Anaerobic Biodegradation of Petroleum Hydrocarbons in Powdered Activated Carbon Groundwater Systems: A Modelling Investigation

by

William Charles McLaren

A thesis
presented to the University of Waterloo
in fulfillment of the
thesis requirement for the degree of
Master of Applied Science
in
Civil Engineering (Water)

Waterloo, Ontario, Canada, 2022

Author’s Declaration

I hereby declare that I am the sole author of this thesis. This is a true copy of the thesis, including any required final revisions, as accepted by my examiners.

I understand that my thesis may be made electronically available to the public.

Abstract

Subsurface contamination by petroleum hydrocarbons (PHCs) is a widespread issue resulting from oil and gas production, distribution, and use. As a result of improved injection methods and particulate materials, injected permeable reactive barriers (PRBs) have gained popularity as a remedial method to cut off groundwater plumes and protect downgradient receptors. The use of particulate activated carbon (AC) as an injected amendment has grown due to its proven capability to adsorb organic contaminants, including PHCs, and potential to enhance biodegradation rates. It has been suggested that AC particulate amendments can establish a dynamic equilibrium between adsorption, desorption, and destruction through biodegradation which prevents downgradient migration of PHC plumes indefinitely.

The overarching goal of this research was to develop a modelling framework to simulate benzene, toluene, and *o*-xylene (BTX) sorption and biodegradation in bench-scale experimental systems containing powdered activated carbon (PAC) and to investigate if biodegradation was enhanced in the presence of PAC. A batch reactor model was developed to simulate non-linear, hysteretic and competitive sorption, and biodegradation representing the conditions of bioaugmentation culture vessels as well as a series of microcosm experiments. The microcosms contained aquifer solids and/or PAC and were subjected to different biological conditions (e.g., bioaugmentation cultures). All microcosms contained either a single compound (toluene) or multiple compounds (BTX). A one-dimensional (1D) reactive transport model was also developed which included the processes simulated in the batch reactor model and was deemed representative of an *in situ* PAC treatment zone. This permitted investigations into sorption hysteresis and PHC breakthrough, as well as exploratory scenarios examining the impact of contaminant mass loading and biodegradation kinetics on the performance of a hypothetical PAC treatment zone.

Using an existing set of single and multi-compound isotherm parameters determined for the PAC used, the batch reactor model was able to simulate the steady-state aqueous BTX concentrations observed in microcosm experiments with no biodegradation. A comparison between simulated and observed solid phase concentrations for microcosms with PAC indicated that desorption hysteresis was minimal. The calibrated kinetic parameters showed improved biodegradation (higher maximum specific growth rate [μ_{max}] and lower half velocity constant [K_S]) for the compound with the highest sorption affinity compared to the bulk solution (toluene in single compound systems and *o*-xylene in

multi-compound systems). 1D investigative scenarios demonstrated that differences in maximum specific growth rate and half-velocity constant (calibrated kinetic parameters for the PHCs) were the most influential factor affecting aqueous effluent PHC concentrations and cumulative PHC mass decayed, while BTX mass loading (a change in flow rate or influent concentration) had a minimal impact. A hypothetical scenario meant to represent biofilm formation on PAC where the maximum specific growth rate was an assumed function of biomass concentration significantly decreased effluent PHC concentrations and increased cumulative PHC mass decayed, suggesting that improved kinetics (i.e., higher maximum specific growth rates) resulting from biofilm formation may lead to more effective long-term PHC treatment.

Overall, the batch reactor and 1D models were able to simulate complex single and multi-compound sorption in bench-scale systems with and without biodegradation. Additionally, there is evidence demonstrating that PAC improves the degradation of compounds with high sorption affinity relative to the bulk solution in a batch reactor system. While mass loading had minimal impact on treatment effectiveness in a column system, improved kinetics (i.e., lower half velocity constant and/or higher maximum specific growth rates, such as through the formation of a biofilm) lead to significant treatment. The developed and validated modelling framework can be used as a foundation for future models to aid in the design and data interpretation of field-scale AC particulate amendment PRBs involving PHCs and other organic contaminants.

Acknowledgements

Firstly, I would like to offer my sincerest thanks to my supervisor Neil R. Thomson. The opportunities and support you have given were vital throughout these last few years, and you have played an integral role in both my professional and personal development. Thank you for everything you have done for me, your past and present students, the university, and our field.

I would also like to thank my thesis readers, Drs. Anh Pham and John Quilty, for taking the time to review this thesis and for providing essential feedback.

Major thanks to Andrea Marrocco, Adam Schneider, and Griselda Raquel Rocha Díaz de León for laying the foundation of all my modelling efforts. My work would lack meaning without the countless hours you spent in the lab generating valuable data sets, and our conversations have been both fun and critical to my understanding over the years. Special thanks to Adam, who I've had the pleasure of suffering through all my post-secondary education with. I will always be grateful not only for your perfectionism – which directly contributed to my success – but also your friendship. I am proud of how far we have come and I am excited to see where we will go.

To Mark Sobon, Mark Merlau, Mark Hummel, and Shirley Chatten for lending their laboratory and field expertise. To Professor Elizabeth Edwards, Dr. Courtney Toth, Amanda Liang, Sandra Dworatzek, and everyone else at BioZone and SiREM for their collaboration and countless fruitful discussions. To Drs. Wayne Parker and Bill Annable for believing in me and providing me with valuable knowledge, perspective, and inspiration throughout my journey.

Funding for this research was provided by the Natural Sciences and Engineering Research Council (NSERC) of Canada Canada Graduate Scholarship – Master's (CGS M), Ontario Graduate Scholarship, NSERC Discovery Grant (PI: N.R. Thomson), and the Ontario Genomics Institute (OGI) and Ontario Research Fund – Genomic Applications Partnership Program (ORF-GAPP) (PI: E.A. Edwards).

And lastly, thank you to my family who fostered my sense of curiosity and instilled in me the confidence I needed to believe in myself. I couldn't have done it without you.

Dedication

To Mom, Dad, Erin, and Grandma for giving me the familial love and support I have relied on; you have given me the opportunity to be here today. To Simone, for being my biggest cheerleader and picking me up when no one else could; you make me excited for the future. To all my friends who provided both welcome and unwelcome distractions from my work; you remind me of the importance of laughter even in difficult times.

And to Grandpa, who I know would have been proud to see where I am today.

Table of Contents

List of Figures

List of Tables

List of Abbreviations

AC	Activated carbon
AGW	Artificial groundwater
AU	Analysis of uncertainty
BAC	Biological activated carbon
BS	Borden sand
BTC	Breakthrough curve
BTEX	Benzene, toluene, ethylbenzene, and the xylene isomers
CAC	Colloidal activated carbon
DDS	Dynamically dimensioned search
DNA	Deoxyribonucleic acid
GAC	Granular activated carbon
IAST	Ideal adsorbed solution theory
ISIAS	Improved simplified ideal adsorbed solution
LUST	Leaking underground storage tank
LV	Large vessel
MDL	Method detection limit
NAPL	Non-aqueous phase liquid
NOM	Natural organic matter
P&T	Pump and treat
PAC	Powdered activated carbon
PAH	Polycyclic aromatic hydrocarbon
PCB	Polychlorinated biphenyl
PFAS	Per- and polyfluoroalkyl substances
PHC	Petroleum hydrocarbon
PRB	Permeable reactive barrier
qPCR	Quantitative polymerase chain reaction
RMSE	Root-mean-square error
USEPA	United States Environmental Protection Agency
VOC	Volatile organic compound
ZVI	Zero valent iron

Chapter 1
Introduction

1.1 General Background

Contamination and migration of organic contaminants in the subsurface is a globally recurring problem and poses both a short and long-term threat to public and ecosystem health. Due to the high variability in extent and severity of this contamination, there are a wide range of remedial technologies available, with minimally intrusive technologies typically preferred from an ecological perspective as they leave the surrounding environment comparatively intact.

The injection of an activated carbon (AC) particulate amendment to create a permeable reactive barrier (PRB) to cut-off a groundwater plume comprised of petroleum hydrocarbons (PHCs) (e.g., benzene, toluene, ethylbenzene, and the xylenes (BTEX)) has gained popularity. The co-injection of AC and beneficial microbial communities is believed to create an environment where sorption and biodegradation are at equilibrium. This AC barrier can theoretically prevent long-term downgradient contamination, and proponents of this technology have touted its ability to quickly remove organics with minimal rebound. However, the *in situ* effectiveness and longevity of AC-based amendments (particularly relating to mass destruction, i.e., biodegradation) remains to be demonstrated. This arises from problems characterizing microbiologic populations and their interaction with physical-chemical processes, a lack of long-term monitoring data, difficulties with adequate AC dosing and effective distribution, and a deficiency in robust mathematical models to assist with design and interpretation (Fan et al., 2017).

The focus of this research effort is on investigating the effect of powdered activated carbon (PAC) on the biodegradation of aqueous BTEX in experimental systems (batch reactors and columns). A modelling framework for bench-scale experiments is developed that simulates the dynamic equilibrium between complex sorption and biodegradation. Insight into the existence of enhanced biodegradation in the presence of PAC, as well as the effects of contaminant loading and transport on treatment effectiveness and longevity is provided. The developed and validated modelling framework can be used as a foundation for future models to aid in the design and data interpretation of field-scale AC particulate amendment PRBs involving PHCs.

1.2 Research Questions

This research will address the following two questions:

1. Can the complex dynamics involving AC particulate amendments be simulated at the bench-scale?
2. Does the presence of AC enhance the biodegradation of PHCs in bench-scale experiments?

To answer these questions, a batch reactor and one-dimensional (1D) model were developed and validated. These were then applied to data sets from culture vessels, soil/PAC microcosm experiments, and a column study emulating an *in situ* AC emplacement. Data sets from the culture vessels were simulated to investigate the capabilities and limitations of the biodegradation portion of the model. Data from a series of soil/PAC microcosm experiments were simulated to determine the representativeness of existing sorption isotherms and to elucidate the effect that PAC sorption has on PHC biodegradation. Then a data set from a column experiment was used to assess the effect of sorption on PHC transport, and the impact of contaminant loading and biodegradation kinetics on PHC treatment was evaluated using a series of investigative scenarios.

1.3 Research Scope and Limitations

To answer the two research questions, a sequential modeling approach was completed:

1. Initially a batch reactor model was developed and used to simulate the behaviour of culture vessels as well as a series of microcosm experiments.
2. Building on (1), a 1D finite volume reactive transport model was developed and used to simulate the behaviour of a column adsorption/desorption experiment as well as a series of investigative scenarios representing a hypothetical *in situ* AC emplacement.

The scope of work was limited to batch reactor and 1D systems. Additionally, simulated PHCs were restricted to benzene, toluene, and *o*-xylene. The impact of additional competitive solutes, such as natural organic matter (NOM), was ignored. Sorption isotherms were limited to those developed for the PAC used in the bench-scale experiments, and sorption processes were assumed to be instantaneous. Biodegradation kinetics and sorption parameters were assumed to be constant and ignored the potential impact of the fouling of AC as biodegradation progresses or variable biodegradation kinetics through culture maturity. Lastly, model calibration was limited to minimizing the error between simulated and observed aqueous phase PHC concentrations only.

This thesis contains four additional chapters. Chapter 2 provides a review of relevant literature that represents the foundation for this research effort. Chapter 3 describes research methods, including

governing equations and assumptions, data sets used, modelling approaches, parameterization, and calibration, uncertainty, and sensitivity analyses. Chapter 4 presents the results and discussion and focuses on the representativeness of PAC isotherm parameters, identification of biodegradation kinetic parameters, and hypothetical 1D column simulations. Lastly, Chapter 5 summarizes the major conclusions and provides recommendations for future work.

Chapter 2
Background and Fundamentals

2.1 General

Groundwater contamination by organic contaminants is a widespread issue which poses a significant risk to public health. As indicated by the Government of Canada, as of August 2022 there are 2,987 Federal sites with contaminated groundwater (Treasury Board of Canada Secretariat, 2022). Some example contaminant classes listed at these sites include petroleum hydrocarbons (PHCs), polycyclic aromatic hydrocarbons (PAHs), per- and polyfluoroalkyl substances (PFAS), metals/metalloids, polychlorinated biphenyls (PCBs), pesticides, and halogenated hydrocarbons, each requiring thorough and appropriate treatment to achieve meaningful remediation.

Groundwater treatment of PHCs is a diverse area of research and development. Example remedial approaches include *ex situ* pump and treat (P&T), bioremediation (e.g., aerobic/anaerobic biodegradation and bioaugmentation), chemical treatment (e.g., *in situ* chemical oxidation/reduction, neutralization), thermal treatment, and other *in situ* treatments like permeable reactive barriers (PRBs), air sparging, phytoremediation, and soil vacuum extraction (Khan et al., 2004; Ossai et al., 2020; USEPA, 2020a). The focus of this research is on the use AC particulate amendments combined with anaerobic bioremediation to treat a dissolved phase PHC plume.

PHCs are a broad category of chemicals which are products of oil and gas, with potential releases occurring at every stage in the supply chain, from production and refinement to distribution and end-use. Comprised of carbon and hydrogen atoms, the two major groups of PHCs are PAHs and monoaromatic compounds. BTEX, a prominent group of monoaromatic compounds and the focus of this research, are ubiquitous to urban and industrial environments contaminated with volatile organic compounds (VOCs) (Abtahi et al., 2018; Miller et al., 2012). Most severely PHC-contaminated sites are associated with crude oil extraction facilities and refineries, but the majority of PHC sites have resulted from leaking underground storage tanks (LUSTs) and pipelines (USEPA, 2020b). In the United States, 84% of USEPA Superfund sites have impacted groundwater, while 59% of these have BTEX present (USEPA, 2020a). Highly volatile and soluble (Table 2.1), these compounds are easily transported in the subsurface (Odermatt, 1994). This causes an increased risk of exposure through inhalation and dermal absorption, with the most significant risk factor being direct ingestion through contaminated drinking water (López et al., 2008). While benzene is a known carcinogen, excess exposure to BTEX can also cause reproductive issues, cardiovascular disease,

respiratory/neurological dysfunction, asthma, and endocrine disruption (Bolden et al., 2015; Brosselin et al., 2009; Ehrlich et al., 2009; McKenzie et al., 2012).

Table 2.1 Canadian Federal drinking water/Ontario Provincial groundwater standards and physical/chemical properties of BTEX compounds.

Parameter	Units	Benzene	Toluene	Ethylbenzene	*o*-Xylene	*m*-Xylene	*p*-Xylene
Formula	[-]	C_6H_6	C_7H_8	C_8H_{10}	C_8H_{10}	C_8H_{10}	C_8H_{10}
GCDWQ MAC[1]	µg/L	5	60	140	90[a]	90[a]	90[a]
Groundwater limit[2]	µg/L	0.5	0.8	0.5	72[a]	72[a]	72[a]
Molecular weight[3]	g/mol	78.1	92.1	106	106	106	106
Density[3]	g/mL	0.877	0.862	0.863	0.876	0.860	0.857
Vapour pressure[3]	torr	94.8	28.4	9.6	6.61	8.29	8.84
Henry's Law constant (K_H^{pc})[3]	atm-m^3/mol	5.55E-03	6.64E-03	7.88E-03	5.18E-03	7.18E-03	6.90E-03
Water solubility[3]	mg/L	1790	526	169	178	161	162
***log* K_{ow}[3]**	[-]	2.13	2.73	3.15	3.16	3.20	3.15
***log* K_{oc}[3]**	[-]	2.16	2.37	2.65	2.58	2.57	2.57

[1]Guidelines for Canadian Drinking Water Quality maximum acceptable concentration (Health Canada, 2020).
[2]Table 1: Full Depth Background Site Condition Standards. Soil, groundwater, and sediment standards for use under Part XV.1 of the Environmental Protection Act (Ontario Ministry of Environment, 2011).
[3]USEPA Superfund Chemical Data Matrix (USEPA, 2021).
[a]Standard is for total xylenes.

There are various mechanisms involved in the immobilization or removal of dissolved BTEX. Because of their high K_{ow} and K_{oc} values (Black & Veatch, 2008), BTEX are good candidates for technologies that rely on sorption, like AC particulate amendments or *ex situ* AC filtration. AC particulate amendments are key to this research and are discussed in Section 2.2.

Biodegradation of dissolved BTEX can be accomplished by indigenous microorganisms, or by more active approaches like biostimulation or bioaugmentation. BTEX compounds are quickly biodegraded aerobically, but due to the rapid depletion of oxygen and its limited supply in the

subsurface these conditions are unsustainable (Lueders, 2017; Scott et al., 2005). As a result, the majority of BTEX biodegradation occurs under anaerobic regimes (Farhadian et al., 2008; Leahy & Colwell, 1990; Weelink et al., 2010; Widdel et al., 2010) detailed in Section 2.2.2.

2.2 Activated Carbon Particulate Amendments

A PRB is a groundwater treatment technology that involves the emplacement of a reactive zone which can immobilize and/or degrade dissolved contaminants. PRBs have been thoroughly explored since the 1990s with reactive material including zero valent iron (ZVI), AC, zeolites, lime, and biomaterials (Al-Hashimi et al., 2021; Faisal et al., 2017; Obiri-Nyarko et al., 2014; Warner, 2015). Conventional installation methods employed are excavation or trenching and backfilling with reactive material; however, recent advancements have allowed less intrusive installation methods using direct push techniques to inject colloidal suspensions or liquid slurries of AC. Often other amendments (i.e., nutrients, bioaugmentation cultures, electron acceptors, buffers) are co-injected to create specific biological and redox conditions as required (Freidman et al., 2017; Ma et al., 2021; Naeimi et al., 2020).

Three main processes that are important in assessing an AC PRB installation include transport, sorption, and degradation (Figure 2.1). Contaminant transport of the dissolved plume is well-understood and involves advection, dispersion/diffusion, and retardation (Barker et al., 1987; Odermatt, 1994; Schirmer et al., 2000). Groundwater flow facilitates contact between the dissolved contaminants and the AC. Sorption to AC results in mass accumulation in the PRB, where enhanced biodegradation is theorized to occur due to higher substrate availability than the surrounding ambient groundwater/soil matrix (Simon, 2015). Mass destruction in the vicinity of the AC frees sorption sites on the AC for further attachment, and the balance between sorption and biodegradation (by indigenous or bioaugmentation cultures) theoretically creates a regenerative system preventing downgradient plume migration. It is this dynamic equilibrium that controls the long-term performance of an AC PRB and remains to be effectively demonstrated (Fan et al., 2017). Detailed discussions regarding the mechanisms and existing research surrounding AC, biodegradation, and simulation of AC particulate amendments are outlined in the following sections.

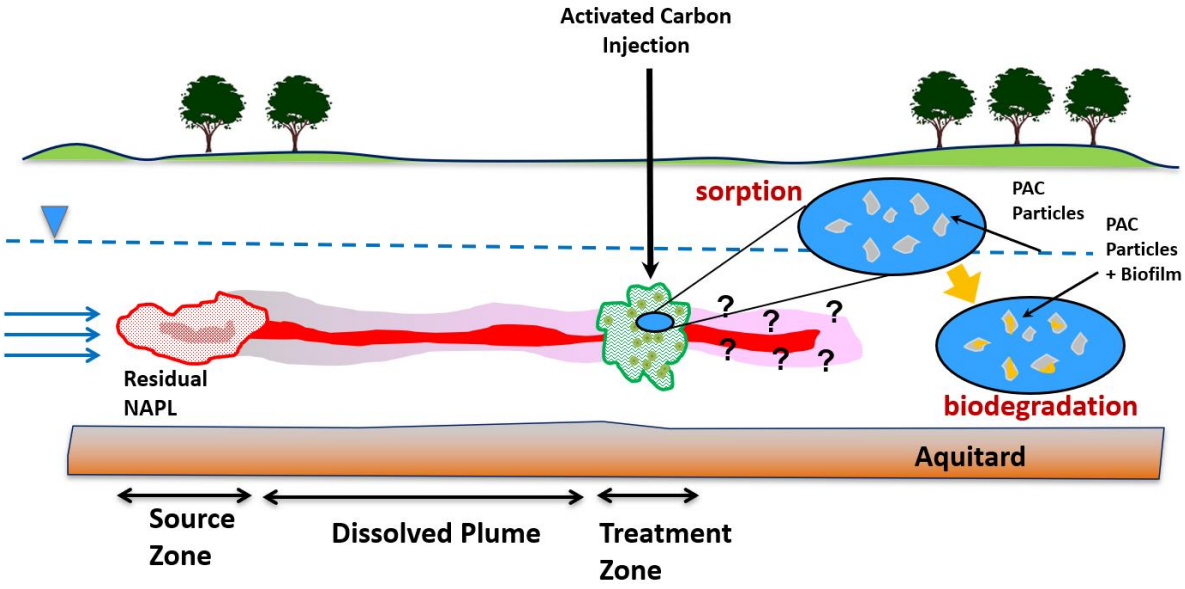

Figure 2.1 Process diagram for field-scale AC particulate amendments (Thomson, 2019), including dissolution of a residual non-aqueous phase liquid (NAPL), migration of the dissolved plume by advection and dispersion, and contaminant sorption and/or biodegradation in an emplacement of powdered activated carbon particulate amendment.

2.2.1 Activated Carbon & Sorption

AC has been used for decades in *ex situ* water and wastewater treatment applications (Çeçen & Aktaş, 2011). AC is used as a general term to describe a family of high-porosity carbonaceous materials, which can be manufactured from a variety of inexpensive sources (e.g., coal, coconut shells, wood, rice husks). The unique properties of AC are the product of a manufacturing process known as activation, which can be accomplished chemically or physically and creates a carbon structure with substantial pore volume and surface area (Çeçen & Aktaş, 2011; Gupta, 2001; Heidarinejad et al., 2020; Teng et al., 1997). The width of pores can vary by 3 to 4 orders of magnitude; micropores, transitional pores (mesopores), and macropores are classified by diameters of < 2 nm, 2-50 nm, and > 50 nm respectively (Çeçen & Aktaş, 2011; Mcdougall, 1991). The structure of AC is similar to graphite, but rather than highly ordered planes of hexagonal rings, carbon rings are randomly oriented, pentagonal (Harris et al., 2008) and hexagonal in shape, and have organic functional groups lying at the edges of these ring systems. These functional groups are a significant factor affecting the degree of sorption occurring on the AC surface and are dependent primarily on the activation method (Figueiredo et al., 1999). Pore volume, surface area, and adsorbate properties (related to surface functional groups) are typically the main parameters considered in assessing the effectiveness of a particular AC-adsorbate combination (Pui et al., 2019). AC is classified according to its grain size; powdered activated carbon (PAC) and granular activated carbon (GAC) have average grain sizes of

15-25 µm (95-100% passing a US standard mesh size of 80 [<0.177 mm]), and 0.2-5 mm respectively (>90% retained in a US standard mesh size of 80 [>0.177 mm]) (ASTM International, 2017, 2019; Çeçen & Aktaş, 2011). Colloidal activated carbon (CAC) has received attention recently due to its low particle size, with average grain sizes of 1-2 µm (Carey et al., 2019; Georgi et al., 2015; Regenesis, 2022). Sorption is broadly defined as the accumulation or concentration of a sorbate (i.e., organics such as BTEX) on a sorbent (i.e., AC, aquifer sediment). There are numerous factors which affect the degree of sorption including the chemical and physical characteristics of the sorbate, the composition of the surface of the sorbent, and the characteristics of the surrounding fluid media (Piwoni & Keeley, 1990). In the case of AC, understanding adsorption requires an understanding of its internal structure.

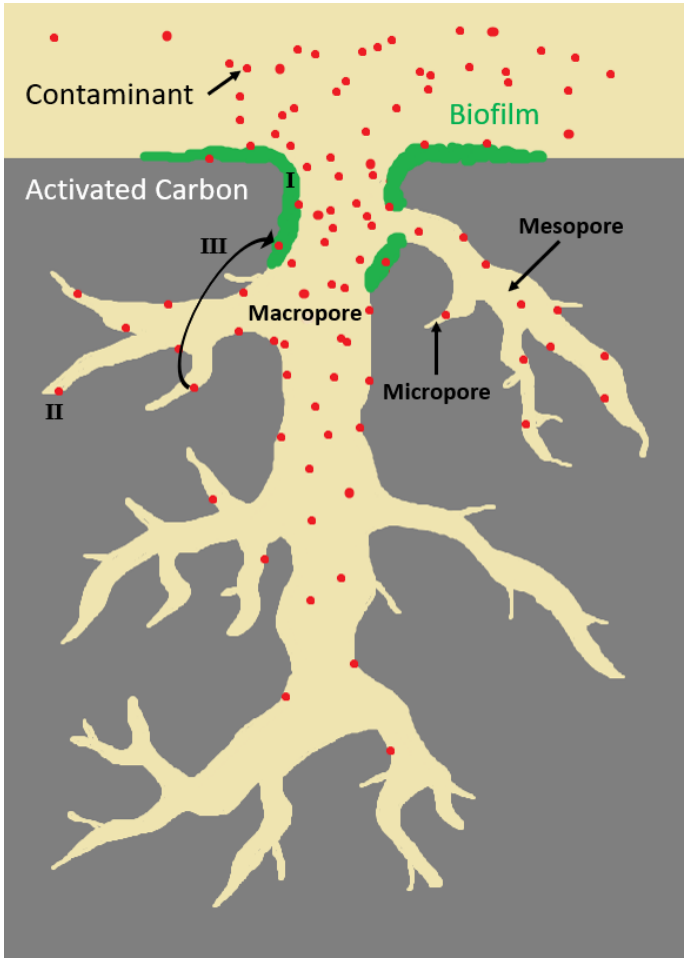

Figure 2.2 Conceptual diagram of PHC removal processes involved in AC particulate amendments: (I) direct adsorption and degradation by microorganisms; (II) adsorption in micropores; (III) desorption, diffusion out of the micropores driven by concentration gradient, and subsequent degradation in microbial biofilm (modified from Fan et al. (2017)).

For sorption to occur, the solute must first be transported from the bulk groundwater to the liquid boundary layer of the sorbate. This is followed by molecular diffusion across the boundary layer and either sorption to the external AC surface or, if the solute is sufficiently small, intraparticle diffusion into the pore space of the AC (Considine et al., 2001; Li et al., 2002; Mcdougall, 1991), as illustrated in Figure 2.2. There are two main sorption processes: physical adsorption (physisorption) and chemical adsorption (chemisorption). Physisorption is driven by the intermolecular attraction at favourable energy sites on carbon planar surfaces (predominantly van der Waals forces) and the sorption energy is relatively low and largely reversible (Aktaş & Çeçen, 2007; Çeçen & Aktaş, 2011; Magne & Walker, 1986; Qu et al., 2019). In contrast, chemisorption occurs when a sorbate reacts with the edges of the planar surface creating a chemical bond. This occurs largely due to the presence of both acidic and basic surface functional groups (Georgi et al., 2015; Julien et al., 1998), and sorption energy is high and largely irreversible. It is difficult to distinguish between physical and chemical sorption, so adsorption is usually simulated using bulk measures like retardation (*R*) and adsorption isotherms (Çeçen & Aktaş, 2011; Yonge et al., 1985; Yonge & Keinath, 1986).

Isotherms are batch experiments used to relate equilibrium aqueous sorbent to sorbed phase concentrations. Isotherms can be linear (Equation (2.1)) and non-linear, like the Freundlich (Equation (2.2)) and Langmuir (Equation (2.3)) isotherms:

$$C_s = K_p C_w \tag{2.1}$$

$$C_s = K_f C_w^{n_f} \tag{2.2}$$

$$C_s = \frac{K_L C_{s_{max}} C_w}{1 + K_L C_w} \tag{2.3}$$

where C_s is the sorbed concentration of the sorbate ($M_{sorbate}\ M_{sorbent}^{-1}$), K_p is the linear partition coefficient ($L^3\ M_{sorbent}^{-1}$), C_w is the aqueous concentration of the sorbate ($M_{sorbate}\ L^{-3}$), K_f is the Freundlich sorption coefficient ($M_{sorbate}^{1-nf}\ L^{3nf}\ M_{sorbent}^{-1}$), n_f is a fitting parameter [-], K_L is the Langmuir sorption coefficient ($L^3\ M_{sorbate}^{-1}$), and $C_{s,max}$ is the maximum observed sorbed concentration of the sorbate ($M_{sorbate}\ M_{sorbent}^{-1}$). Sorption coefficients (K_p, K_f, n_f, K_L, and $C_{s,max}$) are fit to experimental data from single compound batch adsorption experiments. The Freundlich equation assumes that the sorbent has a heterogeneous surface with sites of different sorption potentials with each site adsorbing molecules, while the Langmuir equation assumes the surface of the sorbent is energetically homogenous, with fixed individual sites that can equally sorb only one molecule, creating what is called a *monolayer*. The constants in the Langmuir equation have strictly defined physical meanings,

while the Freundlich equation is empirical in nature. The Freundlich equation arises from a special case in the Langmuir equation where the sorption coefficient varies as a function of the sorbed concentration. The Langmuir equation exhibits a maximum sorbed concentration at high aqueous phase concentrations, while in the Freundlich equation the sorbed concentration increases indefinitely (Çeçen & Aktaş, 2011). While some studies indicate that the Langmuir isotherm is best at describing organic compound sorption onto AC (Luz & Luz, 2013; Pikaar et al., 2006; Zhang & Ou, 2013), the Freundlich isotherm is often adequate and preferable due to its simplicity (Ahmad et al., 2013; Gupta & Gupta, 2016; Hackbarth et al., 2014; Qiu et al., 2012; Yakout & Daifullah, 2014; Yonge et al., 1985).

When discussing the transport of BTEX in the context of contaminant transport and assuming sorption achieves equilibrium instantaneously, sorption processes are summarized by the retardation factor, *R*. Retardation controls the velocity of a simulated BTEX plume relative to the bulk flow of groundwater; an *R* of 1 indicates no retardation, while R > 1 means the plume will be retarded to some degree compared to purely advective-dispersive transport (as with a conservative tracer). Sorption can be linear or non-linear and is empirically represented by an adsorption isotherm. Linear, Freundlich, and Langmuir isotherm equations, sorption rates, and associated retardation factors are described in Table 2.2.

Table 2.2 Expressions of *R* for common sorption isotherm models (modified from Schaffer & Licha (2015).

Sorption model	**Isotherm equation**	**Sorption rate**	**Retardation factor**
Linear	$C_s = K_p C_w$	$\frac{\partial C_s}{\partial t} = K_p \frac{\partial C_w}{\partial t}$	$R = 1 + \frac{\rho_b}{\theta} \cdot K_p$
Freundlich	$C_s = K_f C_w^{n_f}$	$\frac{\partial C_s}{\partial t} = K_f \frac{\partial C_w^{n_f}}{\partial t}$	$R = 1 + \frac{\rho_b}{\theta} \cdot K_f \cdot n_f \cdot C_w^{n_f - 1}$
Langmuir	$C_s = \frac{K_L C_{s_{max}} C_w}{1 + K_L C_w}$	$\frac{\partial C_s}{\partial t} = \frac{K_L C_{s_{max}}}{1 + K_L C_w} \cdot \frac{\partial C_w}{\partial t}$	$R = 1 + \frac{\rho_b}{\theta} \left[\frac{K_L C_{s_{max}}}{(1 + K_L C_w)^2} \right]$

C_w = equilibrium aqueous phase concentration, K_p = linear partition coefficient, K_f = Freundlich sorption coefficient, K_L = Langmuir sorption coefficient, n_f = Freundlich exponent, t = time, C_s = sorbed concentration, $C_{s,max}$ = maximum sorbed concentration, R = retardation factor, ρ_b = bulk density, θ = effective porosity.

Typically, sorption to sediments is assumed to be linear with near-instantaneous kinetics (Chen & Wagenet, 1995; Kan et al., 1994; Schaffer & Licha, 2015). Since *R* is concentration-dependent for non-linear isotherms, it becomes time and space-dependent. Complexity is added if sorption kinetics cannot be neglected. Additional complicating factors include adsorption/desorption hysteresis and competitive sorption between solutes (Sections 2.2.1.1 and 2.2.1.2).

Sorption kinetics for AC, or the rate of approach to equilibrium between the aqueous and sorbed phases, is limited by mass transport mechanisms like advection, dispersion, and diffusion (Çeçen & Aktaş, 2011). Popular models to describe sorption kinetics of PHCs to AC include pseudo-first-order (Hackbarth et al., 2014; Y.-S. Ho, 2004; Lagergren, 1898; Lamichhane et al., 2016) (Equation (2.4)) and pseudo-second-order models (Hackbarth et al., 2014; Y. S. Ho, 1995; Lamichhane et al., 2016) (Equation (2.5)):

$$C_{s_t} = C_{s_{eq}}[1 - \exp(-k_1 t)] \tag{2.4}$$

$$C_{s_t} = \frac{C_{s_{eq}}^2 k_2 t}{1 + k_2 C_{s_{eq}} t} \tag{2.5}$$

where $C_{s,t}$ is the sorbed concentration of the sorbate ($M_{sorbate}\ M_{sorbent}^{-1}$) at time *t* (T), $C_{s,eq}$ is the equilibrium sorbed concentration of the sorbate ($M_{sorbate}\ M_{sorbent}^{-1}$), k_1 is the adsorption constant of the pseudo-first-order model (T^{-1}), and k_2 is the adsorption constant of the pseudo-second-order model (T^{-1}). In batch and continuous flow experiments, adsorption is characteristically a spontaneous ($\Delta G < 0$), endothermic ($\Delta H > 0$), and entropy-increasing ($\Delta S > 0$) process.

2.2.1.1 Hysteresis

It is typically assumed that the amount of mass sorbed from an increase in aqueous phase concentration can be completely desorbed by the same decrease in aqueous phase concentration. However, experimental data often displays desorption data which aberrates from the adsorption isotherm.

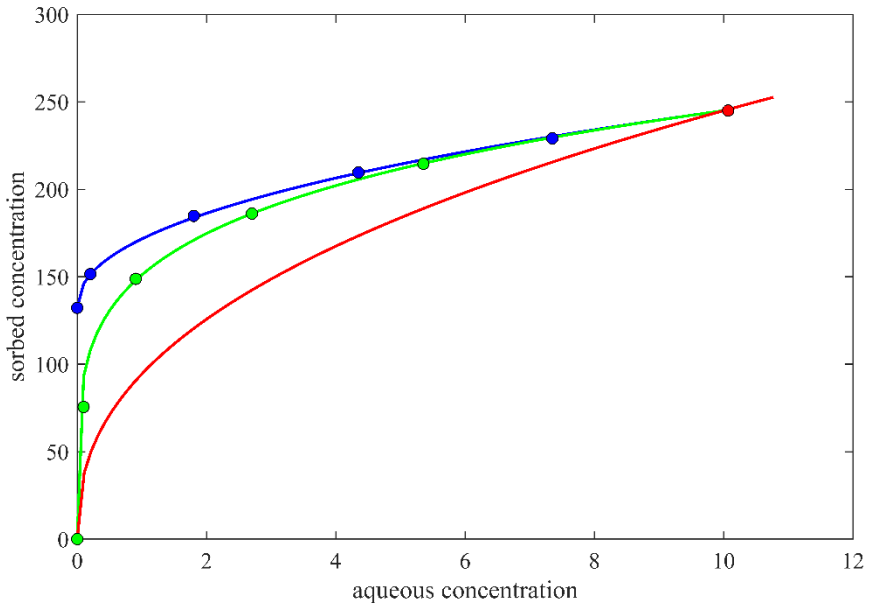

Figure 2.3 Example of hysteretic desorption data: Freundlich adsorption isotherm (—) with hypothetical desorption isotherms from an initial aqueous concentration of 10 (●) displaying desorption hysteresis, including fully reversible (—) or irreversible (—) desorption isotherms. Each desorption data point represents a desorption cycle where the aqueous phase is decanted and replaced with sorbate-free solvent, allowing further desorption until an aqueous concentration of zero is reached, which occurs at a sorbed concentration of zero in reversible hysteresis (●) and 132 in irreversible hysteresis (●).

There is often a portion of sorption sites in virgin AC that cannot be regenerated (Chatzopoulos et al., 1993). Irreversible sorption causes sorption hysteresis (Çeçen & Aktaş, 2011), which manifests as non-zero measured sorbed concentrations at aqueous concentrations of zero in batch isotherm experiments. There are several mechanisms understood to cause irreversible sorption. These can include high-energy permanent chemical bond formation between the sorbate and AC (Chatzopoulos et al., 1993; Kan et al., 1994; Vaccari & Kaouris, 1988; Weber et al., 1998) like oxidative polymerization (de Jonge et al., 1996; Tessmer et al., 1997; Yonge et al., 1985), or physical processes like pore deformation (Braida et al., 2003; Yang & Xing, 2007) and sorption diffusion in restricted microporous channels (Kan et al., 1998). Thermally activated carbon displays a higher degree of irreversible sorption than chemically activated carbon (Aktas & Cecen, 2007; de Jonge et al., 1996).

Evidence of hysteresis can be observed through the development of adsorption and desorption isotherms and fixed-bed column experiments. A distinction must be made between desorption hysteresis caused by irreversible sorption and hysteresis caused by reversible sorption (an experimental artifact resulting from the kinetic limitations of desorption) since each is simulated differently depending on experimental data. The kinetics of desorption are much slower (Hackbarth et

al., 2014; Kan et al., 1994; Yakout & Daifullah, 2014) and adsorption and desorption isotherms may not coincide; if equilibrium has not been established before sampling, the data appears hysteretic. However, if the desorption isotherm passes through the origin, this indicates there is no irreversible sorption. This is referred to as reversible hysteresis, and is possibly a result of inadequate equilibration time, which is typically orders of magnitude higher than adsorption equilibration times and infeasible in most laboratory contexts. Indeed, in many studies the dominant type of sorption is physisorption and is largely reversible (Ahmad et al., 2013; Gupta & Gupta, 2016; Qiu et al., 2012; Zhang & Ou, 2013). In cases where sorption data is hysteretic but appears to pass through the origin (i.e., reversible hysteresis), approaches have been developed to simulate these conditions, mainly through the development of adsorption isotherm and desorption parameters that are functionally related to the maximum concentration observed by the absorbent (Swanson & Dutt, 1973; van Genuchten et al., 1974). To parametrize the Freundlich desorption curves for pesticides, van Genuchten et al. (1974) functionally relate the exponential terms in the adsorption and desorption Freundlich isotherms using an exponential fit:

$$\frac{n_{f_{ads}}}{n_{f_{des}}} = a + bC_{s_{max}}{}^{-c} \tag{2.6}$$

with

$$C_{s,max} = K_{f,ads}C_{w,max}^{n_{f,ads}} \tag{2.7}$$

where $n_{f,ads}$ and $n_{f,des}$ are the Freundlich exponential parameters for the adsorption and desorption isotherms respectively [-], a, b, and c are fitting parameters, $C_{s,max}$ is the maximum simulated solid phase concentration ($M_{sorbate}\ M_{sorbent}^{-1}$), $K_{f,ads}$ is the Freundlich sorption coefficient for the adsorption isotherm ($M_{sorbate}^{1-nf}\ L^{3nf}\ M_{sorbent}^{-1}$), and $C_{w,max}$ is the maximum simulated aqueous phase concentration ($M_{sorbate}\ L^{3}$). By using the equality of the sorption and desorption curves at $C_{w,max}$, $K_{f,des}$ can then be found using

$$K_{f_{des}} = K_{f_{ads}}{}^{n_{f_{des}}/n_{f_{ads}}} \times C_{s_{max}}{}^{(1-n_{f_{des}}/n_{f_{ads}})} \tag{2.8}$$

where $K_{f,des}$ is the Freundlich sorption coefficient for the desorption isotherm ($M_{sorbate}^{1-nf}\ L^{3nf}\ M_{sorbent}^{-1}$). If the simulated aqueous concentration increases beyond the simulated maximum aqueous concentration, the adsorbed concentration is described by adsorption isotherm parameters. If the simulated aqueous concentration decreases below the simulated maximum aqueous concentration, the adsorbed concentration is described by the desorption parameters calculated using Equations (2.6) and (2.8).

In cases where sorption data is hysteretic and appears to not pass through the origin (i.e., irreversible hysteresis) then there is some solute mass that remains sorbed despite an aqueous phase concentration of zero. This sorbed mass is said to be irreversibly sorbed (Yonge et al., 1985). Irreversible hysteresis can be simulated by assuming the adsorption isotherm is the sum of irreversible and reversible sorption isotherms:

$$C_{s_{total}} = C_{s_{irreversible}} + C_{s_{reversible}} \tag{2.9}$$

with

$$C_{s_{irreversible}} = K_{f,irr} C_{w,max}^{n_{f,irr}} \tag{2.10}$$

$$C_{s_{reversible}} = K_{f,rev} C_{w}^{n_{f,rev}} \tag{2.11}$$

where $C_{s,total}$ is the simulated total sorbed concentration of the sorbate ($M_{sorbate}\ M_{sorbent}^{-1}$), $C_{s,irreversible}$ is the simulated irreversibly sorbed concentration of the sorbate ($M_{sorbate}\ M_{sorbent}^{-1}$), $C_{s,reversible}$ is the simulated reversibly sorbed concentration of the sorbate ($M_{sorbate}\ M_{sorbent}^{-1}$), $K_{f,irr}$ and $n_{f,irr}$ are the Freundlich isotherm parameters for irreversibly sorbed mass, $C_{w,max}$ is the maximum simulated aqueous concentration observed by the sorbent ($M_{sorbate}\ L^3$), $K_{f,rev}$ and $n_{f,rev}$ are the Freundlich isotherm parameters for reversibly sorbed mass, and C_w is the simulated aqueous concentration currently observed by the sorbent ($M_{sorbate}\ L^3$). Both the reversible and irreversible sorbed concentrations are simulated using Freundlich isotherms with parameters fit to experimental data (Vaccari & Kaouris, 1988). Parametrizing each sorption type allows for the estimation of an irreversible fraction, which depends on the maximum simulated aqueous phase concentration and does not decrease, and a reversible fraction, which depends on the equilibrium concentration and is allowed to fluctuate freely.

2.2.1.2 Competition

Various solutes (i.e., dissolved organic carbon or PHCs) compete for the limited sorption sites on AC, with the degree of sorption directly depending on the strength of adsorption (ΔG) of the solutes, their individual concentrations, and AC properties (Çeçen & Aktaş, 2011). Efforts to characterize multi-component sorption typically involve estimating isotherm parameters for individual compounds in a multi-component system. These are most typically the Freundlich and Langmuir formulations (Hackbarth et al., 2014; Kilduff & Wigton, 1999; Knettig et al., 1986; Luz & Luz, 2013; Mohamed et al., 2011; Samaddar et al., 2019; Yakout & Daifullah, 2014).

Thermodynamic theory surrounding competitive sorption was initially described for gas mixtures (Myers & Prausnitz, 1965) using a competitive version of the Freundlich isotherm, eventually being extended to the aqueous phase and referred to as Ideal Adsorbed Solution Theory (IAST) (Radke & Prausnitz, 1972) as given by

$$C_{s_i} = {K_f}'^{\left(\frac{{n_f}'-1}{{n_f}'}\right)} \left[K_{f_i} C_{w_i}^{n_{f_i}}\right]^{\frac{1}{{n_f}'}} \left[\sum_i^N \left(\frac{K_{f_i}}{{K_f}'} C_{w_i}^{n_i}\right)^{\frac{1}{{n_f}'}}\right]^{({n_f}'-1)} \tag{2.12}$$

where C_{si} is the sorbed concentration of sorbate i ($M_{sorbate}\ M_{sorbent}^{-1}$), K_f' is the mean value of K_f for all sorbates ($M_{sorbate}^{1-nf}\ L^{3nf}\ M_{sorbent}^{-1}$), n_f' is the mean value of n_f for all sorbates [-], and $i = 1 \ldots N$ is the total number of sorbates. The advantage to IAST is that it utilizes single solute Freundlich adsorption parameters to predict the adsorption behaviour of solutes present in a mixture, foregoing the need to further parameterize a competitive isotherm (DiGiano et al., 1980). While this approach can be effective at predicting the behaviour of bisolute mixtures (Kilduff & Wigton, 1999; Lillo-Ródenas et al., 2006), it is often inadequate. More complex formulations have been developed by implementing various activity or competition coefficients (Kilduff & Wigton, 1999; Knettig et al., 1986; Sochard et al., 2010; Yonge & Keinath, 1986). These coefficients attempt to empirically describe interactions beyond those that are described by the adsorption behaviour represented by the single solute adsorption parameters alone. One of the simplest is the Improved Simplified Ideal Adsorbed Solution (ISIAS) theory, which introduces a competition coefficient derived from the multicomponent adsorption isotherms but maintains the use of single solute isotherm parameters as in IAST (Aktas & Cecen, 2007; Yonge & Keinath, 1986) as given by

$$C_{s_i} = {K_f}'^{\left(\frac{{n_f}'-1}{{n_f}'}\right)} \left[\frac{K_{f_i}}{a_i} C_{w_i}^{n_{f_i}}\right]^{\frac{1}{{n_f}'}} \left[\sum_i^N \left(\frac{K_{f_i}/a_i}{{K_f}'} C_{w_i}^{n_i}\right)^{\frac{1}{{n_f}'}}\right]^{({n_f}'-1)} \tag{2.13}$$

with

$$K_f' = \frac{\sum_i^N (K_{f_i}/a_i)}{N} \tag{2.14}$$

where a_i is the empirical competition coefficient [-].

In competitive systems, PHCs display lower sorbed concentrations at particular aqueous concentrations than they would in non-competitive (i.e., single compound) systems. This is due to the occupation of sorption sites by other PHCs. An additional artifact of competitive sorption in column experiments are breakthrough aqueous PHC concentrations higher than influent concentrations (Lillo-Ródenas et al., 2006). This is due to compounds with low sorption affinity occupying sorption sites at

the leading edge of the adsorption zone which are eventually outcompeted for sorption sites by compounds with a higher sorption affinity. This creates a concentration "front", which is an accumulation of these low sorption affinity compounds and manifests as effluent concentrations higher than what would be predicted by single compound advective-dispersive transport with retardation.

2.2.2 Anaerobic Biodegradation

Anaerobic biodegradation uses electron acceptors in order of energetic favourability, with different microbes and microbial populations taking advantage at various conditions. Table 2.3 provides a summary of the thermodynamics of the primary oxidation pathways of toluene:

Table 2.3 Thermodynamics of toluene oxidation under anaerobic respiration and in syntrophy[a], modified from Lueders (2017).

Electron acceptor (oxidized/reduced)	Stoichiometry	$\Delta G^{0'}$ [kJ (mol C_7H_8)$^{-1}$]
NO_3^-/N_2	$5C_7H_8 + 36NO_3^- + H^+ \rightarrow 35HCO_3^- + 18N_2 + 3H_2O$	-3555 kJ
$Fe(OH)_3/FeCO_3$	$C_7H_8 + 36Fe(OH)_3 + 29\ HCO_3^- + 29\ H^+ \rightarrow 36FeCO_3 + 87H_2O$	-1497 kJ
SO_4^{2-}/HS^- (complete)[b]	$2C_7H_8 + 9SO_4^{2-} + 6H_2O \rightarrow 14HCO_3^- + 9HS^- + 5H^+$	-203 kJ -45 kJ (mol SO_4^{2-})$^{-1}$
SO_4^{2-}/HS^- (incomplete)[b]	$2C_7H_8 + 3SO_4^{2-} + 6H_2O \rightarrow 6CH_3COO^- + 3HS^- + 5H^+$	-61 kJ -41 kJ (mol SO_4^{2-})$^{-1}$
CO_2/CH_4 (sum)	$2C_7H_8 + 15H_2O \rightarrow 9CH_4 + 5HCO_3^- + 5H^+$	-130 kJ
Fermenter	$2C_7H_8 + 18H_2O \rightarrow 6CH_3COO^- + 2HCO_3^- + 8H^+ + 12H_2$	+166 kJ
Hydrogenotroph	$12H_2 + 3HCO_3^- + 3H^+ \rightarrow 3CH_4 + 9H_2O$	-203 kJ
Acetotroph	$6CH_3COO^- + 6H_2O \rightarrow 6CH_4 + 6HCO_3^-$	-93 kJ

[a]Toluene is highlighted as a representative BTEX compound here. The table has been adapted from Weelink et al. (2010) and Widdel et al. (2010).
[b]Complete or incomplete oxidation of toluene.

Differences in energetic favourability create a redox gradient, where electron acceptors are consumed in succession (NO_3^- → $Fe(OH)_3$ → SO_4^{2-} → CO_2); methanogenic conditions prevail at the centre of a plume while nitrate-reducing conditions prevail at the edges. Extensive anaerobic biodegradation of monoaromatic compounds has been achieved at nitrate-reducing (Bender et al., 2001; Cunningham et al., 2001; Rabus & Widdel, 1995; Toth et al., 2021; Ulrich & Edwards, 2003; Xia et al., 2020), iron-reducing (Teramoto & Chang, 2019; Xia et al., 2020), sulfate-reducing (Bartlett et al., 2019; Cunningham et al., 2001; E. Edwards & Grbić-Galić, 1992; Gödeke et al., 2008; Toth et al., 2021; Ulrich & Edwards, 2003; Wei et al., 2018), and methanogenic conditions (E. Edwards &

Grbić-Galić, 1994; Ficker et al., 1999; Luo et al., 2016; Teramoto & Chang, 2019; Toth et al., 2021; Ulrich & Edwards, 2003). Sulfate-reducing and methanogenic conditions are the most extensively studied due to their prevalence, particularly near the centre of mass of PHC plumes.

Assuming decay occurs in the aqueous phase due to biodegradation, the decay of aqueous substrate can be modelled using Monod kinetics (Monod, 1949):

$$\frac{dC_w}{dt} = -k_{max} X \left(\frac{C_w}{K_s + C_w} \right) \tag{2.15}$$

where C_w is the aqueous substrate concentration ($M_{substrate}\ L^{-3}$), k_{max} is the maximum rate of substrate utilization ($M_{substrate}\ M_{biomass}^{-1}\ T^{-1}$), X is the biomass concentration ($M_{biomass}\ L^{-3}$), and K_s is the half-velocity constant ($M_{substrate}\ L^{-3}$), with:

$$k_{max} = \frac{\mu_{max}}{Y} \tag{2.16}$$

where μ_{max} is the maximum specific growth rate (T^{-1}) and Y is the yield coefficient ($M_{biomass}\ M_{substrate}^{-1}$). When substrate concentrations are much higher than the half-velocity constant ($C_w >> K_S$), Equation (2.15) becomes zero-order with respect to aqueous substrate concentration and first order with respect to biomass concentration:

$$\frac{dC_w}{dt} = -k_{max} X \tag{2.17}$$

When substrate concentrations are much lower than the half-velocity constant ($C_w << K_S$), Equation (2.15) becomes first-order with respect to both aqueous substrate and biomass concentration:

$$\frac{dC_w}{dt} = -k'_{max} X C_w \tag{2.18}$$

with:

$$k'_{max} = \frac{k_{max}}{K_S} \tag{2.19}$$

Assuming biomass growth and death rates can be modelled using Monod kinetics and first-order decay respectively, the growth and decay of biomass can be modelled by

$$\frac{dX}{dt} = \mu_{max} X \left(\frac{C_w}{K_s + C_w} \right) - K_d X \tag{2.20}$$

where K_d is the endogenous decay coefficient (d^{-1}). Endogenous decay is represented as a simple first order rate which represents the lump sum of all types of cell decay, including endogenous respiration, predation, and cell lysis (Marais & Ekama, 1976).

2.2.3 Sorption and Biodegradation Interactions

Combining sorption and biodegradation has been investigated in engineered water and wastewater treatment systems, particularly in the context of the biological activated carbon (BAC) process. Essentially the establishment of a microbial community (as a biofilm) on the surface of GAC, BAC has been applied in the treatment of drinking water, industrial and municipal wastewaters, as well as sanitary and hazardous landfill leachates (Çeçen & Aktaş, 2011; Piai et al., 2020; Simpson, 2008). It is well established that the sorption capacity of the AC can be regenerated through biodegradation (Lin, 2016; Shim et al., 2004; Tsuno et al., 2006), extending the lifetime of AC. In turn, adsorption has a positive impact on biodegradation because 1) it increases contact time between microorganisms and substrate, and 2) concentrates the contaminants on and within the AC surface, sequestering contaminant mass which is then available for desorption and degradation (Çeçen & Aktaş, 2011; Fan et al., 2017). Biofilm forms on the outer surface and within macropores, but not within micropores due to the size of microorganisms (~1 μm) (Figure 2.2). This means that sorption and biodegradation are dominant processes in macropores and on the outer AC surface, while adsorption and desorption (driven by concentration gradients created by biodegradation) are dominant in mesopores and micropores (Fan et al., 2017). Biofilms can increase the abundance of microorganisms on particle surfaces, cause nutrient and genetic exchange between populations, and can protect against predation and shear stresses from bulk groundwater flow (Edwards & Kjellerup, 2013). This concept is the foundation of the theorized dynamic equilibrium between sorption and biodegradation suggested for AC particulate amendments (el Gamal et al., 2018; Marchal et al., 2013) and has been demonstrated extensively in BAC systems (Hoang et al., 2008; Lin, 2016; Piai et al., 2022; Zhang & Huck, 1996). BAC employs regular backwashing programs to avoid pore blockages and maintain elevated biodegradation rates on the AC surface (Hoang et al., 2008; Ozis et al., 2007; Rittmann et al., 2002; Shim et al., 2004). Since this degree of control cannot be achieved in the subsurface, the biological management of an AC particulate amendment is reduced to the tuning of redox conditions and other geochemical parameters, and adsorption of degradation products could lead to reduction in the adsorption capacity of the AC (de León, 2021; Smolin et al., 2020). Indeed, direct evidence of biodegradation (Bonaglia et al., 2020; Leglize et al., 2008; Pagnozzi et al., 2021) and regeneration (Chan et al., 2018) in AC products has been mostly limited to the bench scale where solid-phase extraction can be accomplished with ease (to distinguish sorption from biodegradation) and conditions are highly controlled (Fan et al., 2017).

Chapter 3
Methods

A series of microcosm and column experiments were conducted at the University of Waterloo to explore the role of AC-based amendments (Marrocco, 2022; Schneider, 2022). Experiments were performed with and without PAC and/or aquifer solids, using single (toluene) or multiple (BTX) compounds, and under different biological conditions (sterile, killed, indigenous, biostimulated (added sulfate), and bioaugmented). These variations were employed to isolate the effects of sorption and biodegradation. Experimental results elucidated the role of non-linear, hysteretic, and competitive sorption in both the presence and absence of biodegradation. The primary focus was to determine whether mass destruction through biodegradation was enhanced by the presence of AC, and in the case of the columns, in an environment mimicking *in situ* conditions. To develop an understanding of sorption and biodegradation processes in these experiments, both a batch reactor and 1D model were developed. The models were then used to address the questions posed in Section 1.2:

1. Can the complex dynamics (non-linear, hysteretic, and competitive sorption and Monod biodegradation) involving AC particulate amendments be simulated at the bench-scale?
2. Does the presence of AC enhance the biodegradation of PHCs in bench-scale experiments?

This chapter describes the governing equations used to develop both models, as well as the data used in calibration, uncertainty, and sensitivity analyses. Model application and parameterization are also detailed along with the calibration, uncertainty, and sensitivity methods used.

3.1 Batch Reactor Model

This section describes the governing equations, data sets, model application, parameterization, and calibration, uncertainty, and sensitivity analyses for the batch reactor model. Numerical methods and assumptions are detailed, including time discretization and temporal weighting schemes. General trends in the data sets are discussed, followed by key assumptions made for model application. Parameterization of the model input is described, followed by an outline of calibration, uncertainty, and sensitivity analyses methods used.

3.1.1 Batch Reactor Model Development

A batch reactor model was developed to simulate the conditions of a series of microcosm experiments performed with and without PAC and/or aquifer solids, using single (toluene) or multiple (BTX) compounds under different biological conditions. All microcosms consisted of a gaseous phase

(headspace) and an aqueous phase (artificial groundwater (AGW)), with some also having a solid phase (PAC and/or Borden sand (BS)). Mass spikes of PHC were added to the microcosms except in the case of starved controls. Biological conditions included indigenous and/or bioaugmentation cultures, and some were biostimulated through the addition of sulfate or killed through the addition of a biocide. An example diagram of the phases in a biologically active microcosm with PHC addition is displayed in Figure 3.1.

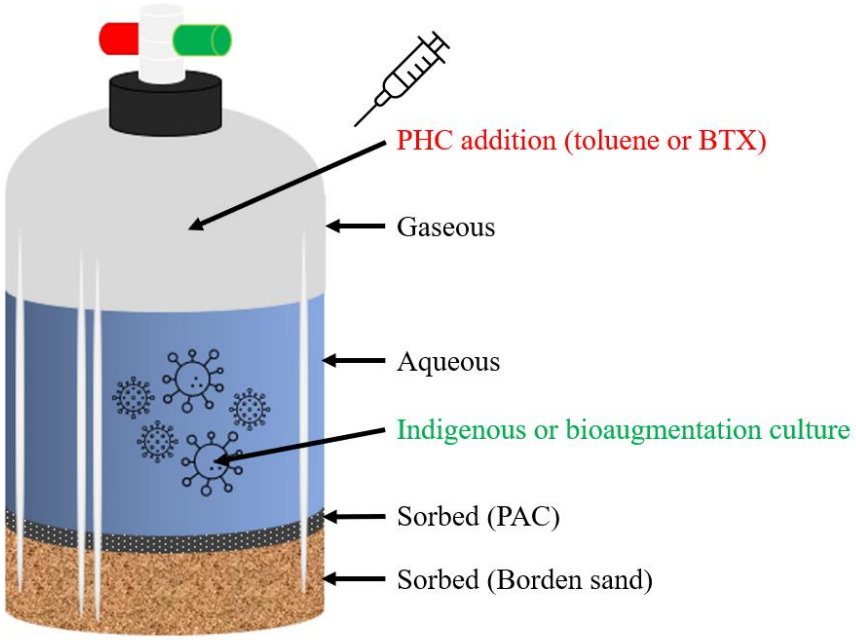

Figure 3.1 Example diagram of a microcosm consisting of gaseous, aqueous, and sorbed (PAC and Borden sand) PHC phases. PHC addition is illustrated as a spike of mass (toluene or BTX), and biological conditions are indigenous or bioaugmentation cultures.

The batch reactor model includes aqueous, sorbed, and/or gaseous (headspace) phases. Some general assumptions were made for the batch reactor model:

1. All phases are fully mixed.
2. Mass partitioning between phases is instantaneous.
3. Reactors are under constant pressure and temperature.
4. Sorption to aquifer solids is linear, non-hysteretic, and non-competitive.
5. Sorption to PAC is non-linear, hysteretic, and competitive.
6. Biomass degrades aqueous PHC mass according to Monod kinetics.

The total mass of PHC compound *i* in a microcosm can be expressed by the addition of aqueous, gas, and sorbed phases as given by

$$M_{T,i} = M_{w,i} + M_{g,i} + M_{s,i} \tag{3.1}$$

with:

$$M_{w,i} = C_{w,i} \forall_w \tag{3.2}$$

$$M_{g,i} = C_{g,i} \forall_{g,i} = H_i C_{w,i} \forall_g \tag{3.3}$$

$$M_{s,i} = M_{s,i}^{aq} + M_{s,i}^{PAC} \tag{3.4}$$

$$M_{s,i}^{aq} = m_{aq} C_{s,i}^{aq} \tag{3.5}$$

$$M_{s,i}^{PAC} = m_{PAC} C_{s,i}^{PAC} \tag{3.6}$$

where *i* is PHC compound *i*, $M_{T,i}$, $M_{w,i}$, $M_{g,i}$, and $M_{s,i}$ are the total, aqueous, sorbed, and gaseous masses of *i* respectively (M_i), $C_{w,i}$ is the aqueous concentration of *i* ($M_i\ L^{-3}$), $\forall_w$ is the liquid volume (L^3) in the microcosm, $C_{g,i}$ is the headspace concentration of *i* ($M_i\ L^{-3}$), $\forall_g$ is the headspace volume (L^3) in the microcosm, H_i is the dimensionless Henry's Law constant of *i* [-], $M_{s,i}^{aq}$ is the mass of *i* sorbed to aquifer solids (M_i), $M_{s,i}^{PAC}$ is the mass of *i* sorbed to PAC (M_i), m_{aq} is the mass of aquifer solids in the microcosm (M_{aq}), $C_{s,i}^{aq}$ is the sorbed concentration of *i* on aquifer solids ($M_i\ M_{aq}^{-1}$), m_{PAC} is the mass of PAC in the microcosm (M_{PAC}), and $C_{s,i}^{PAC}$ is the sorbed concentration of *i* on PAC ($M_i\ M_{PAC}^{-1}$). Equilibrium between phases is assumed.

Sorption of PHCs to aquifer solids is assumed to be linear, reversible, and non-competitive and represented by

$$C_{s,i}^{aq} = K_{p,i} C_{w,i} = f_{oc} K_{oc,i} C_{w,i} \tag{3.7}$$

where $K_{p,i}$ is the linear partitioning coefficient for *i* ($L^3\ M_{aq}^{-1}$), f_{oc} is the organic carbon fraction in the aquifer solids ($M_{oc}\ M_{aq}^{-1}$), and $K_{oc,i}$ is the organic carbon partition coefficient for *i* ($L^3\ M_{oc}^{-1}$). $K_{oc,i}$ can be calculated using empirical relationships with the octanol-water partition coefficient (K_{ow}) (Razzaque & Grathwohl, 2008). The following empirical relationship between K_{ow} and K_{oc} for aromatic hydrocarbons (Doucette, 2003; Karickhoff et al., 1979) was assumed to be applicable:

$$\log K_{oc,i} = \log K_{ow,i} - 0.21 \tag{3.8}$$

where $K_{ow,i}$ is the octanol-water partition coefficient for i ($L^3\ M_i^{-1}$). Adsorption of BTX to AC is assumed to be non-linear according to the Freundlich isotherm:

$$C_{s,i}^{PAC} = K_{f,i} C_{w,i}{}^{n_{f,i}} \tag{3.9}$$

where $K_{f,i}$ is the Freundlich sorption coefficient of i ($M_i^{1-nf}\ L^{3nf}\ M_{PAC}^{-1}$) and $n_{f,i}$ is a fitting parameter [-].

The batch model can simulate both reversible and irreversible hysteretic sorption for a single compound. For reversible hysteretic sorption, the method presented by van Genuchten et al. (1974) was adopted using K_f and n_f values for single compound adsorption and desorption isotherms. An example of simulated reversible hysteresis of toluene on PAC is displayed in Figure 3.2.

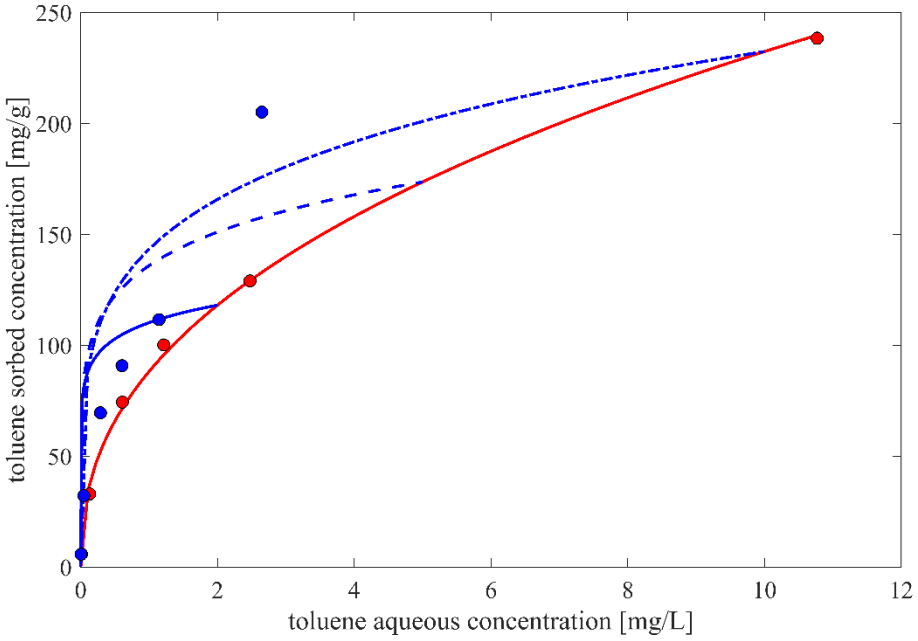

Figure 3.2 Adsorption (●) and desorption (●) of toluene on WPC powdered activated carbon. The simulated Freundlich sorption isotherm (—) is also shown ($K_{f,ads}$ = 88.19, $n_{f,ads}$ = 0.421), with example fully reversible desorption isotherms shown for maximum aqueous concentrations of 2 (—), 5 (— —), and 10 mg/L (— · —). Upon desorption, simulated sorbed concentrations are zero after reaching a simulated aqueous concentration of zero.

A functional form relating $n_{f,i}$ between adsorption ($n_{f,i,ads}$) and desorption ($n_{f,i,des}$) isotherms can be fit to experimental data and is given by the empirical relationship

$$\frac{n_{f,i_{ads}}}{n_{f,i_{des}}} = a + b C_{s,i_{max}}^{PAC}{}^{-c} \tag{3.10}$$

with

$$C_{s,i,max}^{PAC} = K_{f,i,ads} C_{w,i,max}^{n_{f,i,ads}} \tag{3.11}$$

where *a*, *b*, and *c* are fitting parameters, $C_{s,i,max}{}^{PAC}$ is the maximum simulated solid phase concentration of *i* on PAC ($M_i\ M_{PAC}^{-1}$), $K_{f,i,ads}$ is the Freundlich sorption coefficient for the adsorption isotherm of *i* ($M_i^{1-nf}\ L^{3nf}\ M_{PAC}^{-1}$), and $C_{w,i,max}$ is the maximum simulated concentration of *i* observed by the PAC ($M_i\ L^{-3}$). Using the intersection of the adsorption and desorption isotherms (i.e., at the maximum simulated aqueous concentration of *i*), $K_{f,i,des}$ can then be calculated using:

$$K_{f,i_{des}} = K_{f,i_{ads}}{}^{n_{f,i_{des}}/n_{f,i_{ads}}} \times C_{s,i_{max}}^{PAC\ \ (1-n_{f,i_{des}}/n_{f,i_{ads}})} \tag{3.12}$$

Using Equations (3.10) and (3.12), $K_{f,i,des}$ and $n_{f,i,des}$ can be calculated for any $C_{w,i,max}$. If the simulated aqueous concentration increases beyond the simulated maximum aqueous concentration, the adsorbed concentration is described by adsorption isotherm parameters. If the simulated aqueous concentration decreases below the simulated maximum aqueous concentration, the adsorbed concentration is described by desorption isotherm parameters.

For irreversible sorption, the method presented by Vaccari and Kaouris (1988) was followed. An example of simulated reversible hysteresis of toluene on PAC is displayed in Figure 3.3. The total sorbed concentration is represented as the sum of irreversible and reversible portions

$$C_{s,i_{total}}^{PAC} = C_{s,i_{irreversible}}^{PAC} + C_{s,i_{reversible}}^{PAC} \tag{3.13}$$

with

$$C_{s,i_{irreversible}} = K_{f,i,irr} C_{w,i,max}^{n_{f,i,irr}} \tag{3.14}$$

$$C_{s,i_{reversible}} = K_{f,i,rev} C_{w,i}^{n_{f,rev}} \tag{3.15}$$

where $C_{s,i,total}{}^{PAC}$ is the simulated total sorbed concentration of *i* on PAC ($M_i\ M_{PAC}^{-1}$), $C_{s,irreversible}$ is the simulated irreversibly sorbed concentration of *i* ($M_i\ M_{PAC}^{-1}$), $C_{s,reversible}$ is the simulated reversibly sorbed concentration of *i* ($M_i\ M_{PAC}^{-1}$), $K_{f,irr}$ and $n_{f,irr}$ are the Freundlich isotherm parameters for irreversibly sorbed mass, $C_{w,i,max}$ is the maximum simulated aqueous concentration of *i* observed by the sorbent ($M_i\ L^3$), $K_{f,rev}$ and $n_{f,rev}$ are the Freundlich isotherm parameters for reversibly sorbed mass, and $C_{w,i}$ is the simulated aqueous concentration of *i* currently observed by the sorbent ($M_i\ L^3$).

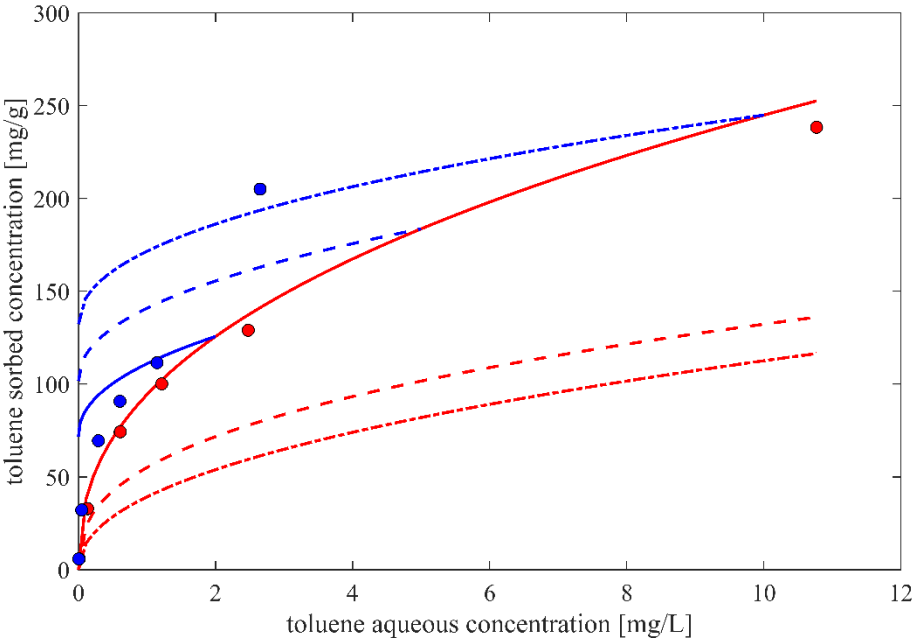

Figure 3.3 Adsorption (●) and desorption (●) of toluene on WPC powdered activated carbon. The simulated Freundlich adsorption isotherm (—) is also shown, which is the sum of example irreversible sorption (— —) and reversible sorption (— · —) isotherms. Desorption isotherms for maximum simulated aqueous concentrations of 2 (—), 5 (— —) and 10 mg/L (— · —). Upon desorption, a simulated irreversibly sorbed concentration remains after reaching a simulated aqueous concentration of zero, which depends on the maximum simulated aqueous concentration observed by the sorbent.

Both the reversible and irreversible sorbed concentrations are calculated using Freundlich isotherms with parameters fit to experimental data (Vaccari & Kaouris, 1988). Parametrizing each sorption type allows for the estimation of an irreversible fraction, which depends on the maximum simulated aqueous phase concentration (which does not decrease), and a reversible fraction, which depends on the equilibrium concentration (which is allowed to fluctuate freely).

Competitive sorption is reflected in the model using ISIAS theory (Yonge & Keinath, 1986), a modification of IAST which uses a competition coefficient as given by

$$C_{s,i}^{PAC} = {K_f}'^{\left(\frac{{n_f}'-1}{{n_f}'}\right)} \left[\frac{K_{f,i}}{a_i} C_{w,i}^{n_{f,i}}\right]^{\frac{1}{{n_f}'}} \left[\sum_i^N \left(\frac{K_{f,i}/a_i}{{K_f}'} C_{w,i}^{n_i}\right)^{\frac{1}{{n_f}'}}\right]^{({n_f}'-1)} \tag{3.16}$$

with

$$K_f' = \frac{\sum_i^N (K_{f,i}/a_i)}{N} \tag{3.17}$$

$$n_f' = \frac{\sum_i^N n_{f,i}}{N} \tag{3.18}$$

where K_f' is the weighted average value of K_f for all PHC compounds ($M^{1-nf}\,L^{3nf}\,M_{PAC}^{-1}$), n_f' is the average value of n_f for all PHC compounds [-], a_i is the competition coefficient for PHC compound i, and $i = 1 \ldots N$ is the total number of PHC compounds. Competition coefficients can be determined using data from competitive sorption experiments.

The developed model can only reflect competitive or hysteretic systems, but not both. Both reversible and irreversible hysteresis are modelled using single compound adsorption and desorption isotherm parameters fit to experimental adsorption and desorption data, so a multi-compound desorption experiment would be required to fit multi-compound desorption isotherms.

The rate of change of mass of PHC compound i is represented by Monod kinetics (Monod, 1949):

$$\frac{dM_{T,i}}{dt} = \dot{M}_{in,i} - k_{max,i} X_i \left(\frac{C_{w,i}}{K_{s,i} + C_{w,i}}\right) \forall_w \tag{3.19}$$

$$\frac{dX_i}{dt} = \mu_{max,i} X_i \left(\frac{C_{w,i}}{K_{s,i} + C_{w,i}}\right) - K_{d,i} X_i \tag{3.20}$$

with

$$k_{max,i} = \frac{\mu_{max,i}}{Y_i} \tag{3.21}$$

where $\dot{M}_{in,i}$ is the rate of PHC compound (substrate) i mass added to the microcosm ($M_{substrate}\,T^{-1}$), $k_{max,i}$ is the maximum rate of substrate utilization ($M_{substrate}\,M_{biomass}^{-1}\,T^{-1}$), X_i is biomass concentration ($M_{biomass}\,L^{-3}$), $K_{s,i}$ is the half-velocity constant ($M_{substrate}\,L^{-3}$), $\mu_{max,i}$ is the maximum specific growth rate (T^{-1}), $K_{d,i}$ is the endogenous decay coefficient (T^{-1}), and Y_i is the yield coefficient ($M_{biomass}\,M_{substrate}^{-1}$). All Monod kinetic parameters are unique for each PHC compound and are independent of other PHCs. Mass spikes are treated as an addition of mass (M_i) that partitions instantaneously across all phases. Additionally, changes in aqueous volume in the microcosm can be modelled as dilutions (aqueous volume increases with no change in system PHC mass) according to

$$\forall_{w,new} = \forall_{w,old} + \Delta \forall \tag{3.22}$$

where $\forall_{w,new}$ is the new aqueous volume after an aqueous addition (dilution) (L^3), $\forall_{w,old}$ is the aqueous volume before an aqueous addition (L^3), and $\Delta\forall$ is the change in aqueous volume (L^3). Changes in aqueous volume can also be modelled as samples (aqueous volume decreases with a loss in aqueous mass) according to

$$\forall_{w,new} = \forall_{w,old} - \Delta \forall \tag{3.23}$$

with

$$\Delta M_{w,i} = \Delta \forall C_{w,i} \tag{3.24}$$

where $\Delta M_{w,i}$ is the aqueous mass of *i* lost (M_i). Occasionally, samples immediately followed by top-ups (i.e., returning the aqueous phase volume to its original value) were simulated. These were represented as a mass loss using Equation (3.24) with no change in aqueous volume.

The PHC compound mass balance equation is developed by combining Equations (3.1) and (3.19):

$$\frac{d(C_{w,i} \forall_w + H_i C_{w,i} + m_{aq} C_{s,i}^{aq} + m_{PAC} C_{s,i}^{PAC})}{dt} = \dot{M}_{in,i} - k_{max,i} X_i \left(\frac{C_{w,i}}{K_{s,i} + C_{w,i}} \right) \forall_w \tag{3.25}$$

Equation (3.25) is non-linear in C_w and coupled across PHC compounds when competition is simulated (through Equation (3.16)) and coupled with the biomass balance described in Equation (3.20) through *X*.

A finite difference discretization was used with a Crank-Nicholson temporal weighting scheme (Crank & Nicolson, 1947). For non-linear problems, Picard iteration (Lindelöf, 1894; Picard, 1890) is employed to solve the system of equations until both aqueous PHC and biomass concentrations converge to a specified tolerance. An arbitrary convergence tolerance of 10^{-10} was selected; the largest change in both aqueous and biomass concentrations from the previous to the current iteration must be $<10^{-10}$ ($M\ L^{-3}$) in order to advance to the next time step. Upon completion of the simulation, the solution yields time series concentrations for both aqueous PHCs and biomass. An adaptive time-stepping method is implemented where a minimum timestep increases by a specified factor until reaching a maximum. The timestep returns to the minimum value when the mass in the system is significantly perturbed (i.e., mass spikes and compartment volume changes).

Verification of the model was completed by comparing simulated concentrations to equilibrium concentrations predicted using Equations (3.1) to (3.6) and assuming biodegradation was negligible. Aqueous, sorbed (BS and PAC), and headspace compartments were turned on and off, and simulated concentrations in each compartment were verified against those predicted.

3.1.2 Data Sets

Data sets were obtained from SiREM in Guelph, Ontario, Canada for their sulfate-reducing and methanogenic benzene-degrading DGG-B culture, as well as a series of aquifer solids/PAC microcosm experiments carried out at the University of Waterloo (Marrocco, 2022; Schneider, 2022).

3.1.2.1 SiREM Culture Vessel Data

The DGG cultures (consisting of DGG-B, DGG-T, and DGG-X for benzene, toluene, and *o*-xylene degradation respectively), named after anaerobic hydrocarbon degradation researcher and Stanford University professor Dunja Grbić-Galić, are sulfate-reducing and methanogenic PHC-degrading microbial consortia originally cultured from oil refinery sites in 1995 (Ulrich & Edwards, 2003). First investigated at the bench scale in the late 1990s (Luo et al., 2014), they have since been significantly scaled up and successfully implemented at field scale (Toth et al., 2021). The cultures are primarily maintained at SiREM in Guelph, Ontario, Canada, and the BioZone Centre for Applied Bioscience and Bioengineering at the University of Toronto in Toronto, Ontario, Canada. A dataset of the DGG-B bioaugmentation culture was provided by SiREM to investigate the capabilities of the Monod kinetics module of the batch reactor model. The culture vessels selected for this investigation were maintained under strictly methanogenic conditions and were chosen because: 1) they have periods of 150+ days of constant aqueous and headspace volume, 2) they have high resolution benzene degradation cycles and are consistently re-spiked, and 3) they represent one of the bioaugmentation cultures (along with DGG-T and DGG-X for toluene and *o*-xylene respectively) used in the microcosms experiments discussed in Section 3.1.2.2.

The following two datasets were used: (1) data from the primary DGG-B culture vessel (LV1) consisting of 69 benzene timepoints with 16 2.5 g benzene re-spikes over 520 days [Figure 3.4(a)], and (2) data from a scale-up vessel seeded from DGG-B-LV1 (LV2) and consisting of 66 benzene timepoints with five 1.9 g and eight 2.5 g benzene re-spikes over 478 days [Figure 3.4(b)]. The total volume (aqueous + headspace) in the reactors was assumed to be 105 L, and aqueous volume changes (due to culture splitting or replenishment of the aqueous phase due to sampling losses over time) were considered. Both vessels display rapid and consistent biodegradation of benzene, which by visual inspection appear to be approximately equal. Both data sets were selected for initial investigations into kinetic parameter calibration.

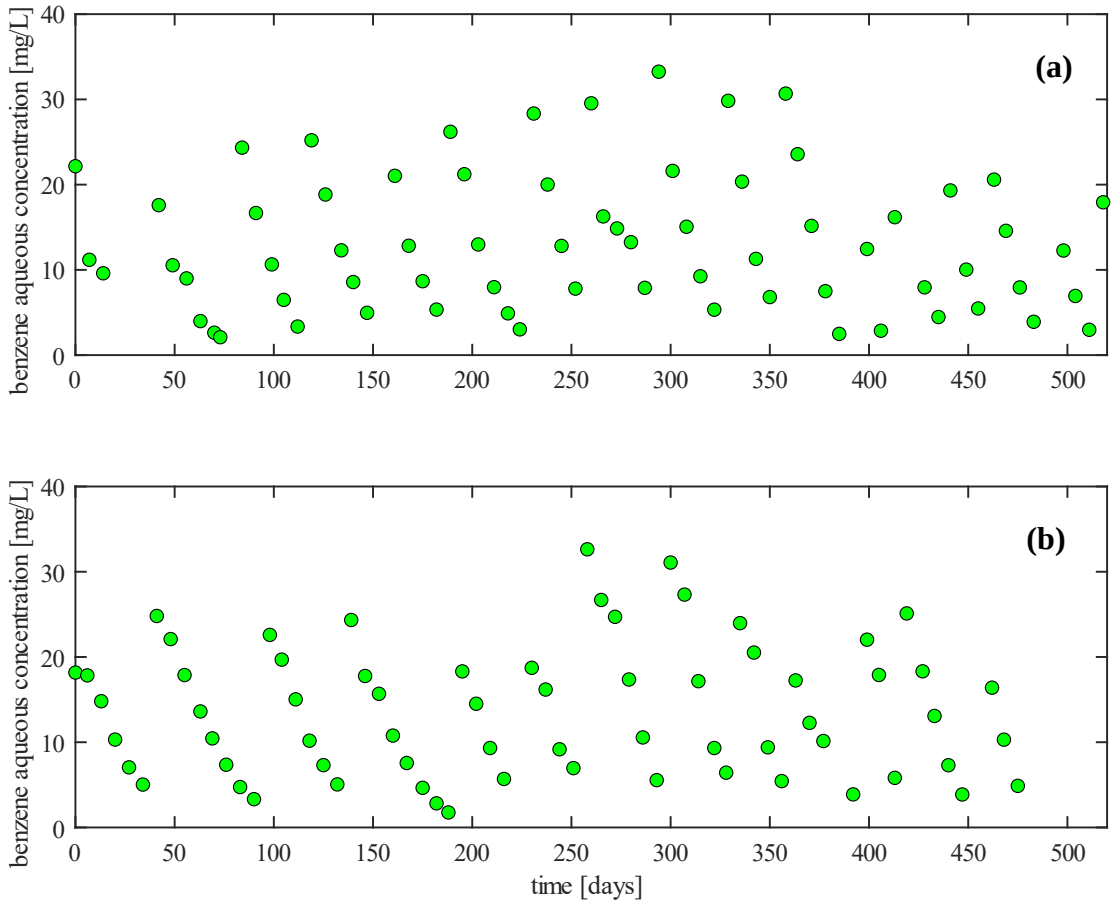

Figure 3.4 (a) LV1 and (b) LV2 culture vessel data: aqueous benzene concentrations (●). Each data point represents a single aqueous phase benzene measurement.

3.1.2.2 Microcosm Data

A series of aquifer solids/PAC microcosm experiments were carried out at the University of Waterloo under a variety of conditions (see Marrocco (2022) or Schneider (2022) for relevant methods). The microcosm systems were used to isolate the effects of indigenous microorganisms, biostimulation, bioaugmentation cultures, and the presence/absence of PAC for a single PHC compound (toluene) or multiple PHC compounds (BTX). Each microcosm system consisted of multiple sets of reactors where, in general, a set was sampled repeatedly over time before being sacrificed. The microcosm systems considered in the work discussed here include:

- Active (A): Isolating the effects of indigenous microorganisms in BS
- Powdered activated carbon (PAC): Isolating the effects of sorption onto PAC (with killed BS and killed bioaugmentation culture)
- A-PAC: Combined effects of indigenous microorganisms in BS and PAC

- Bioaugmented (BA): Isolating the effects of bioaugmentation cultures (this is the only microcosm experiment with no BS)
- A-BA: Combined effects of indigenous microorganisms in BS and bioaugmentation cultures
- A-BA-PAC: Combined effects of indigenous microorganisms in BS, bioaugmentation cultures, and PAC

Each microcosm series was conducted with either toluene only or a BTX mixture. All microcosms were initially spiked with 3.64 mg of toluene only (single compound) or 3.50 mg each of benzene, toluene, and *o*-xylene (multi-compound). If the aqueous phase concentration for a given PHC compound was substantially degraded, the compound was replenished using the same mass as the initial spike. In the following sub-sections, the relevant characteristics of each microcosm system are discussed.

3.1.2.2.1 Active (A) Microcosms

The purpose of the Active (A) microcosm system was to understand the role of indigenous biodegradation. Each microcosm contained ~69 g of BS and 175 mL of AGW. The aqueous concentrations time series for both single and multi-compound A microcosms had 14 data points per PHC compound (Figure 3.5).

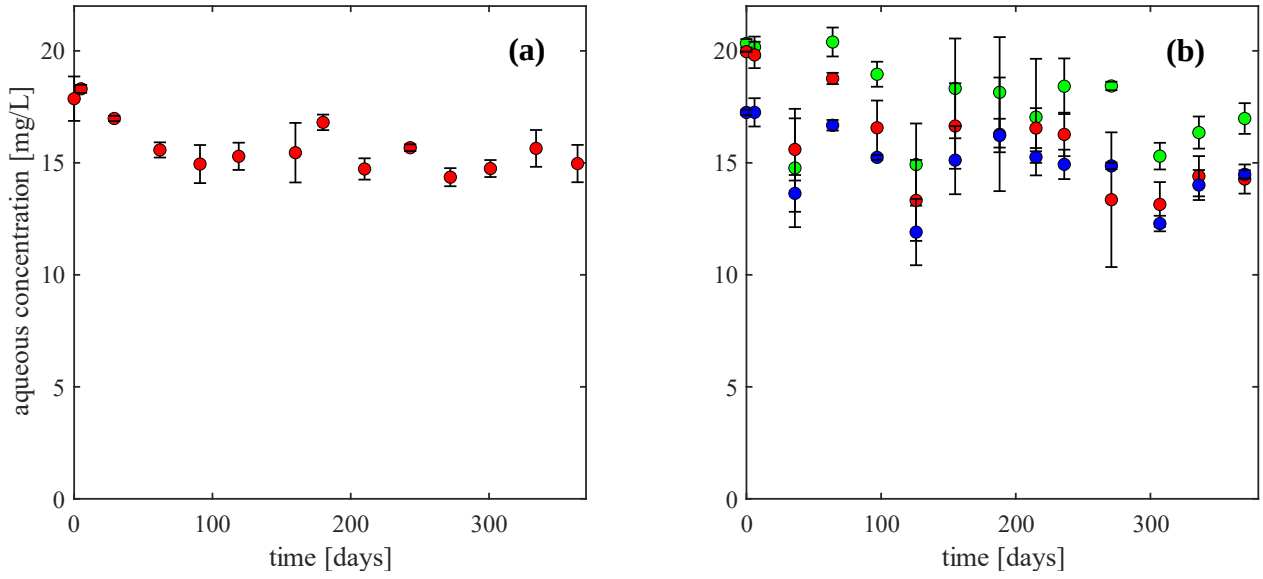

Figure 3.5 Active (A) microcosm data: (a) aqueous toluene concentrations (●) from the single compound system, and (b) aqueous benzene (●), toluene (●), and *o*-xylene (●) concentrations from the multi-compound system. Error bars represent ± one standard deviation.

Toluene concentrations in single compound A microcosms show a negligible amount of degradation with no significant decrease in aqueous phase toluene concentration after Day 60

corresponding to sulfate depletion (data not shown). Irrespective of the presence of sulfate-reducing toluene degradation, all microcosm experiments occur under predominantly methanogenic conditions, so sulfate-reducing activity will be assumed negligible in single compound experiments.

The results from the multi-compound A microcosms are like the single compound A microcosms with negligible degradation of BTX. The rising and falling of BTX concentrations across the time series is perhaps indicative of uncertainty in the mass of the initial spike (multiple bottle sets are sampled and sacrificed over the duration of the time series), but generally the trends are the same. Indigenous biodegradation of BTX will also be ignored in the multi-compound experiments. BTX aqueous concentrations match trends predicted based on physical and chemical constants for each PHC (i.e., partitioning into the sorbed and gas phases using K_p and H_{cc} ([B] > [T] > [X])). Assuming the same amount of mass for each PHC compound in an A microcosm, ~96, ~94, and ~92% of total mass resides in the aqueous phase for benzene, toluene, and *o*-xylene respectively.

3.1.2.2.2 Powdered Activated Carbon (PAC) Microcosms

The purpose of the powdered activated carbon (PAC) microcosm system was to understand the role of PAC. Each microcosm contained ~69 g of autoclaved BS, ~15 mg of PAC, a 1 mL addition of killed bioaugmentation culture (1 mL of DGG-T for single compound and 1 mL of each of DGG-B, DGG-T, and DGG-X for multi-compound) and 175 mL of AGW. The aqueous concentrations time series for both single and multi-compound A microcosms had 14 data points per PHC compound (Figure 3.6).

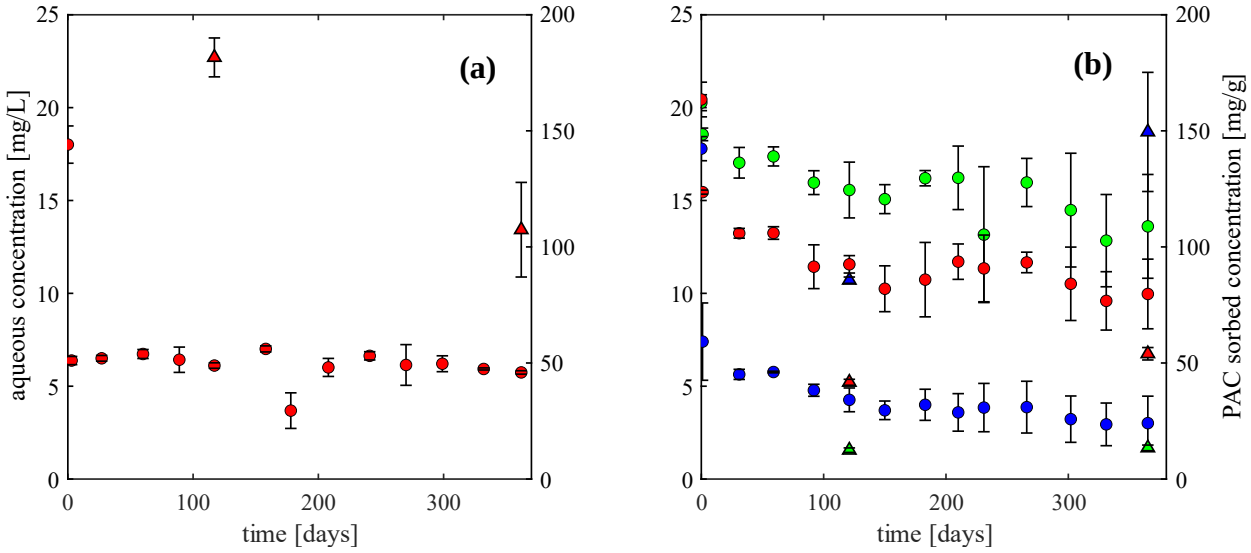

Figure 3.6 Powdered activated carbon (PAC) microcosm data: (a) aqueous (●) and sorbed (▲) toluene concentrations from the single compound system, and (b) aqueous/PAC sorbed benzene (● /▲), toluene (● /▲), and *o*-xylene (● /▲) concentrations from the multi-compound system. Error bars represent ± one standard deviation.

The first data point(s) in the single compound (Day 0) and multi-compound (Day 0 and 1) time series occur before PAC addition. Multi-compound microcosms took nearly 60 days to approach an equilibrium condition, and there is a significant but consistent drop in aqueous concentrations over this period. This could be because there is homogenous mass loss across a given triplicate set due repeated sampling episodes. Unlike other microcosm series, the PAC microcosms only had two triplicate sets; one sampled for the first half and sacrificed at Day 117, and one sampled for the second half and sacrificed at the end of the experiment. This is supported by consistent measured aqueous concentrations in the single compound microcosms since there was significantly less PHC mass removed due to sampling. Overall, these data suggest that biodegradation is not occurring in multi-compound microcosms since the benzene concentration, which is the most recalcitrant of the three PHC compounds, has similar stability to toluene and *o*-xylene. In single compound microcosms, aqueous toluene concentrations remain stable. Additionally, there was no methane generation (data not shown) over the course of the experiments.

3.1.2.2.3 Active Powdered Activated Carbon (A-PAC) Microcosms

The purpose of active powdered activated carbon (A-PAC) microcosms was to understand the combined role of indigenous biodegradation and PAC. Each microcosm contained ~69 g of active BS, ~15 mg of PAC, and 175 mL of AGW. The aqueous concentrations time series for both single and multi-compound A microcosms had 14 data points per PHC compound (Figure 3.7).

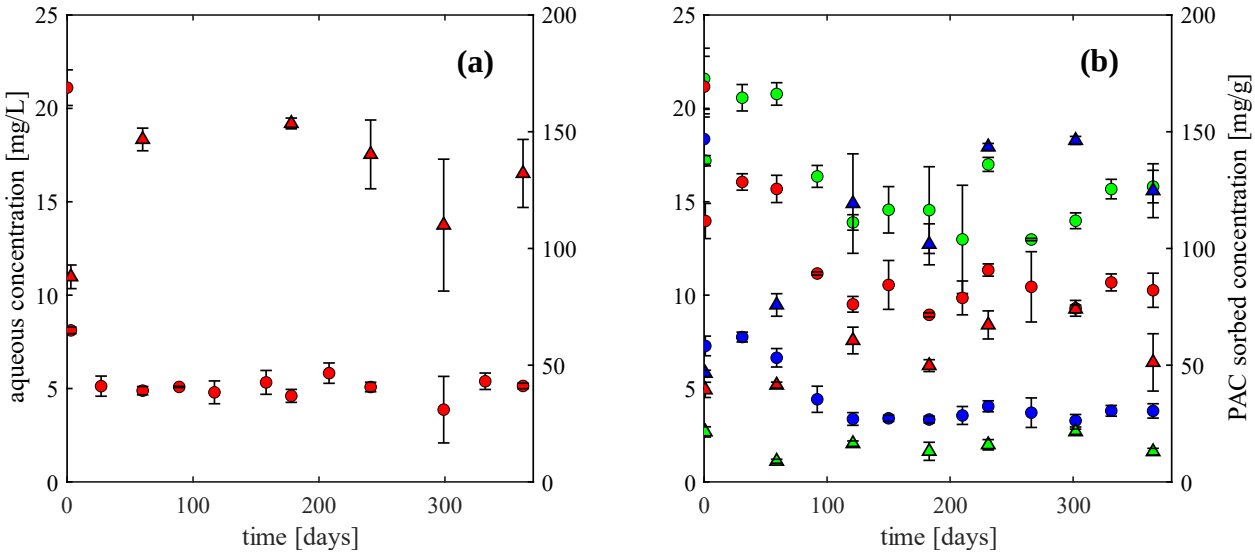

Figure 3.7 Active powdered activated carbon (A-PAC) microcosm data: (a) aqueous (●) and sorbed (▲) toluene concentrations from the single compound system, and (b) aqueous/PAC sorbed benzene (● /▲), toluene (● /▲), and *o*-xylene (● /▲) concentrations from the multi-compound system. Error bars represent ± one standard deviation.

Single compound A-PAC microcosms display the same trends as the PAC microcosms; initial sorption followed by minimal change in aqueous phase toluene concentrations. The variability in the multi-compound A-PAC microcosms is similar to that observed in the multi-compound PAC experiments, including a slight delay in equilibrium conditions until Day 60. Benzene and toluene concentrations fluctuate quite significantly.

3.1.2.2.4 Bioaugmented (BA) Microcosms

The purpose of the bioaugmented (BA) microcosms was to understand the role of bioaugmentation cultures. Each microcosm contained a 1 mL addition of bioaugmentation culture (1 mL of DGG-T for single compound and 1 mL of each of DGG-B, DGG-T, and DGG-X for multi-compound) and 220 mL of AGW. The single compound experiment was re-spiked with toluene at Day 217, while the multi-compound experiment was re-spiked with toluene and *o*-xylene at Day 234. The aqueous concentrations time series for single and multi-compound A microcosms had 15 and 14 data points per PHC compound respectively (Figure 3.8).

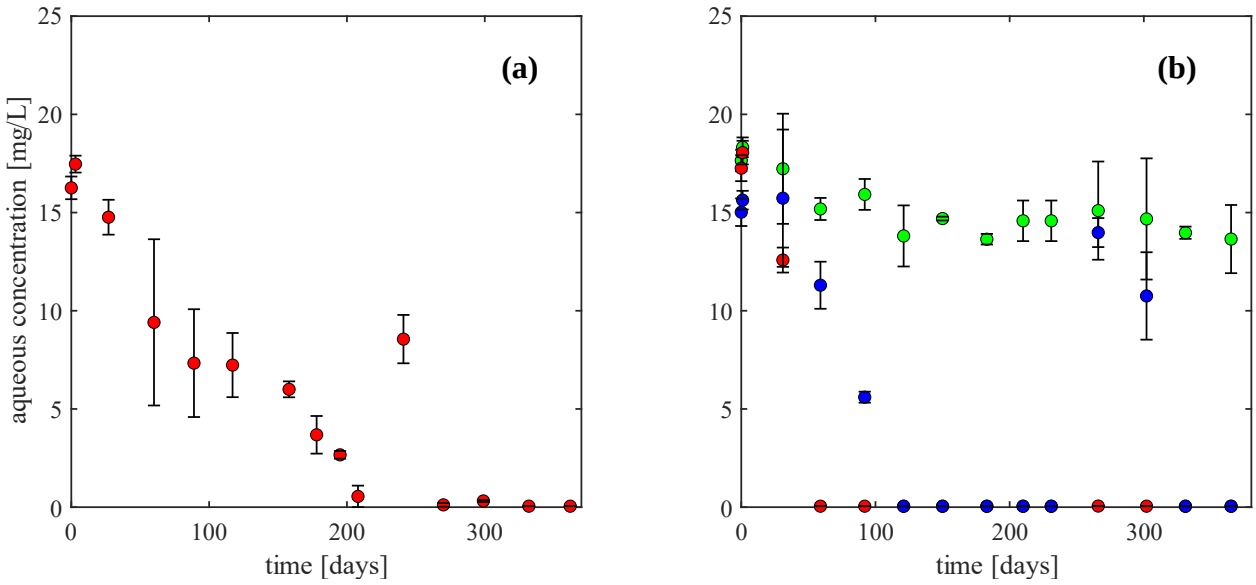

Figure 3.8 Bioaugmented (BA) microcosm data: (a) aqueous toluene concentrations (●) from the single compound system, and (b) aqueous benzene (●), toluene (●), and *o*-xylene (●) concentrations from the multi-compound system. Error bars represent ± one standard deviation.

In the single compound experiment, there was only one toluene re-spike after the initial spike (as opposed to 2-5 in all other bioaugmented microcosm series). This is because toluene degradation was noticeably slower in this microcosm, with aqueous concentrations remaining stable from Day 60 to 158 and eventually depleting sometime after Day 208. After the second spike, however, it appears that toluene degradation increased to the rates observed in the other microcosms.

The multi-compound experimental data shows that toluene degradation occurred much more quickly than in the single compound experiment, being depleted by Day 59. *o*-Xylene degradation was slower but also significant and was depleted by Day 121. Benzene concentration dropped slightly at the beginning of the experiment but remained relatively constant from ~Day 50 until the end of the experiment. This trend is observed in all benzene time series in bioaugmented microcosms and is suspected to be due to an unsuccessful DGG-B bioaugmentation.

3.1.2.2.5 Active Bioaugmented (A-BA) Microcosms

The purpose of active bioaugmented (A-BA) microcosms was to understand the combined role of indigenous biodegradation and bioaugmentation cultures. Each microcosm contained ~69 g of active BS, 1 mL addition of bioaugmentation culture (1 mL of DGG-T for single compound and 1 mL of each of DGG-B, DGG-T, and DGG-X for multi-compound), and 175 mL of AGW. The single compound experiment was re-spiked with toluene at Day 73, 145, 195, 217, and 263, while the multi-compound experiment was re-spiked with toluene and *o*-xylene at Day 186 and 303. The aqueous

concentrations time series for single and multi-compound A-BA microcosms had 16 and 18 data points per PHC compound respectively (Figure 3.9).

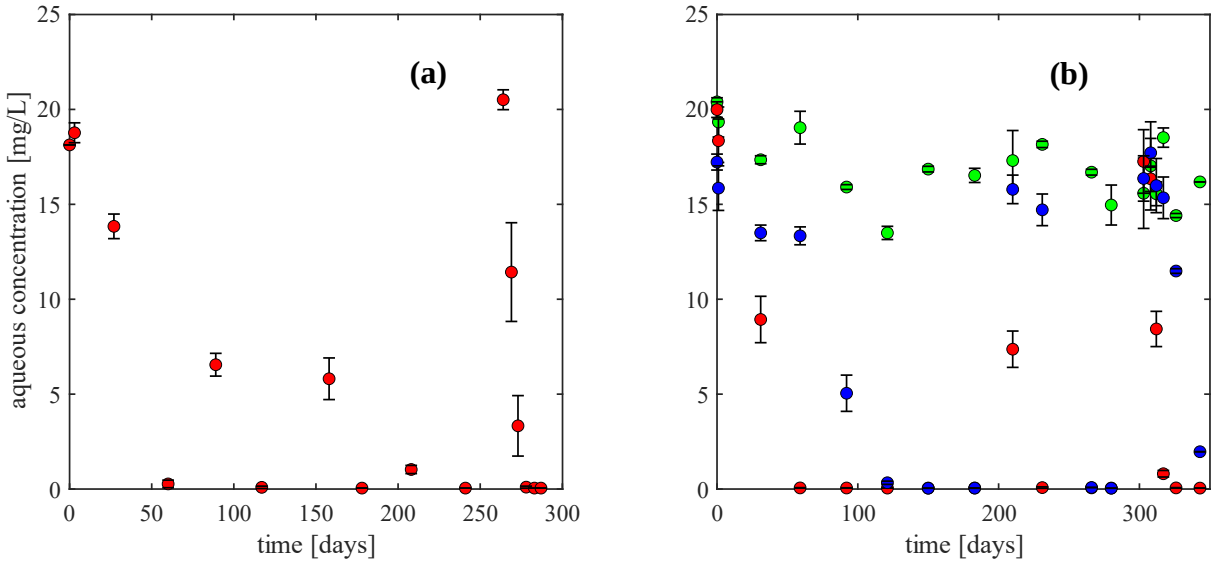

Figure 3.9 Active bioaugmented (A-BA) microcosm data: (a) aqueous toluene concentrations (●) from the single compound system, and (b) aqueous benzene (●), toluene (●), and *o*-xylene (●) concentrations from the multi-compound system. Error bars represent ± one standard deviation.

Aqueous toluene concentrations in the single compound experiments were depleted sometime after Day 60. Degradation rates increased, with concentrations depleted (Day 278) 15 days after re-spike by the last spike (Day 263).

The multi-compound A-BA microcosms displayed similar results to the multi-compound BA microcosms. Toluene and *o*-xylene were depleted by Day 59 and Day 150 respectively. Aqueous benzene concentrations remained stable over the experiment duration. This series was only re-spiked with toluene and *o*-xylene twice (as opposed to five times in the single compound experiment) since toluene and *o*-xylene are preferred substrates, and it was suspected that benzene might degrade in their absence. By the end of the experiment, toluene and *o*-xylene degradation were rapid. Toluene had depleted (Day 326) 23 days after the last spike (Day 303), and *o*-xylene concentrations were at ~2 mg/L (Day 343) 40 days after the last spike (Day 303).

3.1.2.2.6 Active Bioaugmented Powdered Activated Carbon (A-BA-PAC) Microcosms

The purpose of active bioaugmented powdered activated carbon (A-BA-PAC) microcosms was to understand the combined role of indigenous biodegradation, bioaugmentation cultures, and PAC. Each microcosm contained ~69 g of active BS, 1 mL addition of bioaugmentation culture (1 mL of DGG-T for single compound and 1 mL of each of DGG-B, DGG-T, and DGG-X for multi-compound), ~15 mg of PAC, and 175 mL of AGW. The single compound experiment was re-spiked

with toluene at Day 73, 145, 195, 217, and 263, while the multi-compound experiment was re-spiked with toluene and *o*-xylene at Day 186, 234, and 303. The aqueous concentrations time series for single and multi-compound A microcosms had 16 and 18 data points per PHC compound respectively (Figure 3.10).

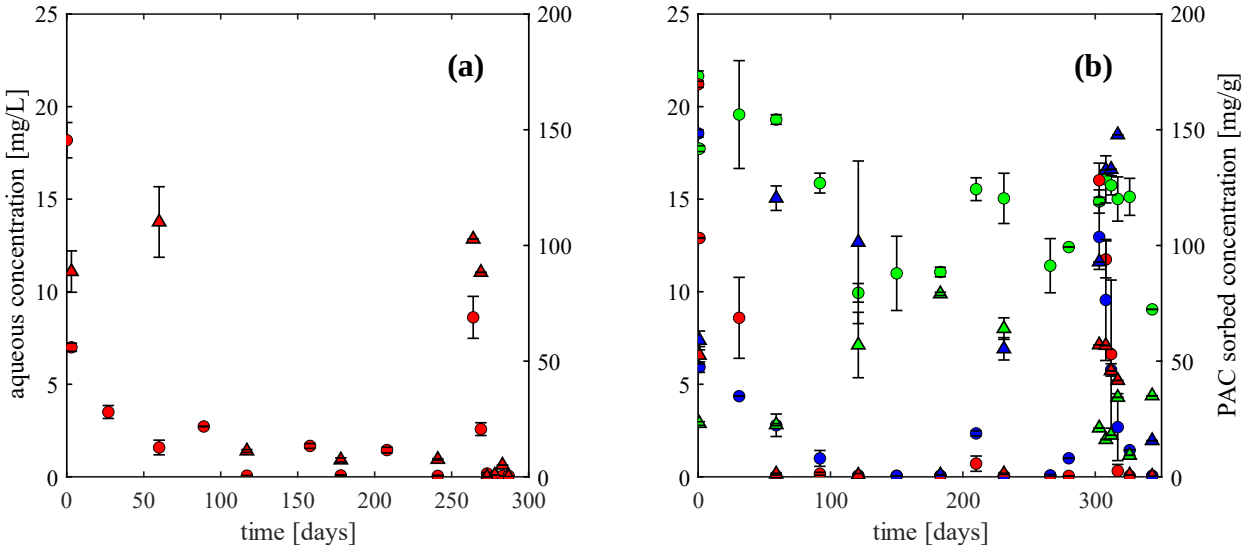

Figure 3.10 Active bioaugmented powdered activated carbon (A-BA-PAC) microcosm data: (a) aqueous (●) and sorbed (▲) toluene concentrations from the single compound system, and (b) aqueous/PAC sorbed benzene (● /▲), toluene (● /▲), and *o*-xylene (● /▲) concentrations from the multi-compound system. Error bars represent ± one standard deviation.

There is initial sorption of toluene which causes a drop in initial aqueous phase concentration. Initial degradation appears slower in single compound A-BA-PAC microcosms than in the single compound A-BA microcosms, as toluene concentrations were higher at Day 60 (2.72 mg/L vs 0.27 mg/L), the last measurement before the second re-spike (Day 73). Degradation rates increased, with concentrations depleted (Day 278) 15 days after the last re-spike (Day 263).

Initial PHC compound sorption to PAC also occurs in the multi-compound experiments and follows the order predicted based on sorption affinity ([X] > [T] > [B]). After the initial spike, *o*-xylene degrades more slowly than toluene, with each being depleted by Day 59 and Day 150 respectively. The effect of competition is also observed in aqueous benzene concentrations, which follow drops in toluene/*o*-xylene aqueous concentrations since more sorption sites become available for benzene. By the last re-spike, toluene depletion is like the other bioaugmented microcosms, being depleted (Day 326) 23 days after the last re-spike (Day 303), and *o*-xylene was depleted (Day 343) 40 days after the last re-spike (Day 303), faster than it did in any other microcosm series.

3.1.3 Model Application

Initial investigations used the data sets from the SiREM DGG-B culture vessels, and lessons learned and methodology from these results were carried forward for analysis of the microcosm experiments. In all cases, uncertainty analyses were used to calibrate Monod kinetics, and sensitivity analyses were completed on specific data sets to identify impactful sorption and kinetic parameters.

3.1.3.1 SiREM Culture Vessel Simulations

Simulation of the SiREM DGG-B culture vessels was completed to explore the limits of the calibration of Monod kinetic parameters using the batch reactor model. Calibration parameters were initially μ_{max}, K_d, K_S, Y, and X_0 for benzene degraders, and then the decision space was narrowed to only μ_{max} and K_S. μ_{max} is of special interest as it is a direct indicator of culture performance and is related to the maximum rate of substrate utilization (k_{max}) through Equation (3.21), which also includes the yield coefficient (Y). Cultures with high μ_{max} are more favourable because they have a higher k_{max}. K_S is difficult to predict, and estimates vary widely depending on the characteristics of the system (Rittmann & McCarty, 2018). At substrate concentrations much greater than K_S, the culture displays predominantly zero-order degradation, while at concentrations much less than K_S it displays predominantly first-order degradation. While no conclusions can be directly drawn from a calibrated K_S value alone, low relative K_S values are considered beneficial due to less dependance on substrate concentration and faster rates of substrate degradation. A sensitivity analysis (Section 3.1.5.2) was conducted on the fixed kinetic parameters (K_d, Y, and X_0).

3.1.3.2 Microcosm Simulations

Simulation of the microcosms was completed to investigate the representativeness of sorption isotherms and highlight differences in Monod kinetic parameters between PHCs and across microcosm series. The calibration of kinetic parameters was completed for the bioaugmented microcosms (BA, A-BA, and A-BA-PAC). Based on the results from the SiREM culture vessels (Section 3.1.3.1), three modelling parameters (X_0, Y, and K_d) were fixed and μ_{max} and K_S and were calibrated. Further investigation was completed by fixing K_S at 20 mg/L to facilitate comparison of μ_{max} alone. The calibration and parameter estimation methods are detailed in Section 3.1.5.1. Additionally, a sensitivity analysis (Section 3.1.5.2) was conducted on the fixed kinetic parameters (K_d, Y, and X_0) and sorption parameters (K_f, n_f, and a_i) for each PHC compound in the A-BA-PAC single and multi-compound models.

3.1.4 Parameterization

This section describes parameterization of initial conditions, the modelling domain, physico-chemical properties of the PHC compounds, sorption isotherms of the AC, and kinetic parameters of the bioaugmentation cultures.

3.1.4.1 Initial Conditions

Rather than assuming the initial spike of PHC mass was the actual spiked mass, the initial simulated PHC compound mass was calculated assuming the first observed aqueous concentration (Day 0, unique for each data set) was in equilibrium with all phases. This strategy was implemented due to variations in initial aqueous phase concentration between different batch reactor data sets. All subsequent mass re-spikes were assumed to be the actual mass spike and allowed to partition between all phases under equilibrium conditions since no corresponding observed aqueous concentrations were available. Initial biomass concentration (X_0, mg/L) estimates were provided by Courtney Toth at the University of Toronto (Table 3.1) and were based on quantitative polymerase chain reaction (qPCR) and relative abundance measurements taken of the cultures used in bioaugmentation experiments (DGG-B, DGG-T, and DGG-X for benzene, toluene, and *o*-xylene respectively). qPCR analyzes deoxyribonucleic acid (DNA) in an aqueous sample to provide estimates in copies/mL for total bacteria and archaea present. Relative abundances are used to estimate the percentage of total bacteria or archaea represented by known benzene, toluene, and *o*-xylene degraders in each culture. Multiplying qPCR and relative abundance measurements provides a copies/mL estimate for known PHC degraders in each culture. Methods for quantifying the volume occupied by a dry cell can then be used to develop biomass estimates in mg/L (Luo et al., 2016).

Table 3.1 Biomass concentration estimates from relative abundance and qPCR measurements for DGG-B, DGG-T, and DGG-X cultures.

	Estimated Biomass Concentration (mg/L)		
	Low	High	Mean
DGG-B	1.94	2.56	2.25
DGG-T	70.0	99.5	49.7
DGG-X	25.8	58.1	41.9

Fixed X_0 values used in simulations are the mean values for each culture. In the bioaugmented microcosms, 1 mL of the concentrated culture was assumed to be injected into the microcosm at Day 0 and diluted in the aqueous phase.

3.1.4.2 Domain Parameters

The physical domain of the batch reactor model is described by aqueous and headspace volumes, $\forall_w$ and $\forall_g$ (L), a mass of aquifer solids, m_{aq} (g), a fraction of organic carbon in the aquifer solids, f_{oc} (g g^{-1}), and a mass of PAC, m_{PAC} (g). The aqueous volume can be altered, as either a dilution (loss in aqueous mass, no change in aqueous volume) or a volume change (loss in aqueous mass resulting from a reduction in aqueous volume, or no change in aqueous mass resulting from an increase in aqueous volume) at a specified time. Aquifer solids used in the experiments were obtained from the University of Waterloo Groundwater Research Facility at the Canadian Forces Base in Borden, ON, Canada and assumed to have an organic carbon fraction (f_{oc}) of ~0.024% (Xu & Thomson, 2008).

The time domain in the batch reactor model is described by a total simulation time and minimum and maximum timesteps (days). The model initializes at the minimum timestep and increases by a specified factor at every timestep until it reaches the maximum timestep; this adaptive timestepping saves computational effort. The timestep size reverts to the minimum timestep immediately before significant changes in system mass (i.e., mass spikes and aqueous volume changes). All batch reactor models used minimum and maximum timesteps of 0.01 and 0.25 days respectively, and a timestep factor of 1.01 was implemented based on preliminary simulations.

3.1.4.3 Physico-Chemical Properties

The PHC compounds simulated include benzene, toluene, and *o*-xylene. Spikes of a PHC compound mass into a batch reactor were represented as instantaneous mass addition at specified times. Each PHC compound is defined by a series of physical constants, including Henry's Law coefficients, H_{cc} [-], octanol-water partition coefficients, $logK_{ow}$ (log(L/kg)), and linear partition coefficients, K_p (L/kg).

Table 3.2 Additional physical constants for modelling BTX partitioning.

Compound	H_{cc}[a] [-]	$logK_{ow}$[b] log(L/kg)	K_p[c] (L/kg)
Benzene	0.225	2.13	2.00×10^{-2}
Toluene	0.274	2.75	8.32×10^{-2}
o-Xylene	0.221	3.13	2.00×10^{-1}

[a]Converted from H_{pc} values (Heath et al., 1993)
[b] Retrieved from Appendix K of the USEPA Superfund Soil Screening Guidance document (USEPA, 1996)
[c]Calculated using Equations (3.7) and (3.8)

3.1.4.4 Sorption Isotherms

A series of single and multi-compound isotherm experiments were carried out using a coconut-based PAC from Calgon Carbon (WPC®, < 325 US mesh) and BTX (experimental results can be found in Marrocco (2022)). Analysis of the isotherm experiments provided estimates of single compound Freundlich sorption parameters for benzene, toluene and *o*-xylene, and multi-compound competition coefficients for a BTX mixture (Table 3.3).

Table 3.3 Freundlich sorption parameters and multi-compound competition coefficients for BTX on Calgon WPC® powdered activated carbon (±95% CI) adapted from Marrocco (2022).

Compound	K_f ($mg^{1-nf}\ L^{nf}\ g^{-1}$)	n_f [-]	a [-]
Benzene	36.1 ± 3.77	0.484 ± 0.045	1.416 ± 0.383
Toluene	88.2 ± 7.70	0.421 ± 0.044	1.432 ± 0.158
o-Xylene	131 ± 20.0	0.371 ± 0.099	1.080 ± 0.078

To understand desorption hysteresis, each reactor was subjected to one desorption step where most of the aqueous phase was decanted and was replaced with AGW. Sorbed concentrations in both the adsorption and desorption experiments were measured through solid phase extraction. Single compound adsorption and desorption data are displayed in Figure 3.11.

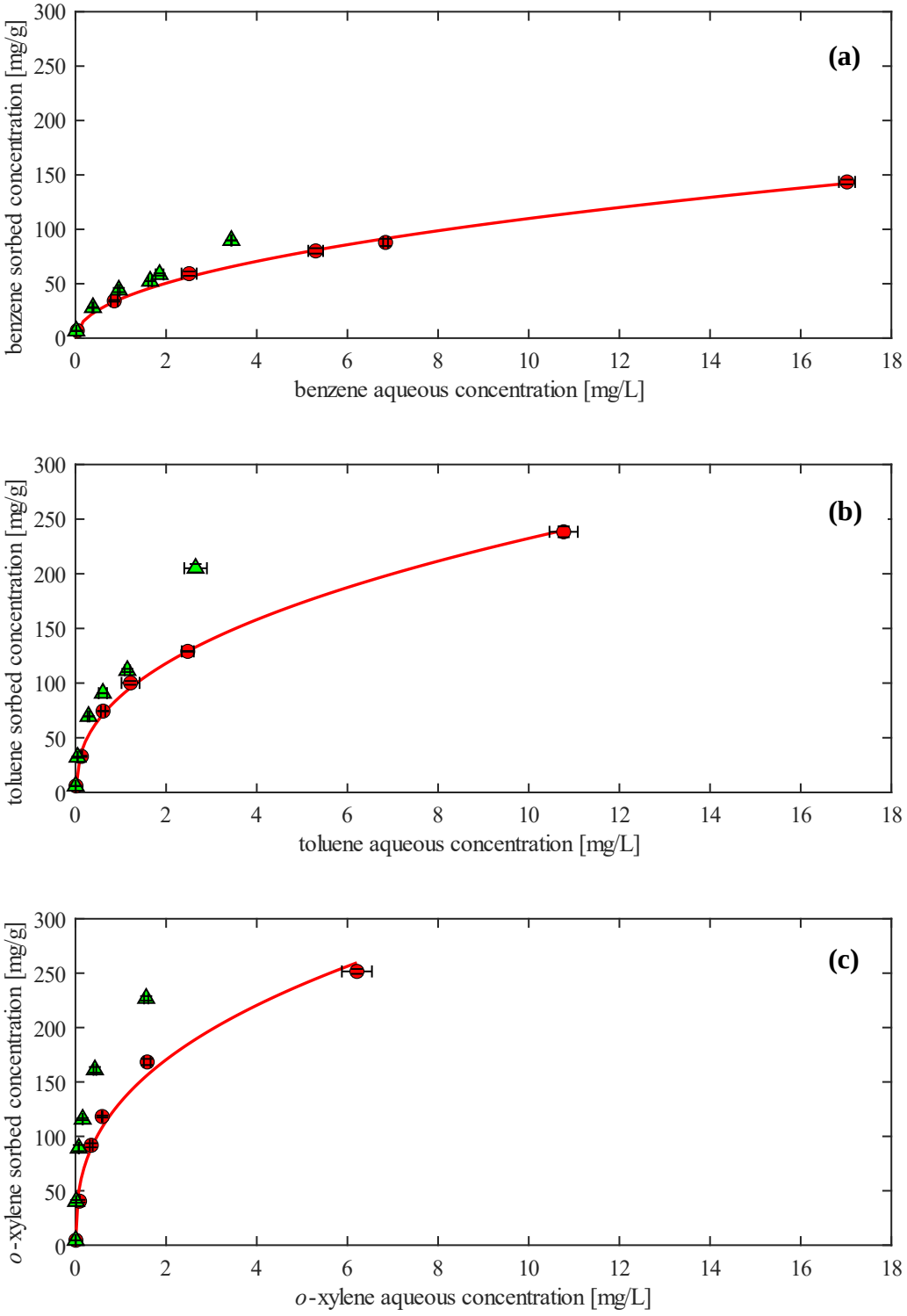

Figure 3.11 Sorption data for BTX on WPC powdered activated carbon: adsorption (●) and desorption (▲) data and adsorption isotherms (—) for (a) benzene, (b) toluene, and (c) *o*-xylene from Marrocco (2022). Error bars represent ± one standard deviation.

Observations suggest that there is some degree of desorption hysteresis, with desorption data lying above the adsorption isotherm. To investigate further an additional set of reactors were developed for a toluene/PAC system and AGW, like the previous single compound experiment but with seven desorption steps. The results of this experiment indicate that there is no irreversible hysteresis and potentially a slight degree of reversible hysteresis. See Appendix A for a description of the experimental method and the associated data.

The multi-compound isotherm experimental results (Marrocco, 2022) are displayed in Figure 3.12, along with concentrations estimated by the ISIAS equations and fitted competition coefficients (a_i) for BTX.

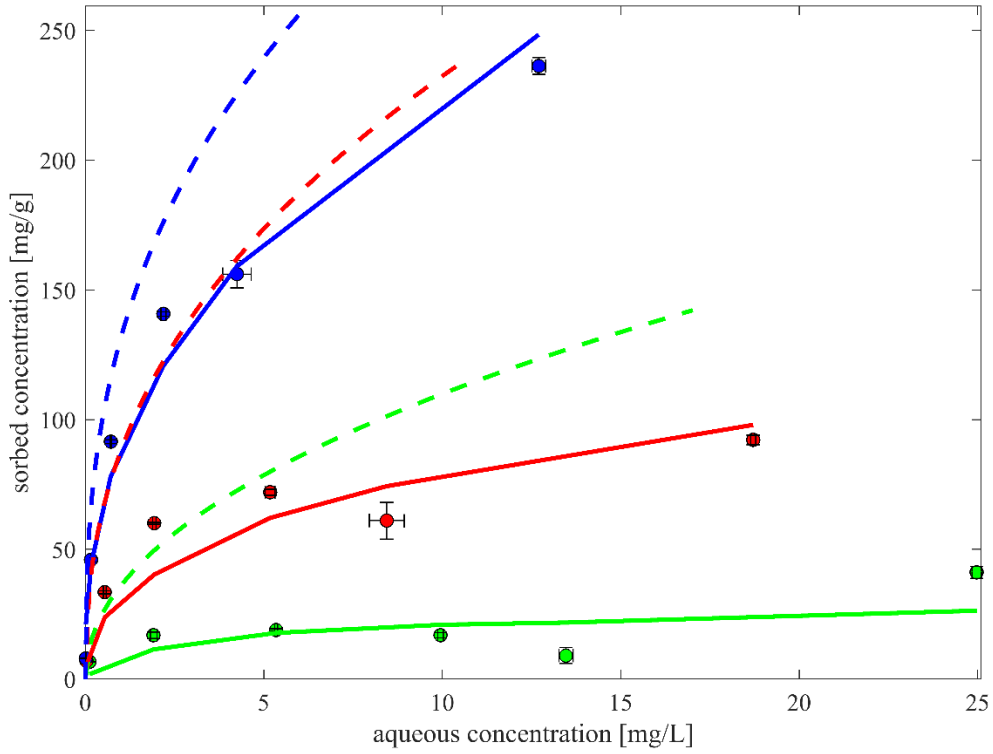

Figure 3.12 Multi-compound sorption data for BTX on WPC powdered activated carbon: adsorption data for benzene (●), toluene (●) and *o*-xylene (●). Also shown are single compound adsorption isotherms using single compound Freundlich parameters in Table 3.3 (— —) and the multi-compound sorbed concentrations predicted using the single compound Freundlich parameters in conjunction with competition coefficients (Table 3.3) and Equation (3.16) (—). Error bars represent ± one standard deviation. Data from Marrocco (2022).

Toluene isotherm parameters (K_f and n_f) from the original single compound experiment were selected for single compound microcosm experiments. Sorption parameters for benzene, toluene, and *o*-xylene from the single compound experiment and multi-compound competition factors were selected for muti-compound microcosms.

3.1.4.5 Kinetic Parameters

A set of kinetic parameters is defined for each simulated PHC compound to represent the chief population degrading that specific compound (i.e., separate kinetics for benzene, toluene, and *o*-xylene degraders). These parameters included the yield coefficient, Y (g/g), the endogenous decay coefficient, K_d (/d), maximum specific growth rate, μ_{max} (/d), and the half-velocity constant, K_S (mg/L). Y has been estimated in past work for the three cultures (E. Edwards & Grbić-Galić, 1994; Ulrich & Edwards, 2003). K_d is slightly more difficult to estimate and is often excluded from Monod kinetics modelling work. Usually, a single re-spike and degradation cycle is observed in a given batch experiment, so endogenous decay is assumed negligible. Estimates of K_d for slow-growing cultures (like sulfate-reducing and methanogenic cultures) are usually < 0.05 /d (Rittmann & McCarty, 2018), and additional efforts to estimate K_d for BTEX compounds have determined a value of ~0.01 /d (Schirmer et al., 1998). A summary of fixed parameter values as well as calibration parameters and their bounds are provided in Table 3.4 and Table 3.5.

Table 3.4 Parameter estimates for Monod kinetics parameters.

Parameter	Units	Benzene	Toluene	*o*-Xylene
Yield (Y)	g/g	0.12[a]	0.12[b]	0.12[b]
Endogenous Decay (K_d)[c]	1/d	0.01	0.01	0.01

[a]Ulrich & Edwards, 2003
[b]Edwards & Grbić-Galić, 1994
[c]Schirmer, 1998

Table 3.5 Bounds for selected Monod kinetics calibration parameters.

Parameter	Units	Low	High
Maximum Specific Growth Rate (μ_{max})	1/d	0.001	0.6[a]
Half-velocity Constant (K_S)	mg/L	0.001	200[c]

[a]Farhadian, 2008
[b]Non-zero to prevent numerical issues when substrate concentration is zero
[c]While no upper limit for K_S could be found, a reasonable value based on the literature was selected to restrict the decision space

3.1.5 Calibration, Uncertainty, and Sensitivity

3.1.5.1 Calibration and Uncertainty

For calibration, the batch model was linked to an optimization package (OSTRICH). OSTRICH allows the configuration of model executables, input files, and output files with various pre-programmed optimization algorithms (Matott, 2017) and simplifies the calculation and output of statistics. Global (as opposed to local) algorithms benefit from being able to search a large decision space and avoid becoming trapped in local maxima or minima but require an analysis of uncertainty to determine statistics on the parameters. A global optimization algorithm, Dynamically Dimensioned Search (DDS) (Tolson & Shoemaker, 2007), was used in this work in conjunction with the root-mean-square error (RMSE) objective function as given by:

$$\mathrm{RMSE} = \sqrt{\frac{\sum_{i=1}^{N}(\hat{C}_i - C_i)^2}{N}} \tag{3.26}$$

where $i = 1 \ldots N$ is the total number of observations, $\hat{C}$ is the simulated value, and C is the observed value.

In cases where statistics on optimization parameters were investigated, a DDS analysis of uncertainty (DDS-AU) (Tolson & Shoemaker, 2008) was implemented by executing multiple optimization trials within the OSTRICH framework.

3.1.5.2 Sensitivity

Sensitivity analyses were conducted to investigate the impact of fixed parameters on μ_{max} and K_S, which included kinetic parameters (K_d, Y, and X_0), single compound sorption parameters (K_f and n_f) in single and multi-compound systems with PAC, and multi-compound competition coefficients (a_i) in multi-compound systems with PAC. This was accomplished by perturbing parameter values individually and running another DDS analysis of uncertainty to generate revised calibration parameters (μ_{max} and K_S). Perturbation values used were ±95% confidence intervals where applicable, which were the sorption parameters (K_f, n_f, and a_i). X_0 values were the mean of high and low estimates based on qPCR and relative abundance measurements of the cultures, so the high and low estimates were taken as the upper and lower bound of the sensitivity analysis. Y and K_d were estimated from literature, so they were perturbed by ±15%, approximately the perturbation of X_0. A summary of values used in the sensitivity analysis are provided in Table 3.6.

Table 3.6 Upper, mean, and lower bounds for perturbation of parameters used in the sensitivity analyses.

Compound	Parameter	Units	Lower Bound	Mean	Upper Bound	Perturbation (%)
Benzene	X_0	mg/L	1.94	2.25	2.56	13.8
	Y	mg/mg	0.102	0.120	0.138	15.0
	K_d	1/d	0.0085	0.0100	0.0115	15.0
	K_f	$mg^{1-nf}\ L^{nf}\ g^{-1}$	32.3	36.1	39.9	10.4
	n_f	[-]	0.439	0.484	0.528	9.10
	a_i	[-]	1.03	1.42	1.80	27.0
Toluene	X_0	mg/L	0.168	0.284	0.400	40.8
	Y	mg/mg	0.102	0.120	0.138	15.0
	K_d	1/d	0.0085	0.0100	0.0115	15.0
	K_f	$mg^{1-nf}\ L^{nf}\ g^{-1}$	80.5	88.2	95.9	8.70
	n_f	[-]	0.377	0.421	0.465	10.5
	a_i	[-]	1.27	1.43	1.59	11.0
o-Xylene	X_0	mg/L	0.147	0.240	0.332	38.3
	Y	mg/mg	0.102	0.120	0.138	15.0
	K_d	1/d	0.0085	0.0100	0.0115	15.0
	K_f	$mg^{1-nf}\ L^{nf}\ g^{-1}$	112	132	152	15.2
	n_f	[-]	0.272	0.371	0.470	26.7
	a_i	[-]	1.00	1.08	1.16	7.20

3.2 One-Dimensional Model

This section describes the governing equations, data sets, application, and parameterization used for the 1D model. Numerical methods and assumptions are detailed, including boundary conditions, space and time discretization, and spatial/temporal weighting schemes. Data sets used for model validation are discussed, followed by the rationale for a series of investigative scenarios which represent a PAC treatment zone.

3.2.1 One-Dimensional Model Development

A 1D model was developed to simulate an experimental column (Figure 3.13) mimicking an *in situ* AC particulate amendment.

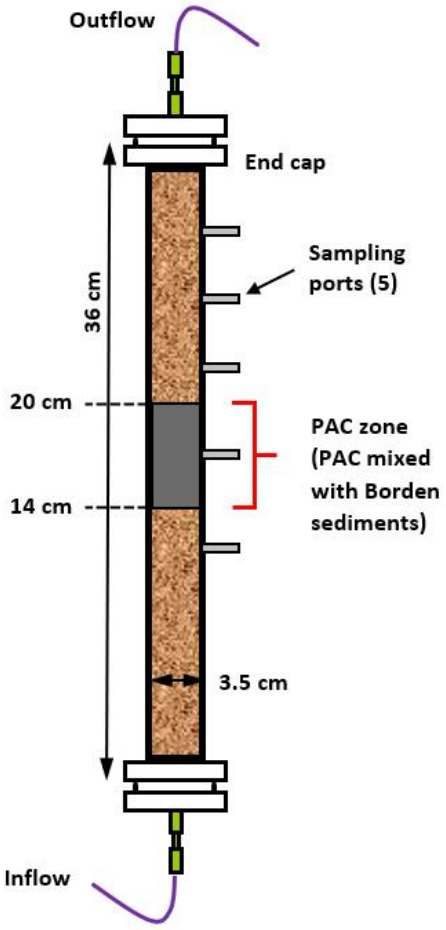

Figure 3.13 Example schematic of a column operating in upflow mode consisting of two Borden sand zones (0-14 and 20-36 cm from bottom) and a Borden sand/PAC zone (14-20 cm from bottom) (Marrocco, 2022).

The 1D model includes aqueous and sorbed phases, and the following general assumptions were adopted:

1. Column system is fully saturated,
2. Flow is steady-state and isotropic (obeys Darcy's Law),
3. Mass partitioning between phases is instantaneous,
4. Column is under constant pressure and temperature,
5. Sorption to aquifer solids is linear, non-hysteretic, and non-competitive,
6. Sorption to PAC is non-linear, hysteretic and competitive, and
7. Biomass is immobile and degrades aqueous mass according to Monod kinetics.

In a fully saturated domain, transport with aqueous phase biodegradation following Monod kinetics is governed by the ADRE given by

$$R_i \frac{\partial C_{w,i}}{\partial t} = D_i \frac{\partial^2 C_{w,i}}{\partial x^2} - v \frac{\partial C_{w,i}}{\partial x} - k_{max,i} X_i \left(\frac{C_{w,i}}{K_{s,i} + C_{w,i}} \right) \tag{3.27a}$$

with

$$R_i = 1 + \frac{\rho_b}{\phi} \frac{\partial C_{s,i}}{\partial C_{w,i}} \tag{3.27b}$$

$$\frac{\partial C_{s,i}}{\partial C_{w,i}} = f_{PAC} \frac{\partial C_{s,i}^{PAC}}{\partial C_{w,i}} + (1 - f_{PAC}) K_{p,i} \tag{3.27c}$$

$$D_i = \alpha_l |q| + \phi \tau_w D_{w,i} \tag{3.27d}$$

$$\tau_w = \frac{(\phi)^{10/3}}{\phi^2} \tag{3.27e}$$

where R_i is the retardation factor for compound i [-], $C_{w,i}$ is the aqueous concentration of i (M_i L^{-3}), t is time (T), D_i is the hydrodynamic dispersion coefficient of i (L^2 T^{-1}), x is the spatial coordinate direction (L), v is the seepage velocity (L T^{-1}), $k_{max,i}$ is the maximum rate of substrate utilization (M_i $M_{biomass}^{-1}$ T^{-1}) using Equation (3.21), X_i is biomass concentration ($M_{biomass}$ L^{-3}) using Equation (3.20), $K_{s,i}$ is the half-velocity constant (M_i L^{-3}), ρ_b is the solids bulk density (M_{solids} L^{-3}), ϕ is the effective porosity [-], $C_{s,i}$ is the total sorbed concentration of i (M_i M_{solids}^{-1}), f_{PAC} is the fraction of PAC [-], $C_{s,i}^{PAC}$ is the sorbed concentration of i on PAC ($M_{substrate}$ M_{PAC}^{-1}) for non-linear (Equation (3.9)), hysteretic (Equations (3.10) to (3.13)), or competitive systems (Equations (3.16) to (3.18)), $K_{p,i}$ is the linear partitioning coefficient of i (L^3 M_{aq}) using Equations (3.7) and (3.8), q is the Darcy velocity (L T^{-1}), α_l is the dispersivity (L), τ_w is a tortuosity factor [-] (Millington, 1959), and $D_{w,i}$ is the free solution diffusion coefficient for i (L^2 T^{-1}). Like the batch reactor model, all Monod kinetic parameters are unique for each PHC compound and independent of other PHCs.

In Equation (3.27a), aqueous mass lost to biodegradation is represented by:

$$-k_{max} X \left(\frac{C_w}{K_s + C_w} \right) \tag{3.28}$$

In many groundwater transport models, it is assumed that $C_w << K_s$ and that biomass is constant, simplifying the biodegradation term to:

$$-k_{max} \frac{X}{K_S} C_w = -k_{bio} C_w \tag{3.29}$$

where k_{bio} is the simplified first-order biodegradation rate coefficient (T^{-1}). Due to fluctuating biomass concentrations and C_w values near or above K_s these assumptions do not hold for the systems of interest in this research, so the complete version of Monod kinetics is used in the developed model. Biomass is assumed to be stationary and degrading aqueous phase mass, therefore biomass concentrations (X in Equation (3.27a)) are tracked separately using Equation (3.20).

Equation (3.27a) is non-linear in C_w and coupled across PHC compounds when competition is considered (through Equations (3.16) to (3.18)) and coupled with the biomass mass balance described by Equation (3.20) through X. The finite volume method was used in conjunction with a Crank-Nicholson temporal weighting scheme (Crank & Nicolson, 1947), and the subsequent system of non-linear equations was solved using Picard iteration (Lindelöf, 1894; Picard, 1890) until both aqueous PHC and biomass concentrations converged to a specified tolerance. An arbitrary convergence tolerance of 10^{-10} was selected; the largest change in aqueous and biomass concentrations across all control volumes in the domain from the previous to the current iteration must be $< 10^{-10}$ (M L^{-3}) in order to advance to the next time step. To ensure solution monotonicity and avoid numerical issues, Peclet and Courant conditions are defined to guide selection of both the number of control volumes and the length of timesteps. A constant time step increment was implemented in the 1D model.

The Peclet number is the ratio of advective transport to dispersive transport, with the grid Peclet number defined as

$$Pe_{CV} = \frac{v\Delta x}{D} \geq 2 \tag{3.30}$$

with

$$\Delta \mathrm{x} = \frac{\mathrm{L}}{\mathrm{nCVs}} \tag{3.31}$$

where Pe_{CV} is the grid Peclet number [-], Δx is the spatial increment (L), L is the length of the domain (L), and $nCVs$ is the number of control volumes [-]. Using the $nCVs$ satisfying Equation (3.31), the timestep increment can be calculated by satisfying the Courant condition

$$Cr = \frac{v\Delta t}{\Delta x} = \frac{(nCVs)v\Delta t}{L} < 1 \tag{3.32}$$

where Δt is the timestep increment (T).

The exit boundary condition was assumed to be Type 2 (Cauchy) while the influent boundary condition can be specified as either Type 1 (Dirichlet) or Type 3 (Robin).

In a single compound system, the derivative of C_s^{PAC} with respect to C_w in Equation (3.27c) can be determined analytically as the derivative of the Freundlich isotherm (Equation (3.9)) given by:

$$\frac{\partial C_s^{PAC}}{\partial C_w} = nK_f {C_w}^{n_f-1} \tag{3.33}$$

However, when competitive sorption is considerd, C_s^{PAC} is a function of all PHC compound concentrations according to the ISIAS Equation (3.16), and in a hysteretic system, C_s^{PAC} is a function of individual PHC compound concentrations (Equations (3.10), (3.12), and (3.13)). In this case, this derivative is approximated using a central finite difference approach:

$$\left.\frac{\partial C_s^{PAC}}{\partial C_w}\right|_{C_w} = \frac{C_s^{PAC}(C_w + \Delta C_w) - C_s^{PAC}(C_w - \Delta C_w)}{2\Delta C_w} \tag{3.34}$$

where $C_s^{PAC}(C_w \pm \Delta C_w)$ is the is the sorbed PAC concentration evaluated at ($C_w \pm \Delta C_w$) for non-linear (Equation (3.9)), hysteretic (Equations (3.10) to (3.13)), or competitive systems (Equations (3.16) to (3.18)) and ΔC_w is an arbitrary finite difference that must be sufficiently small to reflect the local slope, but large enough to provide a numerical estimate (2% of C_w assumed).

Validation of the model to reflect advective-dispersive transport was completed by comparing simulation results with the Ogata-Banks solution (Ogata & Banks, 1961). Verification of the sorption components of the model were completed by comparing the steady-state mass predicted using Equations (3.1) to (3.6) and the mass in each of the compartments.

3.2.2 Data Sets

To investigate adsorption and desorption of a single compound (toluene), influent and effluent data collected from a column (12 cm long, 1.5 cm internal diameter) experiment with the central zone (5.5 to 6.5 cm) packed with a mixture of BS and 0.013% PAC was used. The column was packed with BS above and below the PAC zone. An AGW solution with a target toluene concentration of 8.5 mg/L was injected continuously for 24 hours to observe adsorption and then was switched to AGW for the next 32 hours to observe desorption.

The influent aqueous toluene concentration was initially lower than the target of 8.5 mg/L (Figure 3.14a) but eventually reached 7.9 mg/L after 120 minutes and fluctuated between 7.9 and 8.3 mg/L (last sample taken at 360 minutes). When the influent was switched to only AGW at 1,440 minutes (24 hours), the influent concentration was 2.63 mg/L, and steadily decreased until 1,800 minutes. Surprisingly, influent toluene concentrations fluctuated between 0.09 and 0.19 mg/L between 3,240 and 3,600 minutes more than 24 hours after the influent was switched to only AGW. While stainless

steel lines and sampling ports were used to avoid toluene adsorption it is possible there was residual toluene present in the column system.

Effluent breakthrough started at 136 minutes and rose steadily until 378 minutes but did not reach the injection concentration of 8.5 mg/L at this time (Figure 3.14b). Effluent toluene concentrations fluctuated between 8.24 and 8.42 mg/L from 1,456 to 1,544 minutes, confirming complete breakthrough of the injection solution. Effluent concentrations dropped steadily from 8.24 to 1.36 mg/L from 1,544 to 1,816 minutes as the toluene solution was flushed from the column. Toluene concentrations were still decreasing slowly from 0.35 mg/L at 2,896 minutes to 0.16 mg/L at 3,256 minutes at the end of the experiment. An extended falling limb during desorption was expected to occur, but effluent concentrations < MDL were anticipated. Higher aqueous concentrations near the end of the experiment could possibly be due to the non-zero influent concentrations observed after switching to clean AGW.

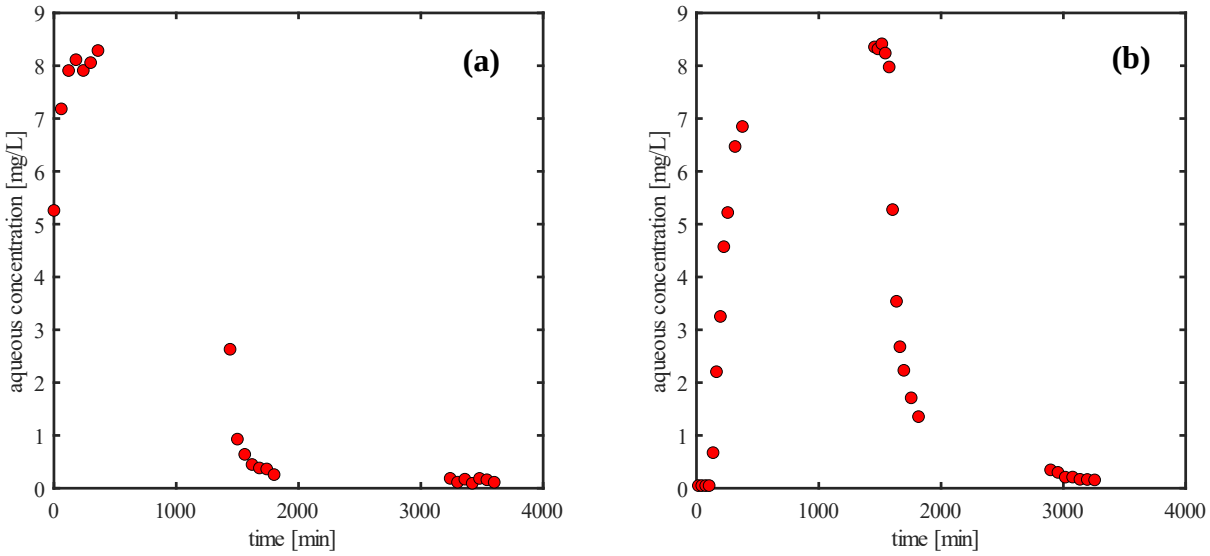

Figure 3.14 (a) Influent and (b) effluent aqueous toluene concentrations from an adsorption/desorption experiment. Each data point (●) is a single aqueous phase toluene measurement.

In addition, a conservative tracer test was conducted using a continuous injection of a 754 mg Br^-/L sodium bromide (NaBr) solution. The data, consisting of 16 effluent bromide concentrations (Figure 3.15), was used to estimate relevant transport parameters (effective porosity and dispersivity) for the 12-cm long column. The 1D model was linked to an optimization package (OSTRICH, described in Section 3.1.5.1), and DDS was used to minimize the RMSE (Equation (3.26)) between simulated and observed bromide effluent concentrations to obtain parameter estimates.

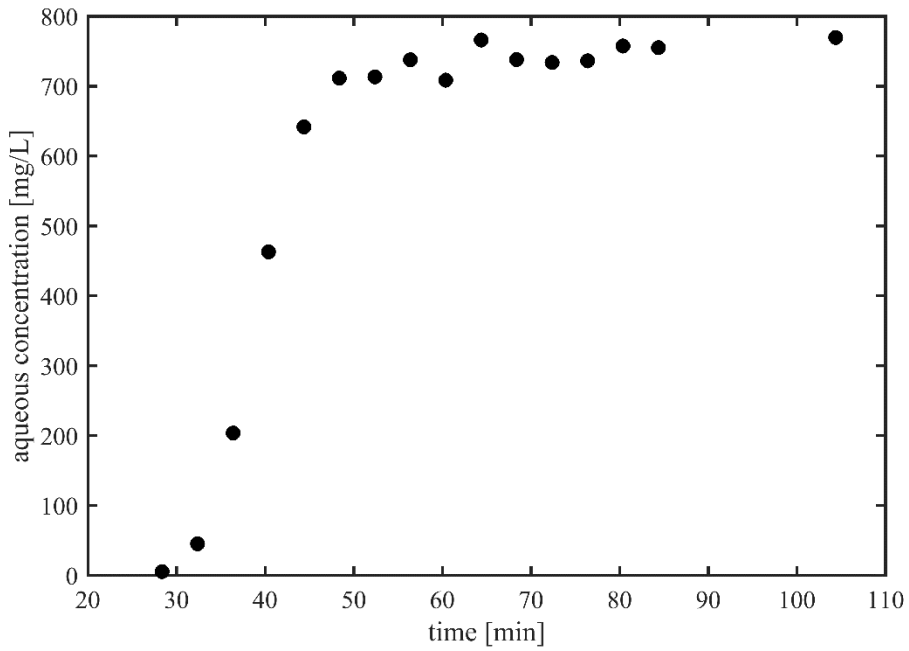

Figure 3.15 12-cm long column tracer test data: column effluent aqueous bromide concentrations. Each data point (●) represents a single aqueous phase bromide measurement.

3.2.3 Model Application

Simulations were completed for the tracer test and toluene adsorption/desorption experiment which permitted validation of the advective and dispersive components of the model and an assessment of desorption hysteresis on toluene transport in a single compound system. Biokinetic parameters obtained in the microcosm simulations (Section 3.1.3.2) were then used in a series of investigative scenarios mimicking an *in situ* AC particulate amendment and a multi-compound PHC plume (consisting of BTX). The scenarios highlight the effects of different hydraulic and contaminant loadings, as well as various biodegradation rates. All investigative scenarios simulated a hypothetical 37-cm long column with and without a central BS+PAC zone subjected to an influent consisting of multiple PHC compounds (BTX). The following five scenarios were simulated:

1. No biodegradation,
2. Biodegradation with kinetic parameters obtained from the batch reactor simulations,
3. A 50% reduction in influent BTX concentrations at 20% of the total simulation time,
4. A 50% reduction in flow rate, and
5. Biomass growth rates were assumed to be proportional to the biomass concentration.

Scenario 1 was used to investigate the characteristics of BTX breakthrough in a column with and without a PAC zone, and no biodegradation. Scenario 2 represents BTX breakthrough and long-term performance in a bioaugmented column with and without a PAC zone and serves as a base case which is modified in Scenarios 3 to 5. Scenario 3 investigates the impact that a change in BTX source strength has on the biological characteristics within the PAC zone, while Scenario 4 represents a similar case where mass loading is reduced through a reduction in flow and a concomitant increase in residence time. Scenario 5 represents a situation with improved kinetics due to biofilm growth, which can increase nutrient exchange and improves resistance against predation (Kjellerup & Edwards, 2013). The arbitrary relationship used in this scenario is described by:

$$\mu^{*}_{max,i} = \begin{cases} 0.6 & \mu_{max,i} > 0.6 \\ X_i \mu_{max,i} & if \quad 0.6 > X_i \mu_{max,i} > \mu_{max,i} \\ \mu_{max,i} & \mu_{max,i} > X \mu_{max,i} \end{cases} \tag{3.35}$$

where $\mu^{*}_{max,i}$ is the new maximum specific growth rate for PHC *i* in the PAC zone (/d), X_i is the biomass concentration for PHC *i* (mg/L), and $\mu_{max,i}$ is the original maximum specific growth rate for PHC *i* in the PAC zone. The maximum and minimum $\mu^{*}_{max,i}$ are 0.6 and $\mu_{max,i}$ respectively. The upper bound is defined by the value used for microcosm calibration (Table 3.5) to avoid exponentially increasing maximum specific growth rates and uncontrolled biomass growth, while the lower bound is defined as the maximum specific growth rate specified to avoid rapid biomass decay (where growth is overcome by endogenous decay). All kinetic parameters used other than $\mu_{max,i}$ were the same as in Scenario 2.

3.2.4 Parameterization

This section describes the parameterization of initial conditions, the modelling domain, physico-chemical properties of the tracer and PHC compounds, sorption isotherms for AC, and kinetic parameters of the bioaugmentation cultures.

3.2.4.1 Initial and Boundary Conditions

The influent and effluent boundary conditions for all simulations were Type 3 (Robin) and Type 2 (Cauchy) respectively. For the tracer simulation, the influent aqueous concentration was assumed to be the average of triplicate measurements (754 mg/L). For the adsorption/desorption experiment, influent toluene concentrations were measured over the duration of the experiment and therefore the toluene concentration at the inlet was assumed to follow a step loading function (Figure 3.16).

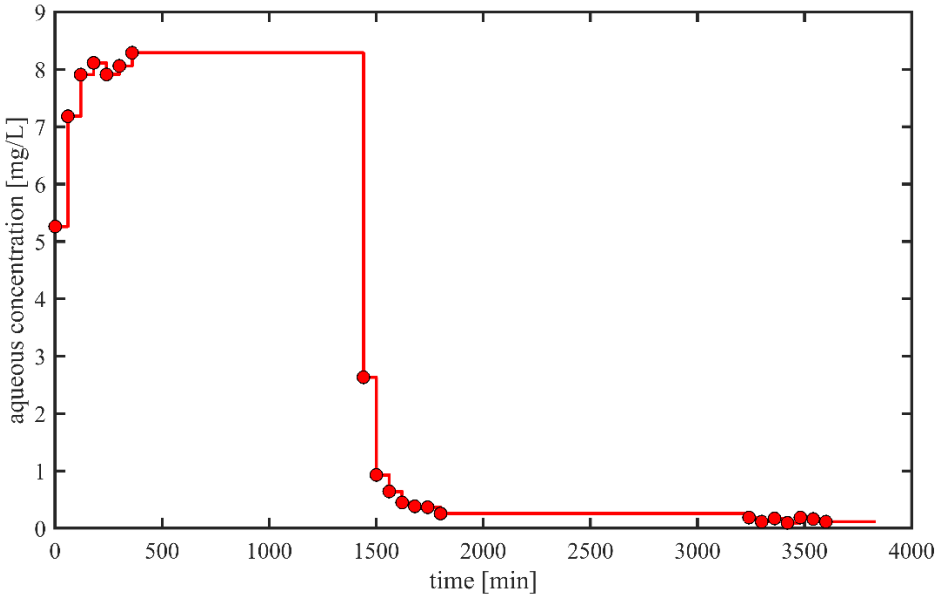

Figure 3.16 12 cm column adsorption/desorption observed (●) and simulated (—) influent aqueous toluene concentrations. Each data point represents a single aqueous phase toluene measurement.

Investigative scenarios using a hypothetical 37-cm long column had an influent solution consisting of multiple compounds (BTX) with a constant aqueous influent concentration of 20 mg/L for each compound unless specified otherwise. The initial biomass concentrations in the treatment zone (central 6 cm) were assumed to be 6.66 mL each of DGG-B, DGG-T, and DGG-X (2.25, 49.7, and 41.9 mg/L for benzene, toluene, and *o*-xylene respectively) and evenly distributed in the pore space.

3.2.4.2 Domain Parameters

The physical domain of the column model is described by its length, L (m), and diameter, D (m), with the area perpendicular to flow assumed circular. The area of the column is only used for mass balance calculations. The column was segmented into a specified number of control volumes, *nCVs* [-] according to the Peclet condition specified in Equation (3.30), and was further subdivided into zones, each with unique lengths, L (m), fractions of PAC, f_{PAC} (g g^{-1}), fractions of organic carbon in the aquifer solids, f_{oc} (g g^{-1}), and bulk density, ρ_b (kg m^{-3}). The length of column used in the 1D simulations were 12 cm (tracer and adsorption/desorption experiment) and 37 cm (investigative scenarios), with internal diameters of 1.5 cm and 3.75 cm respectively. The fraction of PAC (f_{PAC}) used in simulations was 0.013% in the central 1 cm for the 12-cm long glass column, and 0.02% in the central 6 cm for the 37-cm long column. The BS was assumed to be the same as the BS used in the microcosms, so a fraction of organic carbon (f_{oc}) of ~0.024% and an aquifer solids bulk density (ρ_b) of 1,650 kg/m^3 were used.

Flow and transport properties included Darcy flux, q (m/s), effective porosity, ϕ [-], and dispersivity, α_L (m). Darcy flux, q (m/s) was determined for the 12 cm column by measuring the flow rate, Q ($m^3\ s^{-1}$) and dividing by the circular cross-sectional area, A (m^2). Darcy fluxes were 1.77×10^{-5} m/s and 9.04×10^{-6} m/s for the tracer test and adsorption/desorption experiment respectively. In the investigative scenarios, Darcy flux was set to 3.47×10^{-7} m/s. ϕ and α_L were determined experimentally for the 12-cm long column using the tracer test data (Section 3.2.2), and were assumed to be 0.3 [-] and 5.0×10^{-3} m respectively for the 37-cm long column investigative scenarios.

The simulation times for the 12-cm long column reflected the length of the tracer and adsorption/desorption experiments, while the simulation time for the investigative scenarios was set to 1.5×10^{8} seconds (1,736 days or 4.76 years). The timestep increment in all simulations was defined by the Courant condition specified by Equation (3.32).

3.2.4.3 Physico-Chemical Properties

The compounds simulated include PHCs (benzene, toluene, and *o*-xylene) and a conservative tracer (sodium bromide). Each PHC is defined by a series of physical constants including octanol-water partition coefficients, $logK_{ow}$ (log(L/kg)), and linear partition coefficients, K_p (L/kg) (provided in Section 3.1.4.3). Free solution diffusion coefficients (D_w) were 2.0×10^{-9}, 9.8×10^{-10}, 8.6×10^{-10}, and 8.0×10^{-10} m^2/s for bromide, benzene, toluene, and *o*-xylene respectively (Farhat et al., 2012). Sorption isotherms for the PHCs were discussed in Section 3.1.4.4. Reversible hysteresis parameters for toluene were developed by fitting Equations (3.10) to (3.12) to the experimental data (Figure 3.11b) (a = 0, b = 864, c = 1.11 in Equation (3.10)). Reversible and irreversible hysteresis parameters for benzene, toluene, and *o*-xylene can be found in Appendix A.

3.2.4.4 Kinetic Parameters

Kinetic parameters included yield coefficients, Y (g/g), endogenous decay coefficients, K_d (/d) (Table 3.4), maximum specific growth rates, μ_{max} (/d), and half-velocity constants, K_S (mg/L). Parameters (μ_{max} and K_S) for benzene were obtained from simulation of the SiREM DGG-B culture vessels, while parameters for toluene and *o*-xylene were obtained from simulation of the multi-compound active bioaugmented (A-BA) for the BS zones and multi-compound activated bioaugmented powdered activated carbon (A-BA-PAC) microcosms for the PAC zone.

Chapter 4
Results and Discussion

In this chapter, simulation results using the batch reactor and 1D models are presented and discussed. The batch reactor model was used to simulate microcosm experiments and the 1D model was used to simulate various synthetic column systems.

Initial batch reactor simulations of the SiREM DGG-B culture vessel data allowing for a range of Monod kinetics parameters to be calibrated are presented. Upon refining the number of calibration parameters, an uncertainty analysis was completed to identify candidate growth rates and half-velocity constants, and a sensitivity analysis was conducted to highlight impactful kinetic parameters. Investigations into the applicability of estimated isotherm parameters were completed using batch reactor simulations and solid phase concentration data from microcosms containing PAC. Strategies from the SiREM culture vessel simulations were adopted to investigate the effect of PAC in bioaugmented microcosms. These simulations included bioaugmented microcosms that contained no solids, BS, or BS and PAC for data sets containing either toluene-only (bioaugmented with DGG-T) or a mixture of BTX (bioaugmented with DGG-B, DGG-T, and DGG-X). The focus was to determine potential differences in growth rates and half-velocity constants between PAC and non-PAC systems. Sensitivity analyses were conducted to investigate fixed kinetic and sorption parameters.

The 1D model was used to investigate the behaviour of various scenarios representing a PAC treatment zone within an experimental column. The scenarios included no biodegradation, changes in mass loading, reduced flow conditions, and a hypothetical scenario where the biomass growth rate was assumed to be proportional to the biomass concentration in the system.

4.1 Batch Reactor Model

The batch reactor model was used to simulate both the SiREM culture vessels and microcosm experiments. Simulation of the SiREM DGG-B vessels was completed to investigate the capabilities and limitations of the biodegradation portion of the model, leading to the development of an uncertainty analysis strategy to quantify key kinetic parameters. Considering the detailed sorption characteristics of the PAC used in the microcosm experiments, and the negligible effect of indigenous microorganisms on methanogenic biodegradation, uncertainty analysis was applied to the bioaugmented microcosm data sets (toluene and BTX). This facilitated a comparison of kinetic parameters across data sets and permitted speculation on differences in biodegradation rates including

the effect of PAC. Sensitivity analysis of a selection of calibrated kinetic parameters was also completed.

4.1.1 SiREM Culture Vessels

Monod kinetics parameter estimation was completed using the SiREM DGG-B Large Vessel 1 (LV1) and DGG-B Large Vessel 2 (LV2) culture data sets. Optimization parameters and bounds [lower, upper] for these simulations were the initial biomass (X_0) [0, 15 mg/L], the maximum specific growth rate (μ_{max}) [0, 0.6 /d], the half-velocity constant (K_S) [0, 200 mg/L], the yield coefficient (Y) [0, 0.6 mg/mg], and the endogenous decay coefficient (K_d) [0, 0.09 /d]. The objective function used was the RMSE between observed and modelled substrate (benzene) concentrations. Three DDS trials of 1000 iterations, each with a unique seed, were completed for each data set. While all optimization trials obtained a similar RMSE and visually good fits to the observation data (Figure 4.1), there was significant variation in parameter values both across the three trials and within data sets (Table 4.1).

Table 4.1 Three calibrated Monod kinetic parameter sets for DGG-B-LV culture vessels.

		DGG-B-LV1					DGG-B-LV2				
		1	**2**	**3**	**Mean**	**Std. Dev.**	**1**	**2**	**3**	**Mean**	**Std. Dev.**
RMSE	**mg/L**	3.49	3.22	3.25	3.32	0.15	4.01	3.43	3.46	3.63	0.33
X_0	**mg/L**	0.81	8.42	7.70	5.64	4.20	1.54	10.56	7.11	6.40	4.55
μ_{max}	**1/d**	0.480	0.263	0.236	0.326	0.134	0.330	0.247	0.105	0.227	0.114
K_S	**mg/L**	117	154	113	128	22	93	165	36	98	65
Y	**g/g**	0.134	0.262	0.310	0.235	0.091	0.199	0.522	0.590	0.437	0.209
K_d	**1/d**	0.049	0.021	0.024	0.031	0.015	0.040	0.017	0.026	0.028	0.011

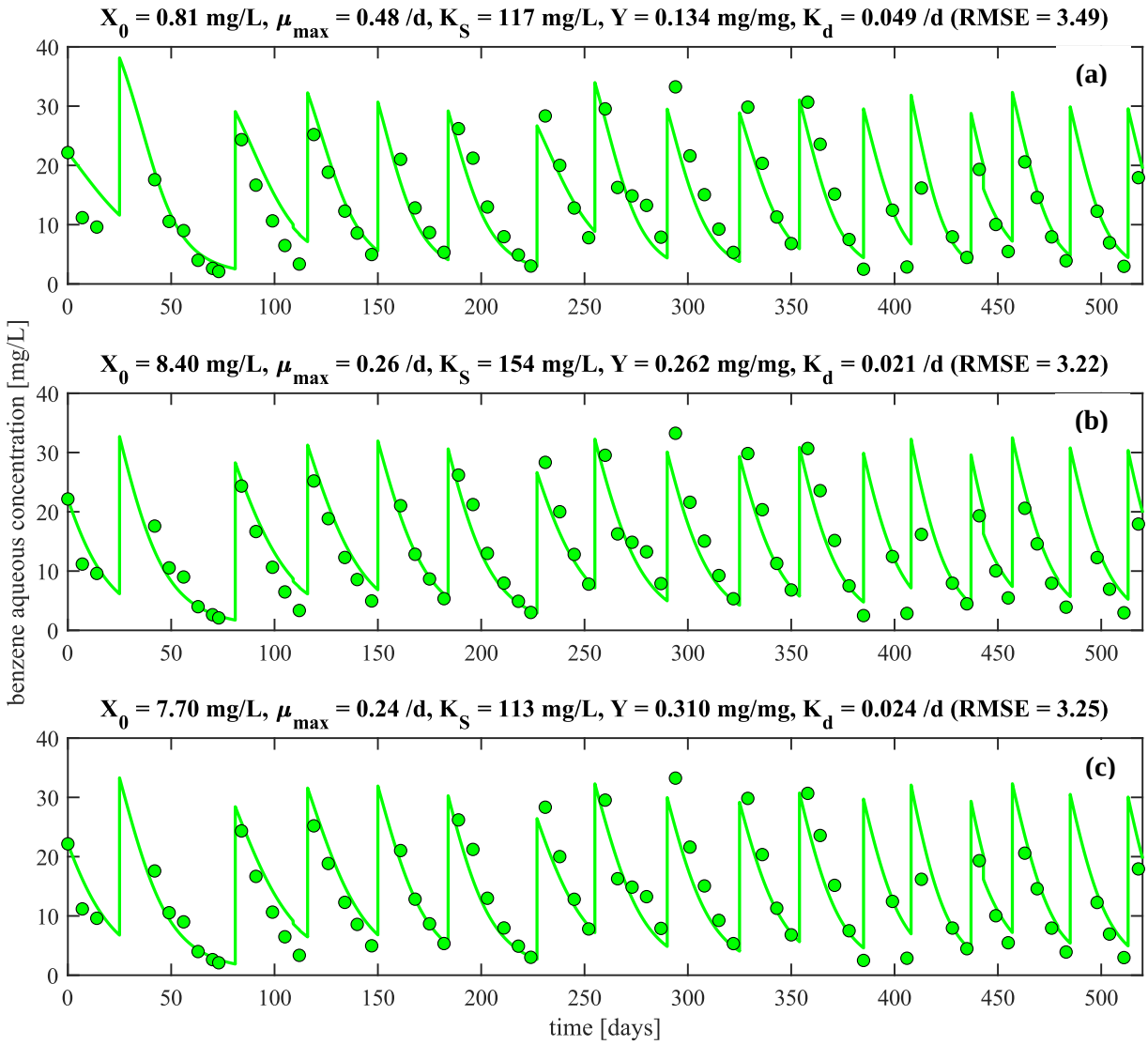

Figure 4.1 LV1 culture vessel data: observed (●) and simulated (—) aqueous benzene concentrations for three different calibrated parameter sets (a, b, and c) each with a unique starting seed.

The variation in best-fit parameter values is a result of significant parameter correlation and interaction (e.g., higher μ_{max} can be compensated by higher K_d) and is discussed at length in the literature (Rittmann & McCarty, 2018). This interplay demonstrates a need to restrict the number of parameters and determine suitable estimates where appropriate. To reduce the dimensionality of the parameter space, X_0 was fixed using estimates from available qPCR data and relative abundance measurements (Table 3.1), and Y and K_d were assumed to be constant across cultures. Estimates of Y and K_d were obtained from the literature (Table 3.4), and μ_{max} and K_S were retained as optimization parameters. DDS-AU was completed for each data set using 500 trials of 100 model iterations per

trial. A scatter plot of μ_{max} vs K_S for all 500 trials for both LV1 and LV2 is shown in Figure 4.2. Example histograms of μ_{max}, $K_{S,}$ and RMSE for LV1 are shown in Figure 4.3 (LV2 data not shown had the same trends).

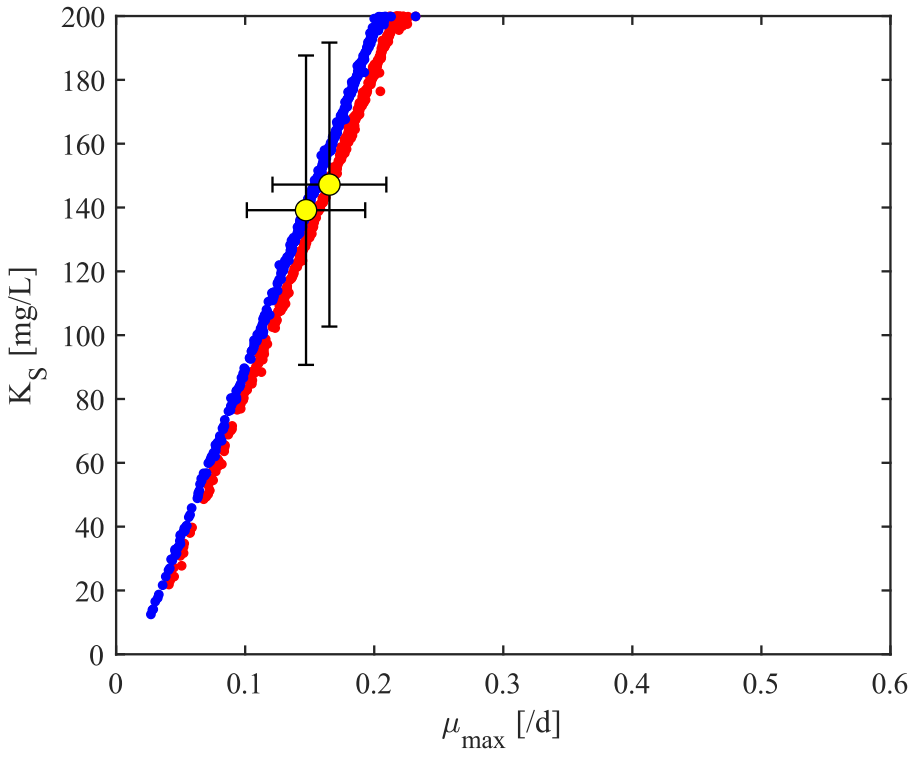

Figure 4.2 Calibrated parameters (μ_{max} and K_S) representing the 500 best solutions of DDS trials with 100 iterations per trial for LV1 (●) and LV2 (●). Mean of calibrated parameters (●) were $\bar{\mu}_{max}$ = 0.165 /d and $\bar{K}_S$ = 147 mg/L for LV1, and $\bar{\mu}_{max}$ = 0.147 /d and $\bar{K}_S$ = 139 mg/L for LV2. Error bars represent ± one standard deviation.

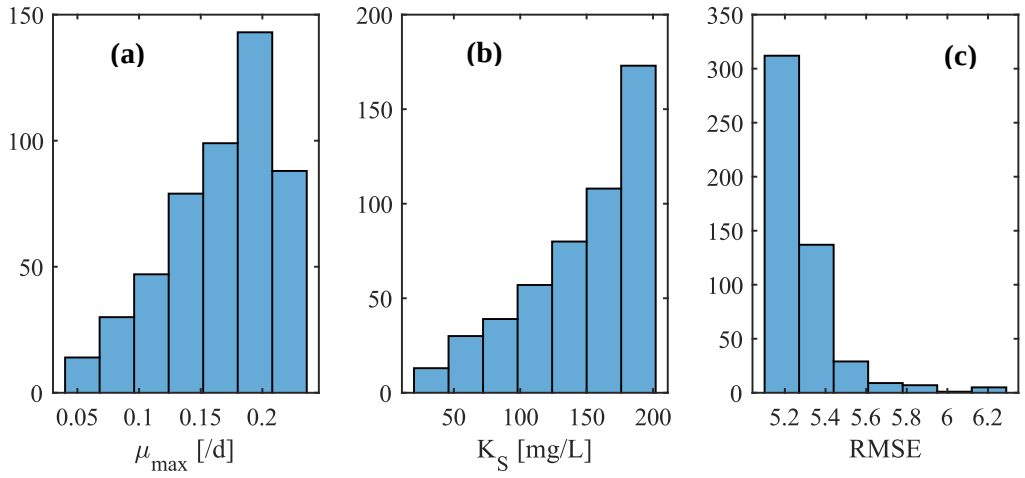

Figure 4.3 Frequency histograms of the best 500 calibrated (a) μ_{max} and (b) K_S values, and (c) model RMSE of DDS trials with 100 iterations per trial for LV1.

There is significant correlation between optimized μ_{max} and K_S values (Figure 4.2). Additionally, the parameter values are not normally distributed (Figure 4.3(a,b)), necessitating non-parametric statistical analyses (e.g., Wilcoxon rank sum test for comparison of medians). The observed and simulated benzene concentrations using the mean calibrated μ_{max} and K_S ($\bar{\mu}_{max}$ and $\bar{K}_S$) for both LV1 and LV2 are provided in Figure 4.4. The model assumes the first observed aqueous phase concentration (Day 0) represents an equilibrium condition partitioned across all phases.

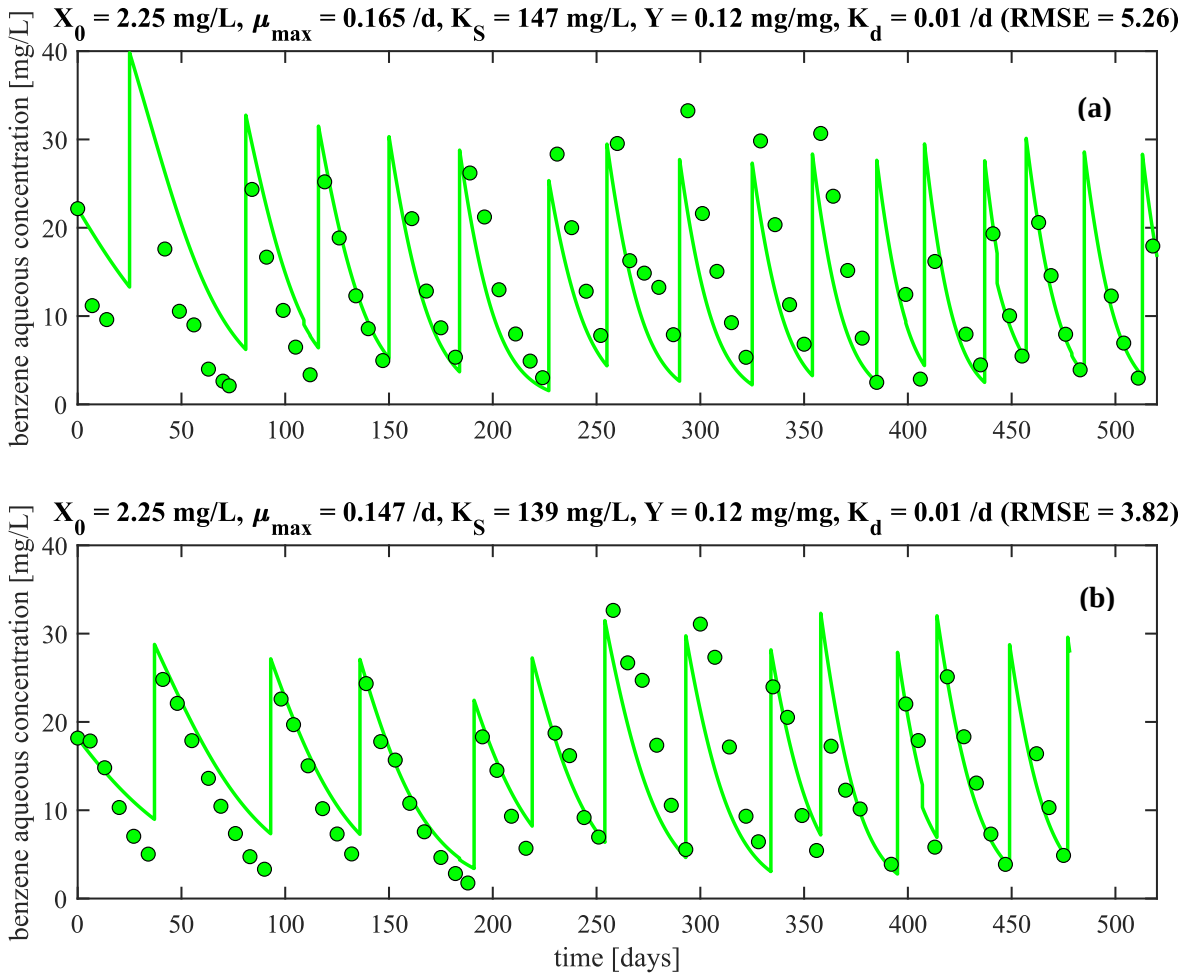

Figure 4.4 LV1 and LV2 culture vessel data: observed (●) and simulated (—) aqueous benzene concentration time series for (a) LV1 ($\bar{\mu}_{max}$ = 0.165 /d and $\bar{K}_S$ = 147 mg/L) and (b) LV2 ($\bar{\mu}_{max}$ = 0.147 /d and $\bar{K}_S$ = 139 mg/L).

Simulated benzene concentrations using the mean calibrated parameter values follow the trends observed in both LV1 and LV2 with benzene concentrations generally following the shape of the degradation cycles; however, randomness is not observed in the residuals for LV1 or LV2 (Figure 4.5). This is perhaps indicative of an underlying bias in the model. Non-random residuals may occur due to the uncertainty in the actual benzene mass spiked into each vessel at various times to sustain the culture. The batch model is assigned the target benzene mass, which then partitions instantaneously across phases. Error is introduced if the actual mass spike deviates from this target. For example, the simulated mass spike that occurs at Day 227 in LV1 causes an instantaneous increase in simulated aqueous benzene concentration of 23.6 mg/L (from 3 to 26.6 mg/L), but the observed increase in aqueous benzene concentration was 25.3 mg/L (from 3 to 28.3 mg/L). Uncertainty in the actual spiked benzene mass in the SiREM culture vessels (~2.5 g benzene added to

each 105 L vessel for each spike) leads to discrepancies between measured and simulated benzene concentrations for the duration of the experiment.

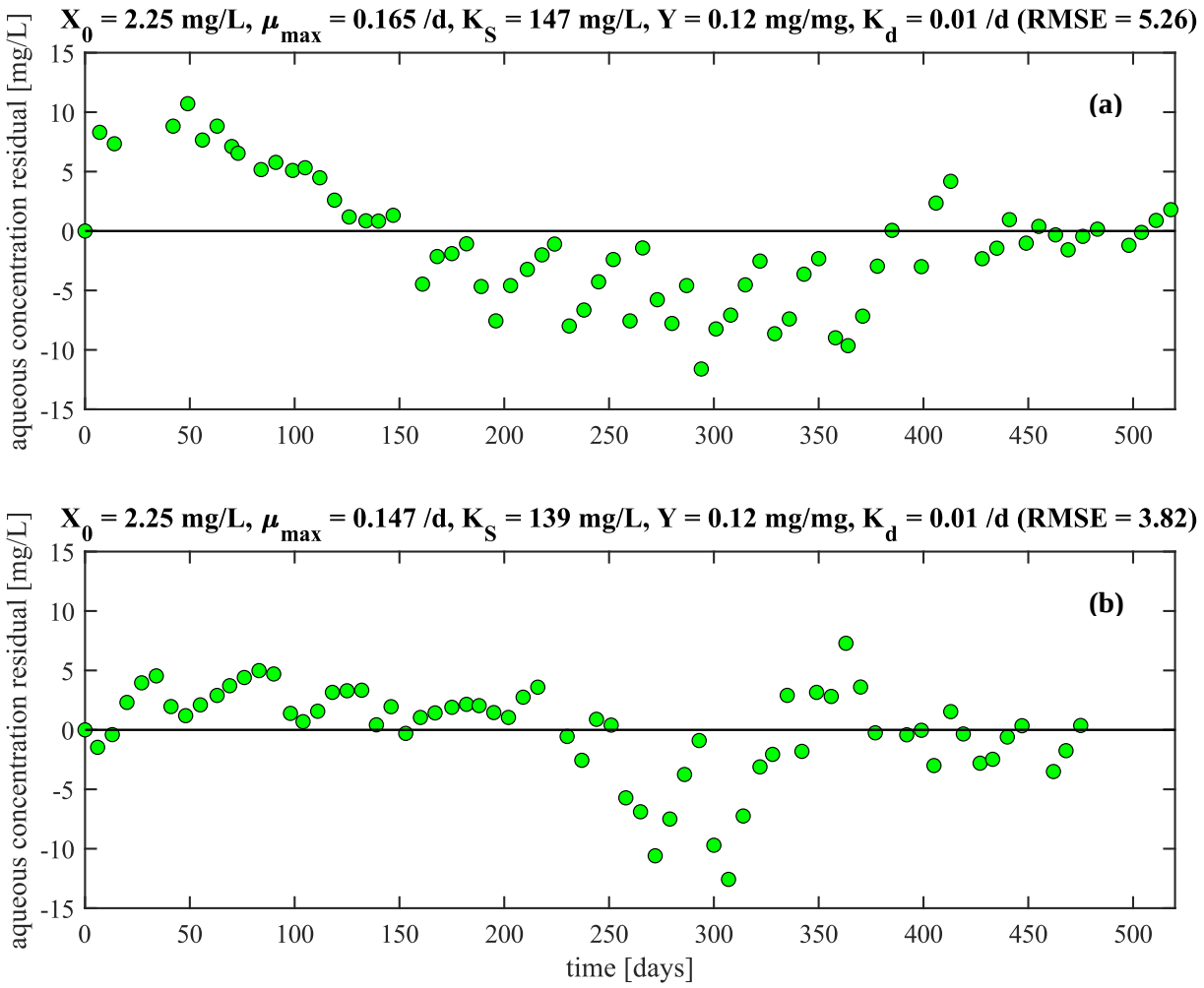

Figure 4.5 Aqueous benzene concentration residuals (simulated – observed) (●) for (a) LV1 and (b) LV2.

The median μ_{max} and K_S for LV1 were 0.175 /d and 158 mg/L respectively, whereas the median μ_{max} and K_S for LV2 were 0.156 /d and 149 mg/L respectively. Results from the Wilcoxon rank sum test showed that differences in the median μ_{max} and K_S values were statistically significant ($p < 0.05$). While LV2 was developed as a split from LV1 and thus expected to have essentially the same kinetic behaviour, the higher growth rate in LV1 is perhaps due to LV1 being the more established of the two culture vessels. For example, escalating substrate consumption rates can be observed in both LV1 and LV2 as they mature, with the time interval between successive benzene spikes decreasing over time. This is particularly pronounced in LV2 where the time between the first (Day 37) and second (Day 93) benzene spikes was 56 days, while the time between spikes 12 (Day 449) and 13 (Day 477) was

28 days, representing a 50% reduction in time between re-spikes and an increasing rate of substrate utilization as the culture matures.

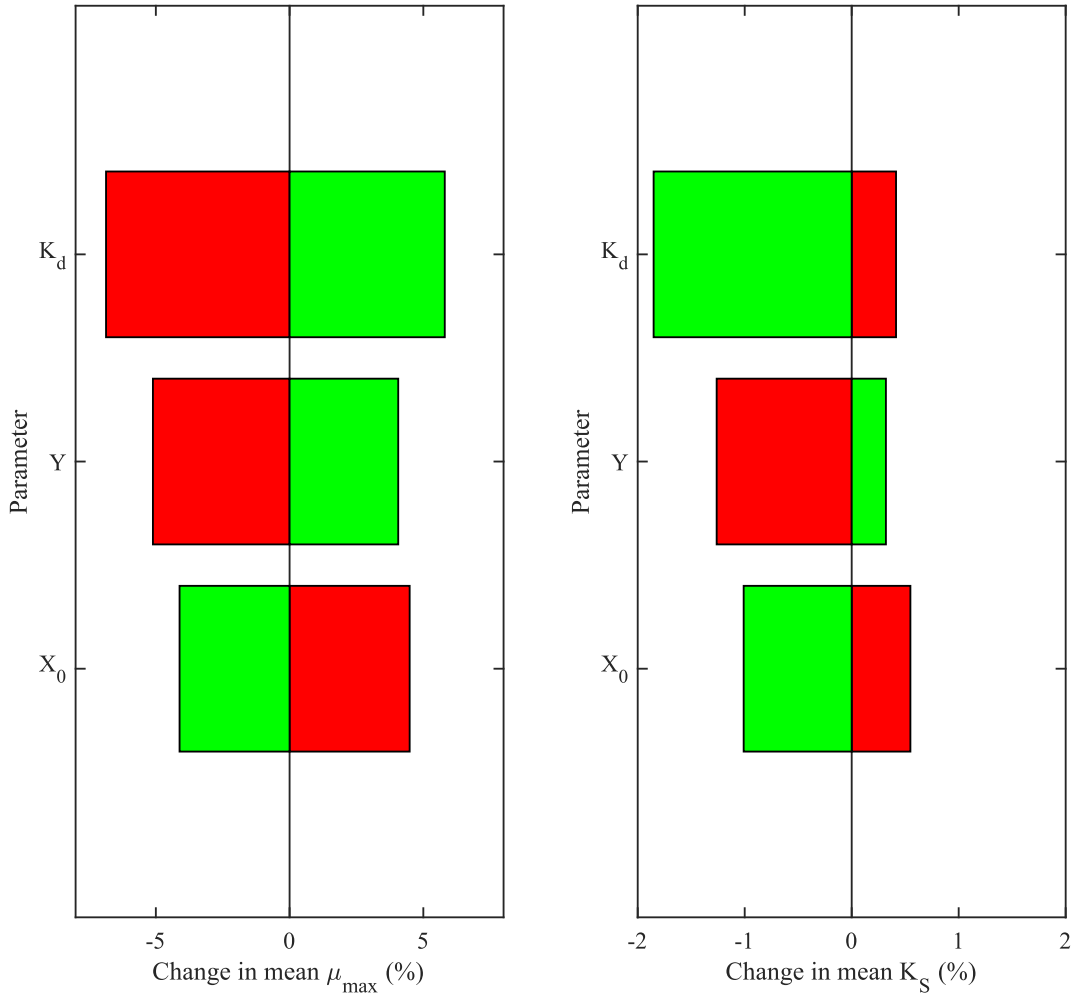

Figure 4.6 Sensitivity analysis on calibrated kinetic parameters for LV1 ($\bar{\mu}_{max}$ = 0.165 /d and $\bar{K}_S$ = 147 mg/L). Bars represent the percent change in the mean calibrated parameter ($\bar{\mu}_{max}$ or $\bar{K}_S$) value in response to an increase (■) or decrease (■) in a fixed parameter (X_0, Y, and K_d) value.

LV1 was selected for sensitivity analysis to investigate impactful parameters (Figure 4.6). Both calibration parameters were most sensitive to K_d, followed by Y and X_0. Impacts of increasing or decreasing the examined parameters were expected based on biomass growth and substrate consumption (see Equations (3.19), (3.20), and (3.21)). $\bar{\mu}_{max}$ was the most sensitive, with shifts of magnitude ±7%. In contrast, shifts in $\bar{K}_S$ were between +0.3 and -2%.

4.1.2 Microcosms

Different microcosm series were selected for simulation and analysis. Assuming indigenous biodegradation is negligible (based on analysis of the observation data presented in Section 3.1.2.2), useful observations were made from sets of simulations and analyses which informed subsequent simulations including:

1. Comparing aqueous phase data from the PAC and A-PAC microcosms to simulated aqueous phase concentrations, the single compound Freundlich adsorption parameters and the multi-compound competition coefficients can predict aqueous concentrations in PAC systems at steady-state (no degradation) based on mass balance considerations.
2. With 1), based on the aqueous and solid phase data from PAC, A-PAC, and A-BA-PAC microcosms and simulated values using single compound Freundlich adsorption parameters and multi-compound competition coefficients
    a. PAC sorbed phase data was collected under non-equilibrium conditions, and in most cases simulated sorbed concentrations overpredict observed values, and
    b. At aqueous concentrations < the method detection limit (MDL), sorbed concentrations are at or near-zero, suggesting there is no significant irreversible hysteresis in the PAC microcosms.
3. With 1) and 2), kinetic parameters can be determined for the BA, A-BA, and A-BA-PAC microcosms using calibration.

A subset of the microcosms was simulated to assess the role that PAC plays in bioaugmented systems. This included toluene and BTX bioaugmented microcosms with no solids, BS, or BS and PAC. In all cases, DDS-AU (500 trials of 100 model iterations each) was completed. For the single compound systems, optimization parameters were μ_{max} and K_S for toluene, and for the multi-compound systems, they were μ_{max} and K_S for both toluene and *o*-xylene. While the kinetics for benzene were ignored because it was not observed to biodegrade in the microcosms, it was simulated because it plays an important role competing for sorption sites on PAC. For all comparisons of the simulated kinetic behaviour between microcosm sets, "improved" kinetics refers to both an increase in μ_{max} and a decrease in K_S (Equations (3.19) to (3.21)). Following optimization efforts using two calibration parameters (μ_{max} and K_S), K_S was fixed to observe the behaviour of μ_{max} as the sole calibration parameter and to facilitate more direct comparison between the simulated microcosms.

4.1.2.1 Active and Killed Powdered Activated Carbon Microcosms

The active powdered activated carbon (A-PAC) and killed powdered activated carbon (PAC) microcosms contained substrate (toluene or BTX) with BS and PAC present. PAC microcosms differed in that they contained an addition of killed bioaugmentation culture (1 mL of DGG-T for single compound and 1 mL of each of DGG-B, DGG-T, and DGG-X for multi-compound). Simulated toluene and BTX concentrations in single and multi-compound A-PAC and PAC microcosms are displayed in Figure 4.7(a,b) and Figure 4.8(a,b). Due to the variability in initial aqueous concentration across microcosm series, the model assumes the first observed aqueous phase concentration (Day 0) represents an equilibrium condition partitioned across all phases. After PAC addition, mass is redistributed to a new equilibrium condition including a PAC sorbed phase. Additionally, it was assumed that there was no PHC biodegradation.

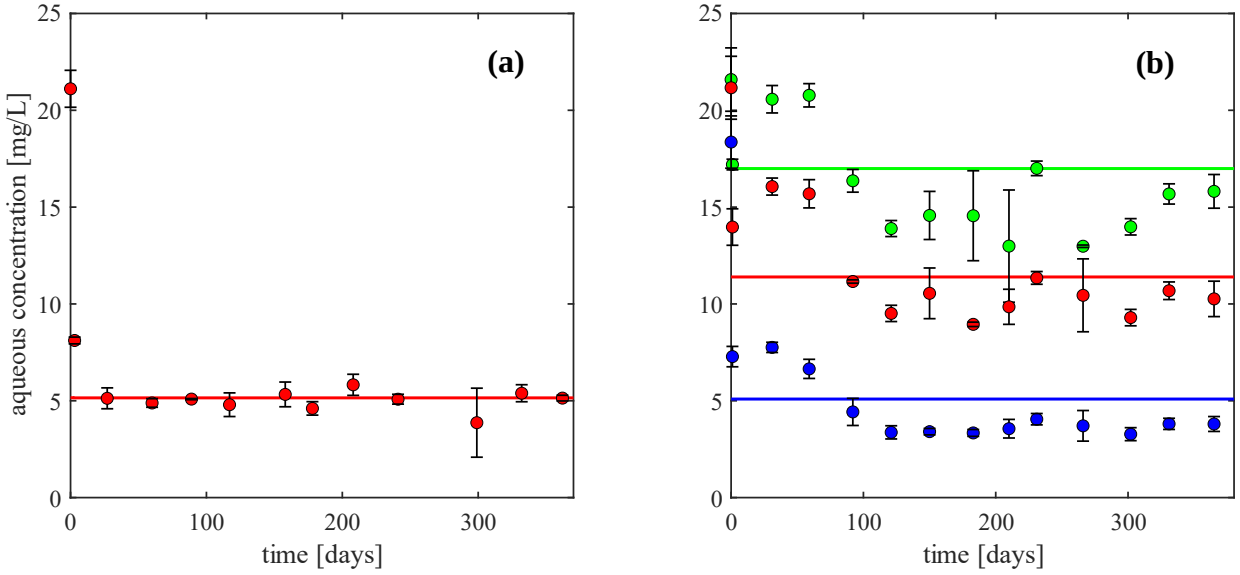

Figure 4.7 Active powdered activated carbon (A-PAC) microcosm data: (a) aqueous toluene concentrations (●) from the single compound system, and (b) aqueous benzene (●), toluene (●), and *o*-xylene (●) concentrations from the multi-compound system. Solid lines represent simulated aqueous concentrations for benzene (—), toluene (—), and *o*-xylene (—) which assumes the first observed aqueous concentration (Day 0) of each compound is in equilibrium with all phases. Error bars represent ± one standard deviation.

In the A-PAC microcosms, the steady-state aqueous concentration (5.2 mg/L for toluene in single compound systems; 17.0, 11.4, and 5.1 mg/L for B, T, and X respectively in multi-compound systems) is predicted by the model using single compound sorption coefficients in the single compound microcosms and single compound sorption coefficients and competition coefficients in the multi-compound microcosms. Likewise, in the PAC microcosms, the steady-state aqueous

concentration (5.2 mg/L for toluene in single compound systems; 16.5, 11.4, and 4.5 mg/L for B, T, and X respectively) is also predicted by model using single compound sorption coefficients in single compound microcosms and single compound sorption coefficients and competition coefficients in multi-compound microcosms.

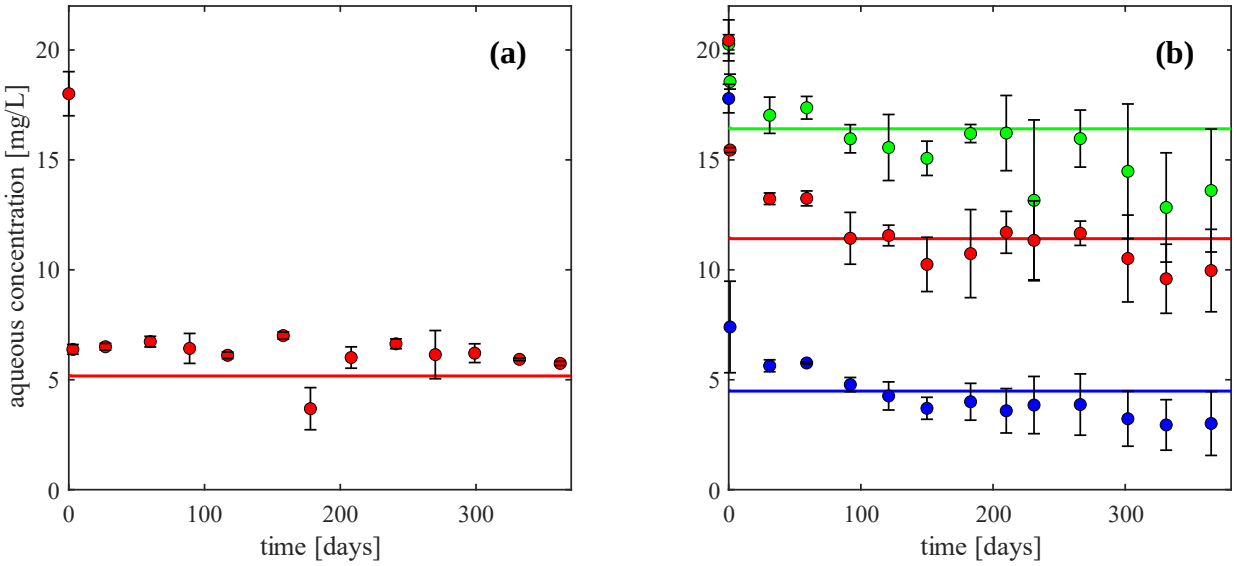

Figure 4.8 Powdered activated carbon (PAC) microcosm data: (a) aqueous toluene concentrations (●) from the single compound system, and (b) aqueous benzene (●), toluene (●), and *o*-xylene (●) concentrations from the multi-compound system. Solid lines represent simulated aqueous concentrations for benzene (—), toluene (—), and *o*-xylene (—) which assumes the first observed aqueous concentration (Day 0) of each compound is in equilibrium with all phases. Error bars represent ± one standard deviation.

Since the A-PAC and PAC microcosms are analogous to the conditions in a batch isotherm (assuming no decay), after equilibrium is reached between phases the final aqueous concentration should be estimated based on the isotherm properties of the PAC and PHC compound alone. Indeed, the results from the A-PAC and PAC microcosms provide evidence that single compound sorption parameters for toluene (single compound microcosms) and single compound sorption parameters and competition coefficients for BTX (multi-compound microcosms) are sufficient to estimate the steady-state concentration of BTX for a system with PAC and no biodegradation.

4.1.2.2 Bioaugmented Control Microcosms

The bioaugmented control (BA) microcosms contained bioaugmentation culture (either DGG-T or DGG-B, DGG-T, and DGG-X) and substrate (toluene or BTX) with no BS and/or PAC present.

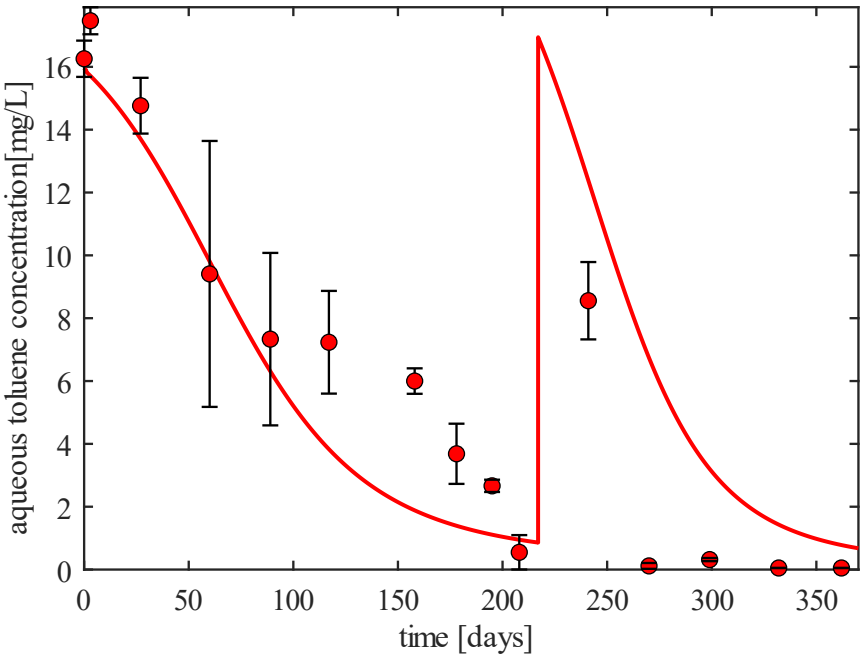

Figure 4.9 Single compound BA microcosm observed (●) and simulated (—, $\bar{\mu}_{max}$ = 0.324 ± 0.105 /d, $\bar{K}_S$ = 133 ± 46 mg/L) aqueous toluene concentrations. Error bars represent ± one standard deviation.

Single compound BA microcosms had the lowest number of toluene re-spikes (one) of all the bioaugmented microcosms which are reflected reasonably well by the model. Biodegradation is captured over the first ~80 days, but discrepancies arise when observed aqueous toluene concentrations remain constant between Day 80 and 120, and then continue to degrade to Day 217 before the toluene re-spike. Additionally, the calibrated simulation does a poor job representing the rate of toluene degradation after the Day 217 spike. Simulated toluene values are consistently greater than observed values and remain elevated until Day 370 when observed toluene falls below the MDL at Day 332. Calibrated toluene kinetic parameters were $\bar{\mu}_{max}$ = 0.324 ± 0.105 /d and $\bar{K}_S$ = 133 ± 46 mg/L.

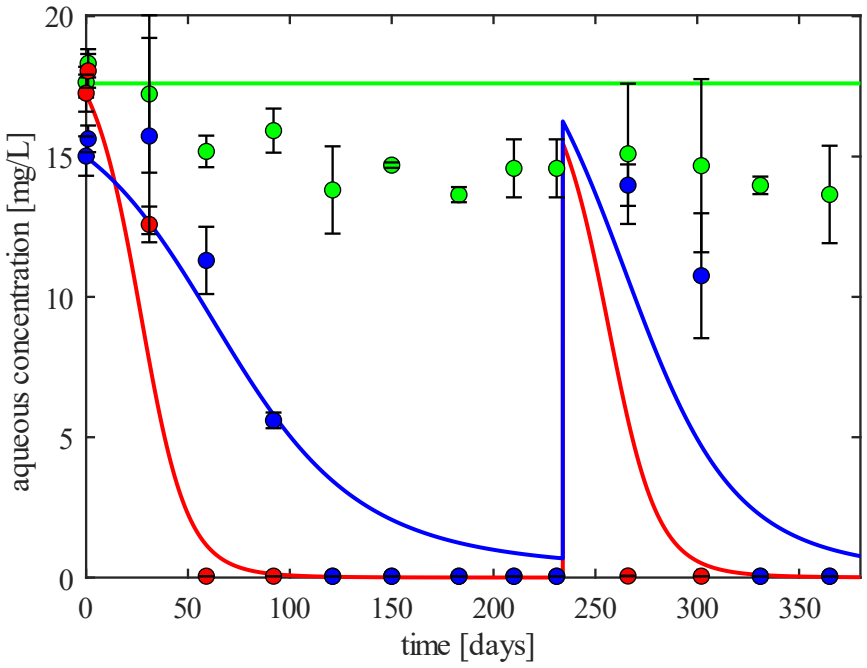

Figure 4.10 Multi-compound BA microcosm observed (●) and simulated (—) aqueous concentrations for benzene, (—, no degradation), toluene (—, $\bar{\mu}_{max}$ = 0.401 ± 0.139 /d, $\bar{K}_S$ = 69 ± 28 mg/L), and *o*-xylene (—, $\bar{\mu}_{max}$ = 0.325 ± 0.121 /d, $\bar{K}_S$ = 123 ± 50 mg/L). Error bars represent ± one standard deviation.

Simulated B, T, and X concentrations in the multi-compound BA microcosm system using mean calibrated kinetic parameters from DDS-AU are presented in Figure 4.10. Benzene degradation was assumed negligible, leading to a constant aqueous phase concentration of 17.6 mg/L. This microcosm system had only one re-spike of toluene and *o*-xylene. Despite the same number of re-spikes (one) as the single compound experiment, toluene degradation was significantly faster. Simulated toluene and *o*-xylene concentrations reflected the trends observed in the microcosms, with perhaps the greatest discrepancy being the slower rate of *o*-xylene biodegradation. While benzene kinetics were assumed to be negligible, the simulated constant aqueous benzene concentrations were higher than the observed values. This may be due to minor benzene biodegradation at the beginning of the experiment followed by a plateau presumably due to unsuccessful establishment of the DGG-B culture. Calibrated toluene kinetics in this microcosm system were improved compared to the single compound BA microcosm system ($\bar{\mu}_{max}$ = 0.401 ± 0.139 /d, $\bar{K}_S$ = 69 ± 28 mg/L compared to $\bar{\mu}_{max}$ = 0.324 ± 0.105 /d, $\bar{K}_S$ = 133 ± 46 mg/L). *o*-Xylene kinetics were lower than toluene kinetics in the multi-compound BA microcosm ($\bar{\mu}_{max}$ = 0.325 ± 0.121 /d, $\bar{K}_S$ = 123 ± 50 mg/L compared to $\bar{\mu}_{max}$ = 0.401 ± 0.139 /d, $\bar{K}_S$ = 69 ± 28 mg/L).

4.1.2.3 Active Bioaugmented Microcosms

Active bioaugmented (A-BA) microcosms contained BS, bioaugmentation culture (either DGG-T or DGG-B, DGG-T, and DGG-X), and substrate (toluene or BTX).

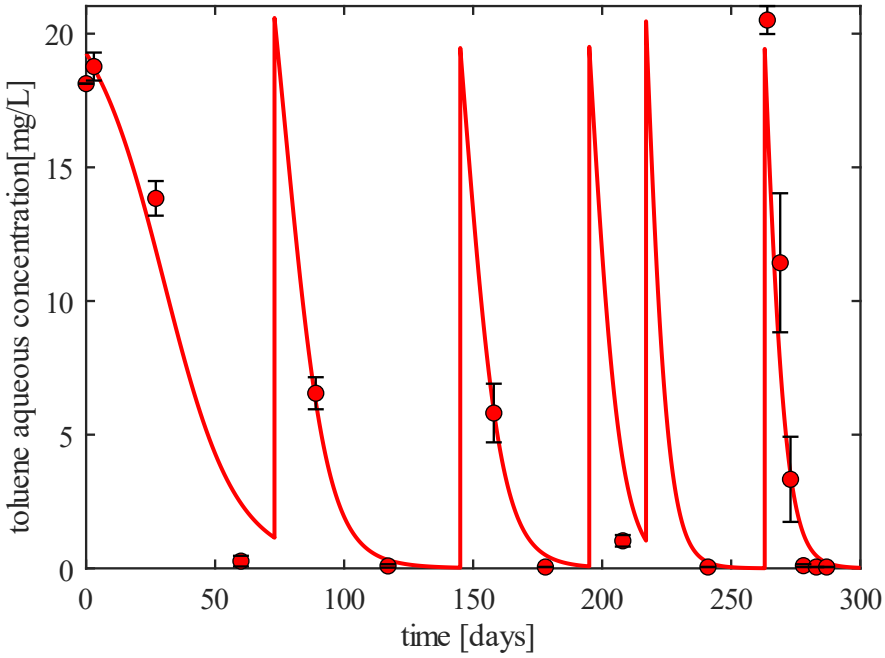

Figure 4.11 Single compound A-BA microcosm observed (●) and simulated (—, $\bar{\mu}_{max}$ = 0.382 ± 0.145 /d, $\bar{K}_S$ = 88 ± 38 mg/L) aqueous toluene concentrations. Error bars represent ± one standard deviation.

Single compound A-BA microcosms had significantly more re-spikes (five) than the BA microcosms and displayed much higher rates of toluene biodegradation. The shape of the observed toluene data is captured well by calibrated model, with perhaps an overestimation after the last mass spike (Day 263 to 287). The calibrated toluene kinetics in this microcosm system were improved compared to the single compound BA microcosms ($\bar{\mu}_{max}$ = 0.382 ± 0.145 /d, $\bar{K}_S$ = 88 ± 38 mg/L compared to $\bar{\mu}_{max}$ = 0.324 ± 0.105 /d, $\bar{K}_S$ = 133 ± 46 mg/L).

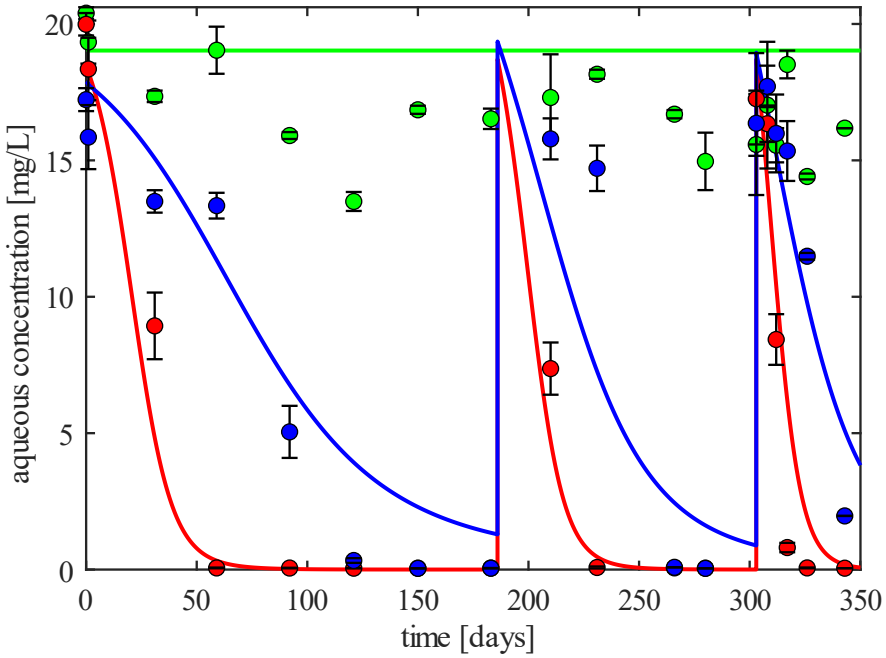

Figure 4.12 Multi-compound A-BA microcosm observed (●) and simulated (—) aqueous concentrations for benzene, (—, no degradation), toluene (—, $\bar{\mu}_{max}$ = 0.420 ± 0.131 /d, $\bar{K}_S$ = 62 ± 23 mg/L), and *o*-xylene (—, $\bar{\mu}_{max}$ = 0.304 ± 0.102 /d, $\bar{K}_S$ = 133 ± 49 mg/L). Error bars represent ± one standard deviation.

Benzene degradation was assumed negligible in the multi-compound A-BA microcosms, leading to a constant aqueous phase concentration of 19.0 mg/L. Multi-compound A-BA microcosms were not re-spiked the same number of times as the single compound A-BA microcosms (two vs five) since a decision was made to see if the DGG-B culture would acclimatize and benzene would begin to degrade. Nonetheless, toluene and *o*-xylene degradation rates were reflected well by the calibrated model. The same overestimation of *o*-xylene as in the multi-compound BA microcosms is observed here. Even with the lower number of re-spikes, these microcosms had improved toluene kinetics compared to the multi-compound BA microcosms ($\bar{\mu}_{max}$ = 0.420 ± 0.131 /d, $\bar{K}_S$ = 62 ± 23 mg/L compared to $\bar{\mu}_{max}$ = 0.401 ± 0.139 /d, $\bar{K}_S$ = 69 ± 28 mg/L) but had slightly lower calibrated *o*-xylene kinetics ($\bar{\mu}_{max}$ = 0.304 ± 0.102 /d, $\bar{K}_S$ = 133 ± 49 mg/L compared to $\bar{\mu}_{max}$ = 0.325 ± 0.121 /d, $\bar{K}_S$ = 123 ± 50).

The mass distribution in the simulated multi-compound A-BA microcosm using mean calibrated kinetics is displayed in Figure 4.13.

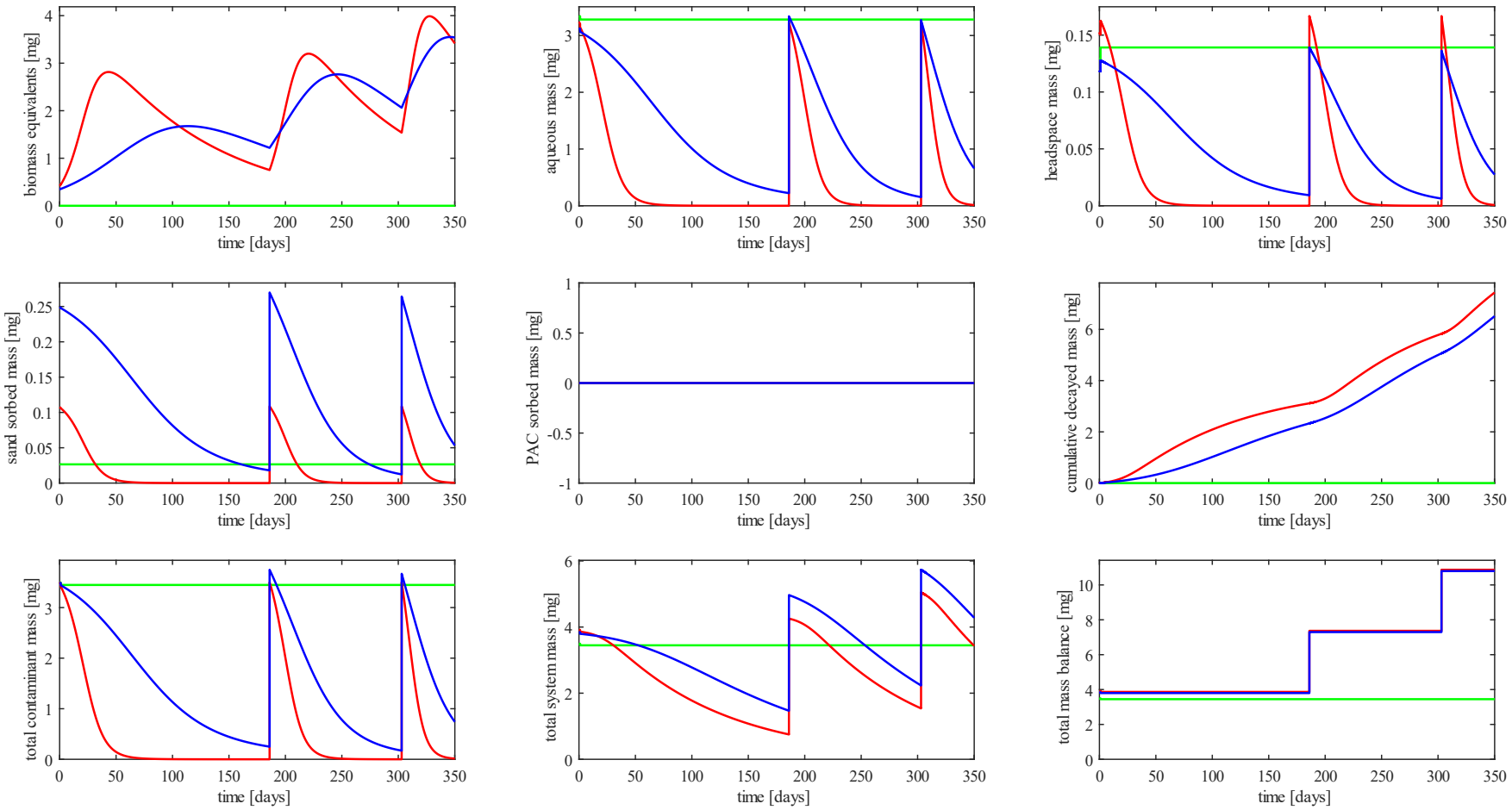

Figure 4.13 Temporal variation of BTX mass in each compartment for the simulated multi-compound A-BA microcosm system using mean calibrated kinetic parameters for toluene (—, $\bar{\mu}_{max}$ = 0.420 ± 0.131 /d and $\bar{K}_S$ = 62 ± 23 mg/L) and *o*-xylene (—, $\bar{\mu}_{max}$ = 0.304 ± 0.102 /d and $\bar{K}_S$ = 133 ± 49 mg/L). Benzene (—) was assumed not to biodegrade.

Most BTX mass resides in the aqueous phase since PAC is not present in this system, with the changes in the aqueous mass matching aqueous concentrations (Figure 4.12). Headspace and sorbed mass to the BS fluctuate in tandem with aqueous phase mass according to H_{cc} and K_p for each compound. The growth and decay cycles of biomass are observed and correspond to mass spikes, and result in a consistent increase in cumulative decayed mass of each substrate (TX).

4.1.2.4 Activated Carbon Sorption

Solid phase concentrations were measured when microcosm reactors were sacrificed in an experimental series containing PAC (i.e., the PAC, A-PAC, A-BA-PAC series). These data enable comparison between measured and simulated sorbed concentrations to investigate sorption behaviour, verification of the representativeness of developed isotherm parameters, and possible determination of the presence or absence of hysteresis. Figure 4.14(a) shows single compound measured aqueous and solid phase concentrations and the adsorption isotherm for toluene. The chronological order of each data point is indicated for each microcosm (e.g., a 4 indicates that it was the fourth solid phase sample collected and analyzed). To visualize the impact of sampling time on the measured and simulated solid phase concentrations, Figure 4.14(b) shows solid phase concentration residual (simulated – observed) as a function of the length of time after a toluene re-spike that the sample was collected. For illustration, Table 4.2 lists the data for the single compound A-BA-PAC microcosm which had re-spikes on Day 0, 73, 145, 195, 217, and 263. The observed solid phase concentrations are consistently overpredicted by the toluene isotherm perhaps indicating fouling of the PAC or measured solid phase concentrations not representative of equilibrium conditions. The latter hypothesis is supported by data points A-PAC (▲ 1) and A-BA-PAC (■ 1) & (■ 6) on Figure 4.14(a) where the samples were collected one to three days after an addition (spike) of toluene mass. Additionally, data from the A-BA-PAC microcosms show that the solid phase concentrations were low even at the end of the experimental period and after numerous re-spikes of toluene, suggesting irreversible hysteresis to PAC was insignificant at the analytical resolution used. Hysteretic behaviour is expected to manifest as observed solid phase concentrations that lie above the sorption isotherm, and irreversible sorption should manifest as non-zero observed solid phase concentrations corresponding to observed aqueous phase concentrations < MDL. Both the reversible and irreversible hysteretic desorption models would overpredict simulated sorbed concentrations during desorption (i.e., sorbed concentrations using desorption isotherms lie above the adsorption isotherm), and as such would never reflect the observed data (see Figure 2.3).

Table 4.2 Example data of measured and simulated sorbed concentrations and corresponding time after re-spike for the single compound A-BA-PAC microcosms. Highlighted rows illustrate sorbed concentrations with a high residual (simulated – observed) which occur shortly after mass spikes.

ID	Sample (Day)	Most Recent Re-spike (Day)	Time After Re-spike (Days)	Observed Concentration		Simulated Concentration	Residual
				Aqueous (mg/L)	Sorbed (mg/g)	Sorbed (mg/g)	Sorbed (mg/g)
1	3	0	3	7.00	88.7	200	111
2	60	0	60	1.58	110	107	-3.12
3	117	73	44	0.06	11.2	27.3	16.2
4	178	145	33	0.07	7.29	29.3	22.0
5	241	217	24	0.05 (MDL)	7.51	25.0	17.5
6	264	263	1	8.61	103	218	116
7	269	263	6	2.58	88.4	131	43.0
8	273	263	10	0.18	0.01	42.6	42.5
9	278	263	15	0.05 (MDL)	0.72	25.0	24.3
10	283	263	20	0.05 (MDL)	5.04	25.0	20.0
11	287	263	24	0.05 (MDL)	0.04	25.0	25.0

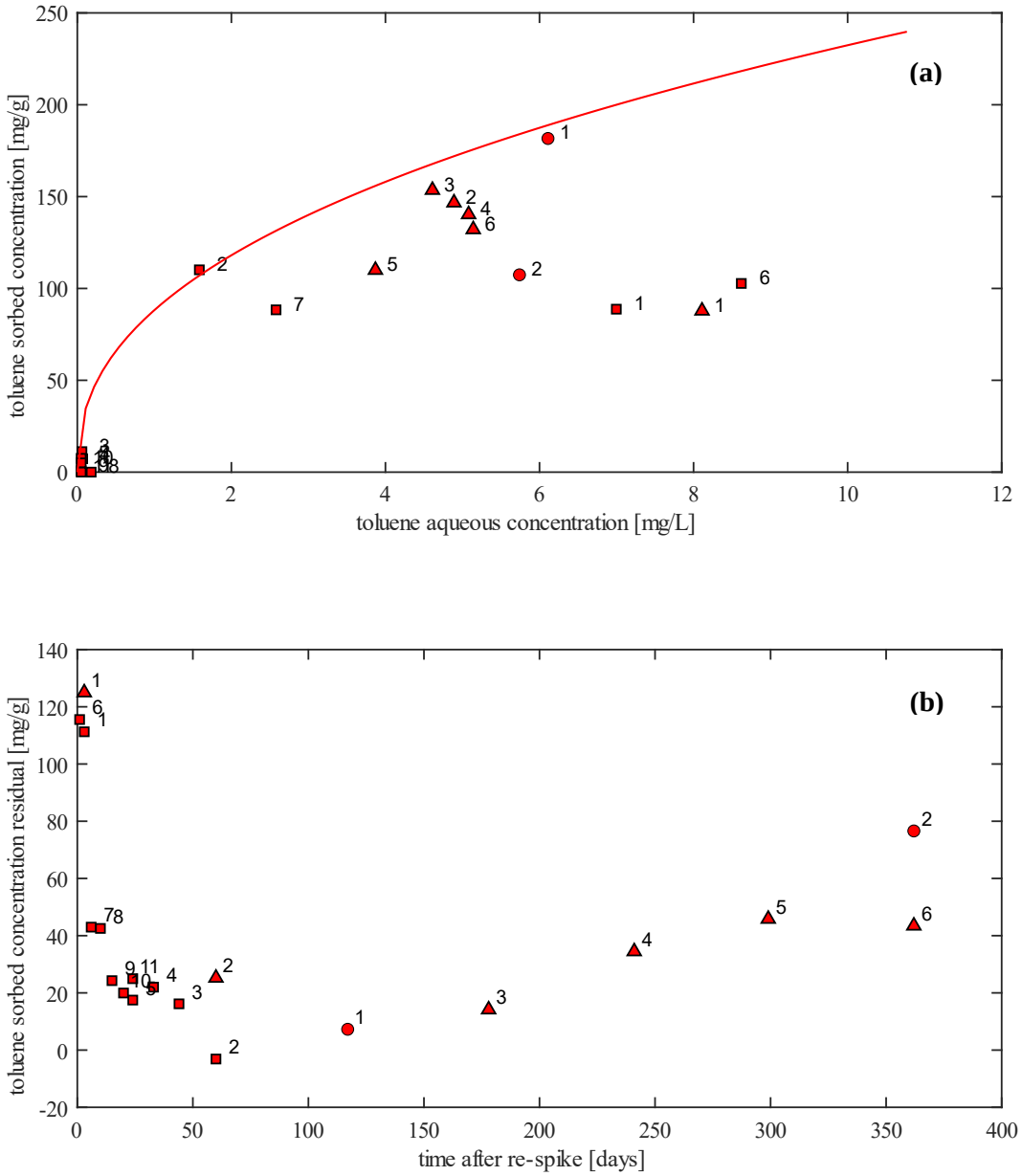

Figure 4.14 (a) Single compound sorbed and aqueous concentration data for PAC (●), A-PAC (▲) and A-BA-PAC (■) microcosms, and the adsorption isotherm for toluene (—, K_f = 88.19, n_f = 0.421). (b) Sorbed concentration residuals (simulated using sorption isotherm – observed) as a function of time after a toluene re-spike the measurement was taken. ID numbers represent the chronological order of sampling ("1" is the first sample, "2" is the second, etc.); examples are provided in Table 4.2. Clustered at the origin in (a) are sample 3, 4, 5, 8, 9, 10, and 11 for the A-BA-PAC microcosms.

Figure 4.15 shows the multi-compound sorbed concentration residuals (simulated – measured) using the adsorption isotherms and competition coefficients for benzene, toluene, and *o*-xylene and the ISIAS (Equations (3.16) to (3.18)). Simulated sorbed concentrations mostly overpredict aqueous

concentrations, except for one solid phase measurement for toluene in A-BA-PAC ([■] 14 days after re-spike) and three solid phase measurements for *o*-xylene in A-BA-PAC ([■] 23, 45, and 121 days after re-spike) which display residuals between -37 and -118 mg/L. Ignoring these points, simulated sorbed concentrations using single compound sorption parameters and competition coefficients either adequately predict or overpredict observed sorbed concentrations. Additionally, except for the four data points mentioned previously, there is a trend indicating that the residual decreases as time after re-spike increases, supporting the hypothesis that measured solid phase concentrations are not representative of an equilibrium condition.

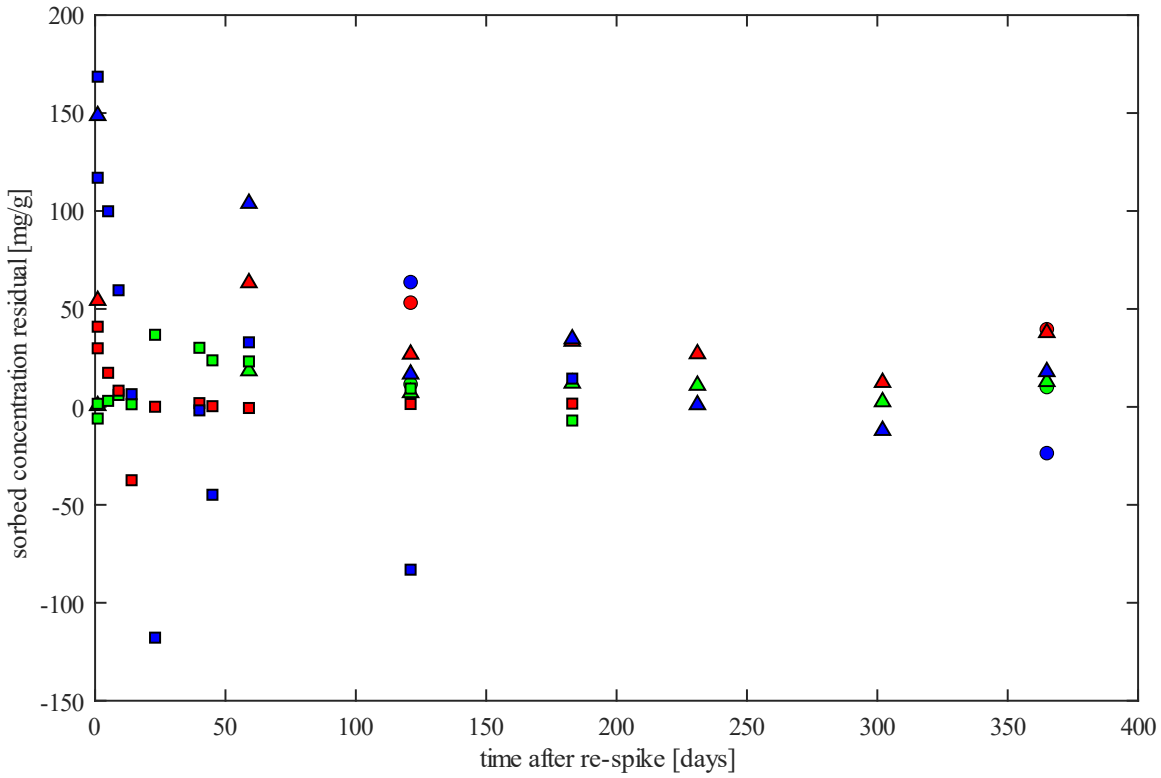

Figure 4.15 Sorbed concentration residuals (simulated using sorption isotherm – observed) for benzene (●, K_f = 36.10, n_f = 0.484, a_i = 1.416), toluene (●, K_f = 88.19, n_f = 0.421, a_i = 1.432), and *o*-xylene (●, K_f = 131.76, n_f = 0.371, a_i = 1.080) as a function of time after a toluene re-spike the measurement was taken in PAC (●), A-PAC (▲) and A-BA-PAC (■) microcosms.

Based on the observations made regarding simulated and observed sorbed concentrations in single compound microcosms, hysteresis was ignored in all simulations. Adsorption isotherms alone overpredict sorbed concentrations, and this mismatch would be compounded in simulations implementing either reversible or irreversible hysteresis. Additionally, trends in residual and time after re-spike in the multi-compound microcosms indicate there may be kinetic considerations not accounted for by single compound adsorption isotherms and competitive theory.

4.1.2.5 Active Bioaugmented PAC Microcosms

Active bioaugmented PAC (A-BA-PAC) microcosms contained BS, PAC, bioaugmentation culture (either DGG-T or DGG-B, DGG-T, and DGG-X), and substrate (toluene or BTX).

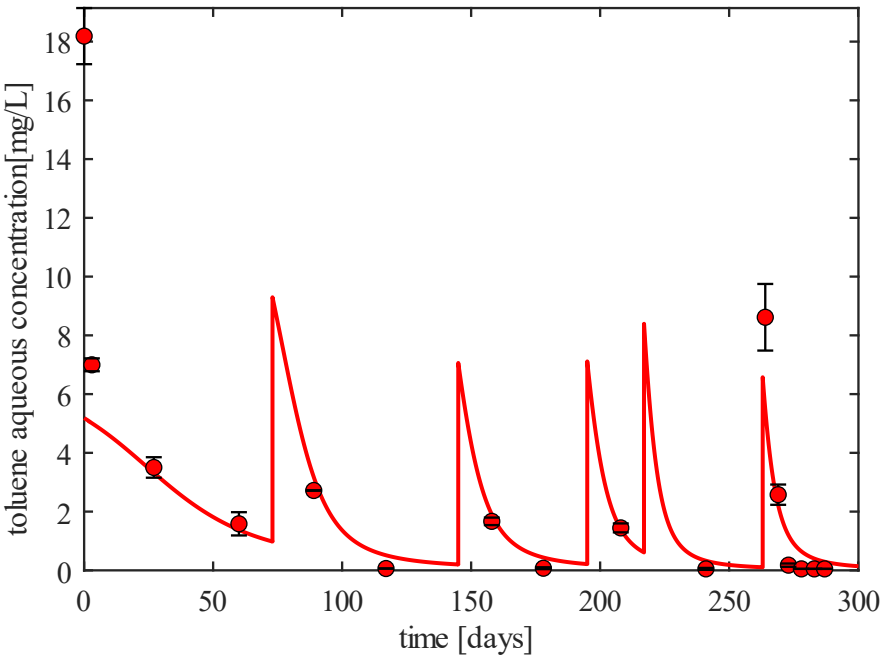

Figure 4.16 Single compound A-BA-PAC microcosm observed (●) and simulated (—, $\bar{\mu}_{max}$ = 0.422 ± 0.128 /d, $\bar{K}_S$ = 37 ± 13 mg/L) aqueous toluene concentrations. Error bars represent ± one standard deviation.

A-BA-PAC microcosms had the same number of re-spikes (five) as the single compound A-BA microcosms and displayed similar toluene biodegradation behaviour. The decrease in aqueous toluene concentration (from Day 0 to Day 3) is due to sorption onto PAC. Anywhere from 60-96% of total toluene mass in the microcosm resides as PAC sorbed phase during the simulation. Again, there is an overestimation of toluene concentration which is especially evident following the last re-spike at Day 263. Calibrated toluene kinetics for these microcosms were the fastest of all the single compound microcosm systems ($\bar{\mu}_{max}$ = 0.422 ± 0.128 /d, $\bar{K}_S$ = 37 ± 13 mg/L compared to $\bar{\mu}_{max}$ = 0.324 ± 0.105 /d, $\bar{K}_S$ = 133 ± 46 mg/L [BA] and $\bar{\mu}_{max}$ = 0.382 ± 0.145 /d, $\bar{K}_S$ = 88 ± 38 mg/L [A-BA]).

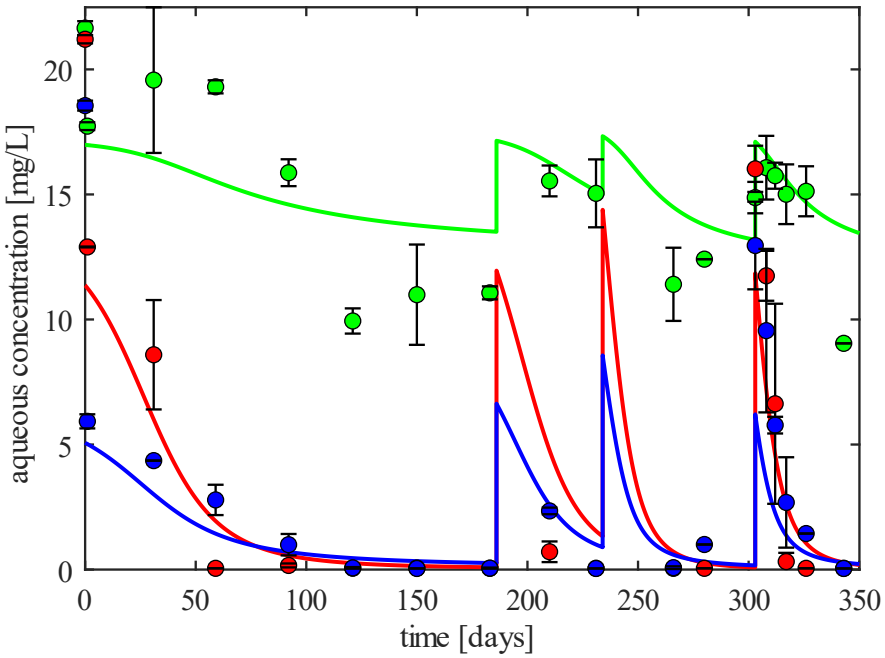

Figure 4.17 Multi-compound A-BA-PAC microcosm observed (●) and simulated (—) aqueous concentrations for benzene (—, no degradation), toluene (—, $\bar{\mu}_{max}$ = 0.419 ± 0.137 /d, $\bar{K}_S$ = 62 ± 23 mg/L), and *o*-xylene (—, $\bar{\mu}_{max}$ = 0.414 ± 0.143 /d, $\bar{K}_S$ = 35 ± 13 mg/L). Error bars represent ± one standard deviation.

Benzene degradation was assumed negligible in the multi-compound A-BA-PAC microcosms, but aqueous benzene concentrations fluctuated due to competitive sorption. Aqueous benzene concentrations decrease as toluene and *o*-xylene degrade and benzene sorbs and increase after re-spikes of toluene and *o*-xylene due to desorption. The multi-compound A-BA-PAC microcosms had one more re-spike (three) than the multi-compound A-BA microcosms (two) after waiting for benzene degradation. Concentration trends are like the multi-compound A-BA microcosms, but aqueous concentrations are depressed due to sorption onto PAC. This effect is most pronounced for *o*-xylene, which has the highest sorption affinity compared to benzene and toluene. Calibrated toluene kinetics were like the other multi-compound microcosms ($\bar{\mu}_{max}$ = 0.419 ± 0.137 /d, $\bar{K}_S$ = 62 ± 23 mg/L compared to $\bar{\mu}_{max}$ = 0.401 ± 0.139 /d, $\bar{K}_S$ = 69 ± 28 mg/L [BA] and $\bar{\mu}_{max}$ = 0.420 ± 0.131 /d, $\bar{K}_S$ = 62 ± 23 mg/L [A-BA]), but the calibrated *o*-xylene kinetics were improved compared to all other microcosms ($\bar{\mu}_{max}$ = 0.414 ± 0.143 /d, $\bar{K}_S$ = 35 ± 13 mg/L compared to $\bar{\mu}_{max}$ = 0.325 ± 0.121 /d, $\bar{K}_S$ = 123 ± 50 [BA] and $\bar{\mu}_{max}$ = 0.304 ± 0.102 /d, $\bar{K}_S$ = 133 ± 49 mg/L [A-BA]). Simulated concentrations underestimate the aqueous mass after the final mass re-spike (Day 303-350) for both toluene and *o*-xylene, but this is presumably due to non-equilibrium between the sorbed and aqueous phases as discussed in Section 4.1.2.4.

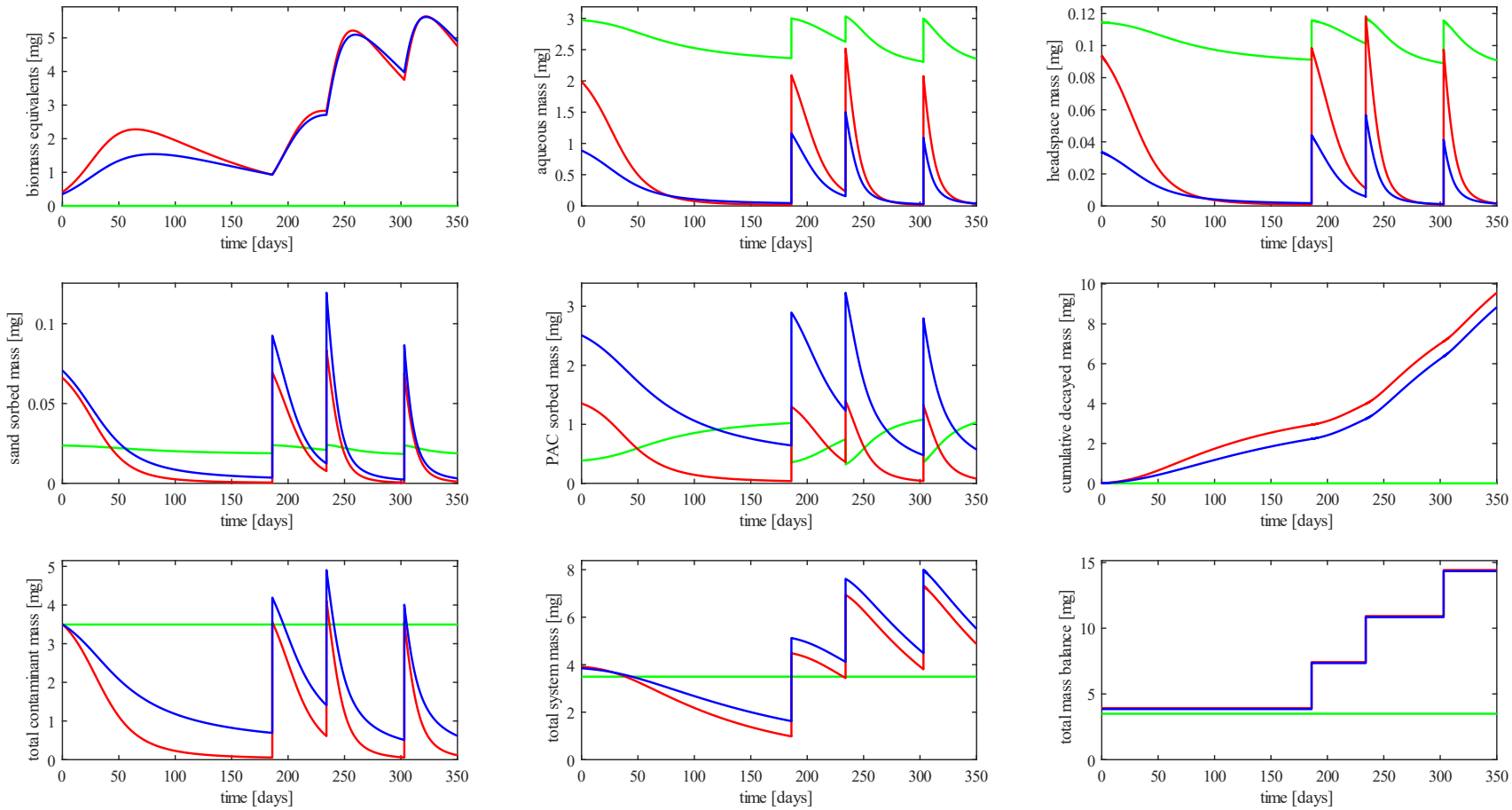

Figure 4.18 Temporal variation of BTX mass in each compartment for the simulated multi-compound A-BA-PAC microcosm system using mean calibrated kinetic parameters for toluene (—, $\bar{\mu}_{max}$ = 0.419 ± 0.137 /d and $\bar{K}_S$ = 62 ± 23 mg/L) and *o*-xylene (—, $\bar{\mu}_{max}$ = 0.414 ± 0.143 /d and $\bar{K}_S$ = 35 ± 13 mg/L). Benzene (—) was assumed not to biodegrade.

As shown in Figure 4.18, most of the mass resides in the aqueous phase or is sorbed to PAC, and the aqueous mass matches aqueous concentrations (Figure 4.17). Headspace and sorbed mass to the sand fluctuate in tandem with the aqueous phase mass according to H_{cc} and K_p for each compound. The mass sorbed to PAC fluctuates in response to aqueous mass. Additionally, even though benzene is not degrading, benzene mass fluctuates in each compartment due to adsorption of benzene on PAC as toluene and *o*-xylene degrade. Conversely, desorption of benzene from PAC occurs after re-spikes of toluene and *o*-xylene. The growth and decay cycles of biomass correspond to mass spikes, and result in a consistent increase in cumulative decayed mass of T and X. Additionally, compared to Figure 4.13, higher biomass and cumulative decayed mass of toluene and *o*-xylene are observed in the A-BA-PAC microcosms compared to A-BA microcosms, but this is perhaps due to an additional PHC mass re-spike (three in A-BA-PAC vs two in A-BA).

Sensitivity analysis results for the fixed kinetic (X_0, Y, K_d) and sorption (a_i, K_f, and n_f) parameters for the single and multi-compound A-BA-PAC simulations are presented on Figure 4.19 and Figure 4.20.

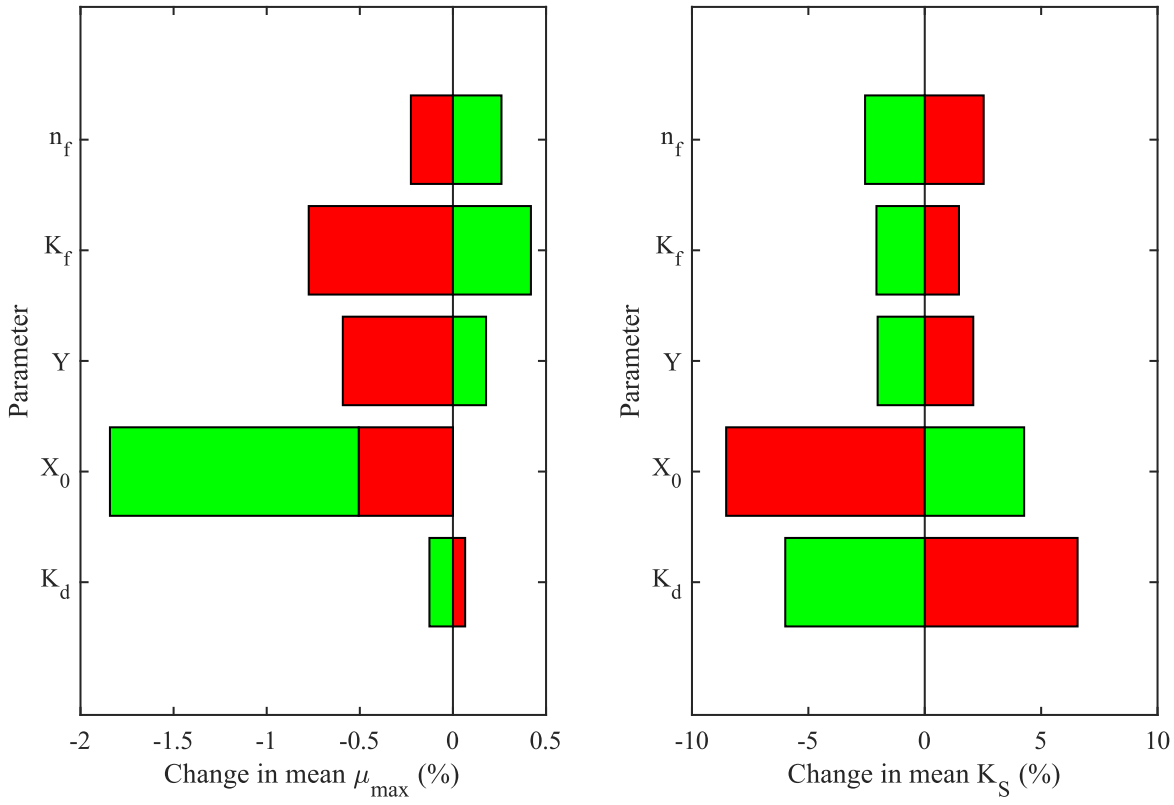

Figure 4.19 Sensitivity analysis on calibrated kinetic parameters for the single compound A-BA-PAC microcosms ($\bar{\mu}_{max}$ = 0.422 /d and $\bar{K}_S$ = 37 mg/L). Bars represent the percent change in calibrated parameter ($\bar{\mu}_{max}$ and $\bar{K}_S$) value in response to an increase (■) or decrease (■) in a fixed parameter (K_f, n_f, X_0, Y, and K_d) value.

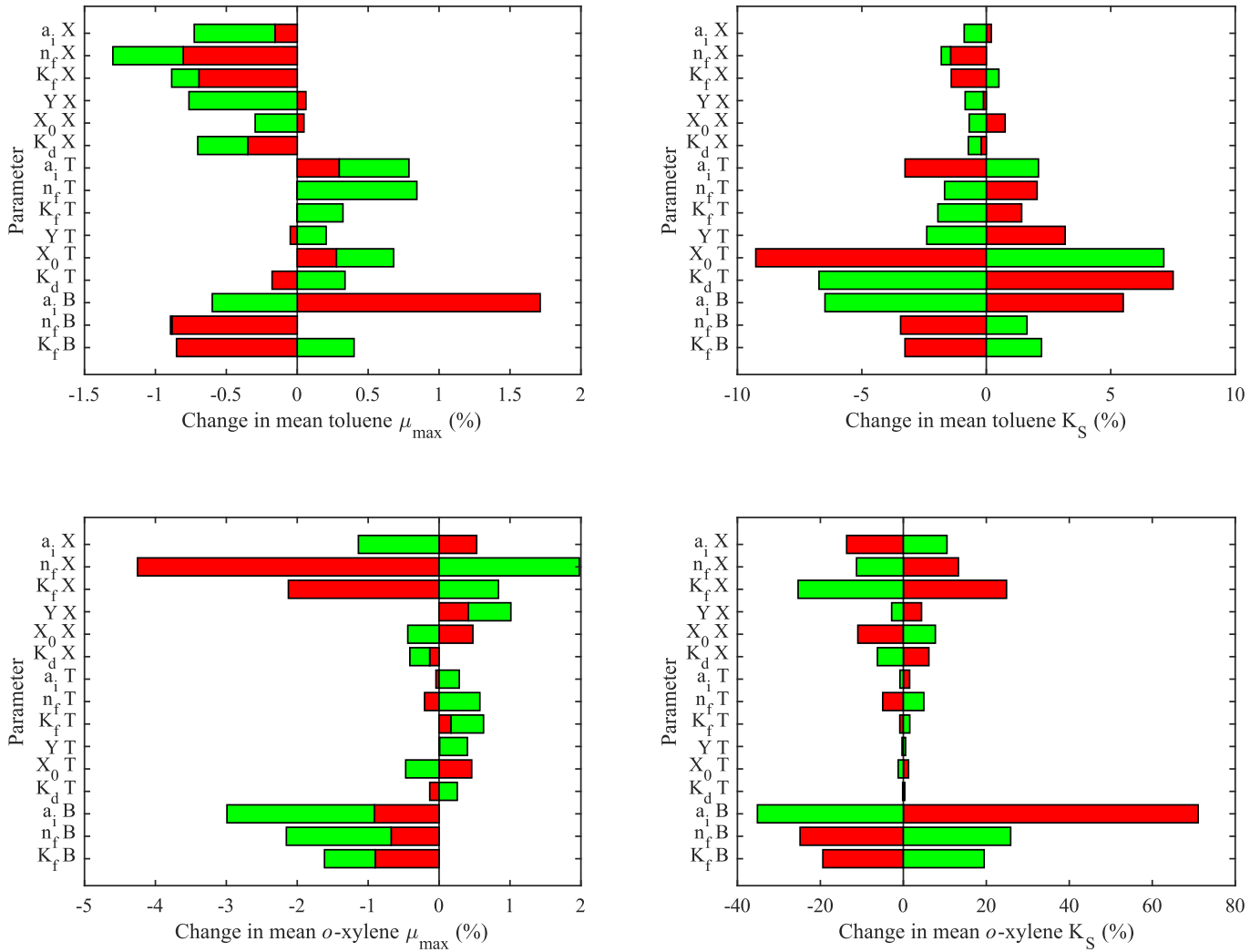

Figure 4.20 Sensitivity analysis on calibrated kinetic parameters for the multi-compound A-BA-PAC microcosms (toluene [$\bar{\mu}_{max}$ = 0.419 ± 0.137 /d, $\bar{K}_S$ = 62 ± 23 mg/L] and *o*-xylene [$\bar{\mu}_{max}$ = 0.414 ± 0.143 /d, $\bar{K}_S$ = 35 ± 13 mg/L]). Bars represent the percent change in calibrated parameter ($\bar{\mu}_{max}$ and $\bar{K}_S$) value in response to an increase (■) or decrease (■) in a fixed parameter (K_f, n_f, a_i, X_0, Y, and K_d) value. If the bars are both positive or negative (i.e., both lie on the same side of the vertical axis), they are stacked and do not overlap.

Shifts in the kinetic parameters for toluene ($\bar{\mu}_{max}$ and $\overline{K_S}$) were < 8% relative to mean calibrated parameters for both single and multi-compound microcosm systems. The most sensitive parameter in the single compound A-BA-PAC microcosm simulations was X_0, which decreased toluene $\bar{\mu}_{max}$ by 2% to 6% and shifted $\overline{K_S}$ by -3% to 2%. This is due to the influence X_0 has on initial degradation in the system, as the rate of degradation of the initial mass spike is largely controlled by the initial biomass. Higher or lower initial biomass would be compensated by shifts in calibrated kinetic parameters. This was also true for calibrated toluene $\overline{K_S}$ in the multi-compound system, which was shifted by a change in X_0 by -6% to 4%. Conversely, the most sensitive parameter with respect to calibrated toluene $\bar{\mu}_{max}$ in the multi-compound system was a_i for benzene, which shifted $\bar{\mu}_{max}$ by -2% to 7%. Since benzene is present in high concentrations for the duration of the experiment (no degradation), its competitive influence has a significant impact on the aqueous concentrations of the other PHCs (toluene and *o*-xylene), which directly influence biodegradation due to a change in substrate availability. *o*-Xylene kinetic parameters were significantly more sensitive than those of toluene. The most sensitive parameter with respect to calibrated *o*-xylene $\bar{\mu}_{max}$ in the multi-compound system was n_f for *o*-xylene, which shifted $\bar{\mu}_{max}$ by -18% to 8%. Because *o*-xylene has the highest sorption affinity of the PHCs, its own adsorption parameters have a significant impact on its aqueous concentrations and thus substrate availability for biodegradation. The most sensitive parameter with respect to the calibrated *o*-xylene $\overline{K_S}$ in the multi-compound system was a_i for benzene, which shifted $\overline{K_S}$ by -12% to 25%. Again, since benzene is present in high concentrations, its competitive influence has an impact on the availability of *o*-xylene in the aqueous phase, and significantly alters substrate availability.

4.1.2.6 Single Parameter Calibration

Due to significant correlation between calibrated $\bar{\mu}_{max}$ and $\overline{K_S}$, K_S was fixed to facilitate comparison between $\bar{\mu}_{max}$ (directly related to substrate utilization rate, k_{max}) across bioaugmented microcosms. K_S was set to 20 mg/L for all microcosms (the lower end of calibrated $\overline{K_S}$ values) and DDS-AU was performed [Figure 4.21].

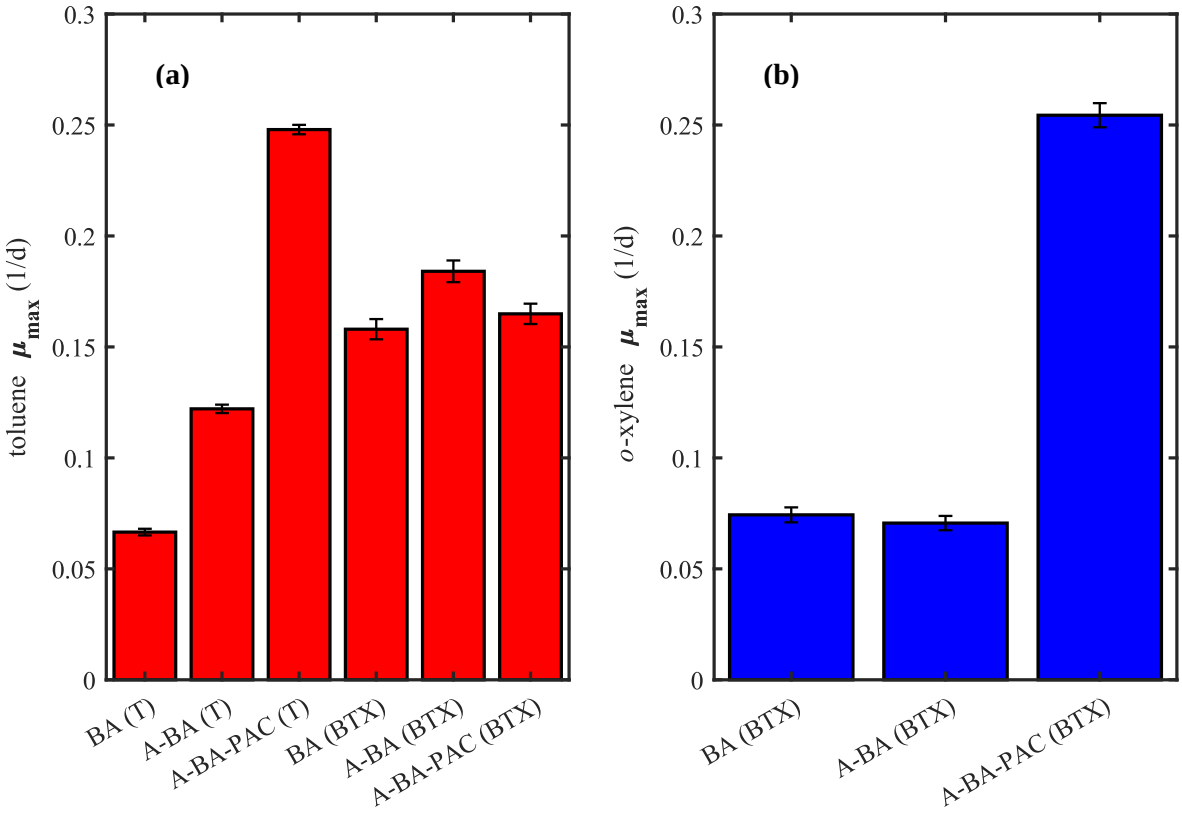

Figure 4.21 Mean calibrated maximum specific growth rate ($\bar{\mu}_{max}$) for (a) toluene and (b) *o*-xylene in the BA, A-BA, and A-BA-PAC microcosms in response to a fixed half-velocity constant (K_S = 20 mg/L). Error bars represent ± one standard deviation.

Optimal μ_{max} values were normally distributed, allowing the comparison of means using a *t*-test. The Student's *t*-test was used in cases of equal variance (for toluene, BA-BTX vs. A-BA-BTX, BA-BTX vs. A-BA-PAC-BTX, and A-BA-BTX vs. A-BA-PAC-BTX; for *o*-xylene, BA-BTX vs. A-BA-BTX) and the Welch's *t*-test was used in cases of unequal variance. Paired statistical tests between all combinations of microcosms showed that $\bar{\mu}_{max}$ values were statistically different ($p < 0.05$) (Appendix A).

4.1.2.7 Summary

The DDS-AU optimization results (for toluene and o-xylene) are presented in Figure 4.22, and a summary of the mean calibrated Monod kinetic parameters ($\bar{\mu}_{max}$ and $\bar{K}_S$) is listed in Table 4.3.

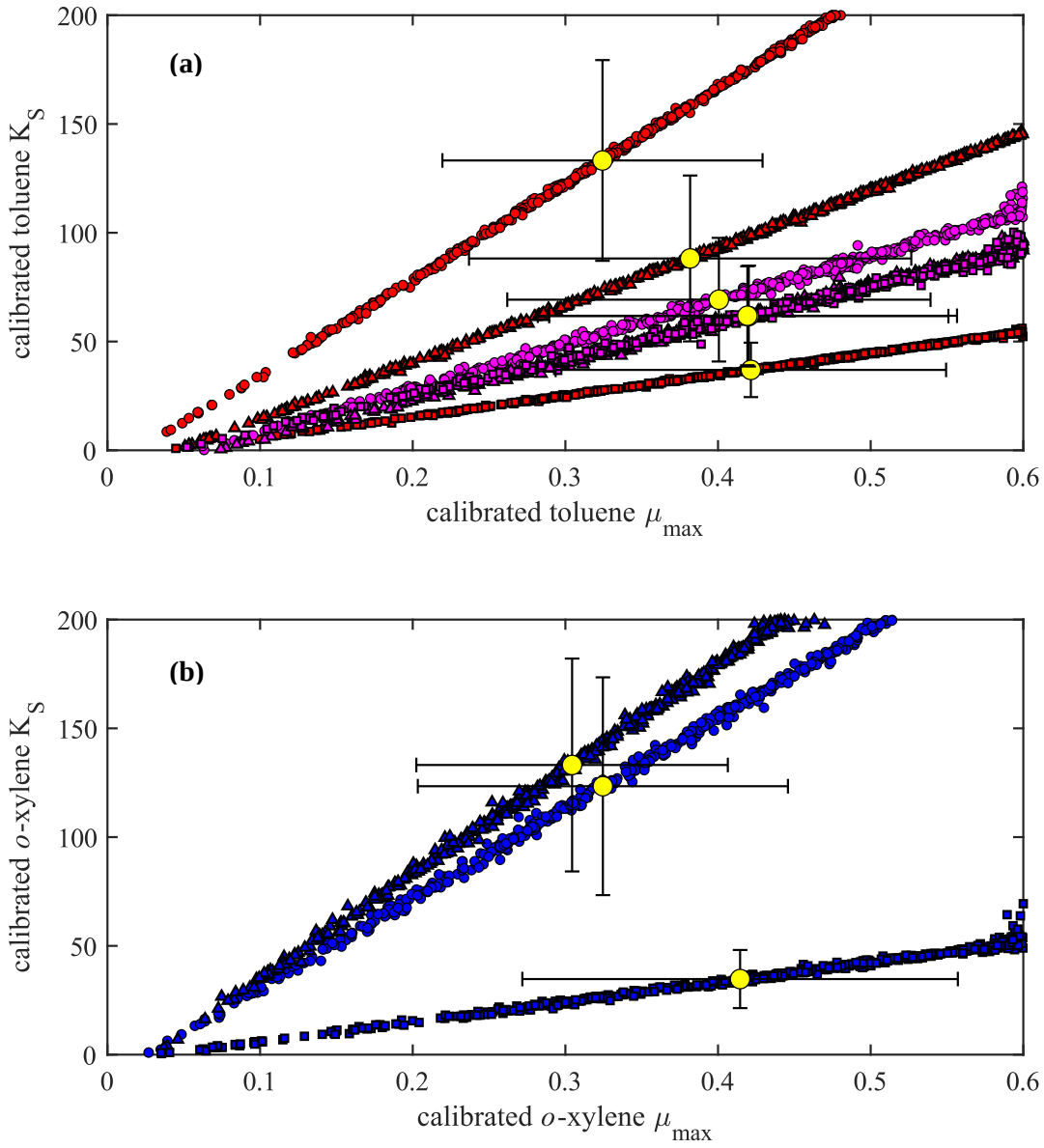

Figure 4.22 Calibrated parameters (μ_{max} and K_S) for (a) toluene in single (●) and multi-compound (●) microcosms and (b) *o*-xylene (●) in multi-compound microcosms representing the 500 best solutions of DDS trials with 100 iterations per trial for BA (●), A-BA (▲) and A-BA-PAC (■) microcosms. Mean calibrated parameters (●) are listed in Table 4.3.

Table 4.3 Summary of mean calibrated maximum specific growth rates ($\bar{\mu}_{max}$) and half-velocity constants ($\bar{K}_S$) for BA, A-BA, and A-BA-PAC microcosms.

		BA	A-BA	A-BA-PAC
		Toluene		
Single compound	$\bar{\mu}_{max}$ (1/d)	0.324 ± 0.105	0.382 ± 0.145	0.422 ± 0.128
Multi-compound	$\bar{\mu}_{max}$ (1/d)	0.401 ± 0.139	0.420 ± 0.131	0.419 ± 0.137
Single compound	$\bar{K}_S$ (mg/L)	133 ± 46	88 ± 38	37 ± 13
Multi-compound	$\bar{K}_S$ (mg/L)	69 ± 28	62 ± 23	62 ± 23
		o-Xylene		
Multi-compound	$\bar{\mu}_{max}$ (1/d)	0.325 ± 0.121	0.304 ± 0.102	0.414 ± 0.143
	$\bar{K}_S$ (mg/L)	123 ± 50	133 ± 49	35 ± 13

Like the SiREM culture vessel simulations, there is significant correlation between the mean calibrated $\bar{\mu}_{max}$ and $\bar{K}_S$ values. Parameter values are not normally distributed, necessitating non-parametric statistical analyses. Application of the Wilcoxon rank sum method was used to compare the median calibrated kinetic parameters for all combinations of microcosms (Appendix A), but comparisons between PAC (A-BA-PAC) and non-PAC (BA and A-BA) microcosms in single and multi-compound systems were of particular interest. For toluene in single compound microcosms, median μ_{max} and K_S values for non-PAC microcosms were statistically different from those in PAC microcosms ($p < 0.05$). For toluene in multi-compound microcosms, the median μ_{max} and K_S in the BA microcosms were statistically different than those in the PAC microcosms ($p < 0.05$), but the median μ_{max} and K_S in A-BA microcosms were not statistically different from those in PAC microcosms ($p > 0.05$ for μ_{max} and K_S respectively). For *o*-xylene in the multi-compound microcosms, the median μ_{max} and K_S for non-PAC microcosms were statistically different from those in the PAC microcosms ($p < 0.05$). As discussed in Section 4.1.2.6, when K_S is fixed at 20 mg/L and μ_{max} is the only calibration parameter, calibrated μ_{max} values become normally distributed facilitating comparison using a *t*-test. Paired statistical tests between all combinations of microcosms showed that $\bar{\mu}_{max}$ values were statistically different ($p < 0.05$) (Appendix A).

Based on the sensitivity analyses of the simulation of the A-BA-PAC microcosms, the results are most sensitive to changes in the individual sorption characteristics of compounds and the initial biomass in the microcosm. In the single compound microcosms, X_0 for toluene was the most sensitive parameter (with respect to both $\bar{\mu}_{max}$ and $\bar{K}_S$ for toluene). In this case, the calibrated kinetic parameters were most dependent on the initial concentration of toluene-degrading biomass in the microcosm, as opposed to the sorption characteristics of toluene. This is likely due to the impact

initial biomass has on the degradation rate of the first mass spike of toluene, which will have a direct impact on both calibrated kinetic parameters. Similarly, in the multi-compound microcosms, X_0 for toluene was the most sensitive parameter with respect to $\overline{K_S}$ for toluene. However, in the multi-compound systems, a_i for benzene was the most sensitive parameter with respect to $\bar{\mu}_{max}$ for toluene, indicating that the sorption of benzene has a more significant impact on the mean calibrated biomass growth rate ($\bar{\mu}_{max}$) than in a single compound system, perhaps due increased competition for sorption sites as a result of the elevated concentrations of benzene (which was assumed to not biodegrade). Sorption parameters were much more sensitive with respect to the mean calibrated *o*-xylene kinetics; n_f for *o*-xylene was the most sensitive parameter with respect to $\bar{\mu}_{max}$ for *o*-xylene, and a_i for benzene was the most sensitive parameter with respect to $\overline{K_S}$ for *o*-xylene. n_f for *o*-xylene impacts the sorbed concentration of *o*-xylene, and a change in *o*-xylene availability in the aqueous phase had the most significant impact on the growth rate ($\bar{\mu}_{max}$) of *o*-xylene degraders. a_i for benzene, as described above, indicates that a change in the degree of competition between benzene (present at elevated concentrations due to an absence of biodegradation) has a significant impact on $\overline{K_S}$ for *o*-xylene.

In single compound microcosms, the calibrated toluene kinetics were all statistically different ($p < 0.05$) and improved ($\bar{\mu}_{max}$: 0.324 < 0.382 < 0.422 /d [BA < A-BA < A-BA-PAC], $\overline{K_S}$: 133 > 88 > 37 [BA > A-BA > A-BA-PAC]) as the simulated sorbed fraction of toluene increased (sorbed percentage of toluene in a single compound system: 0% < 3% < 67-96% [BA (no solids) < A-BA (BS) < A-BA-PAC (PAC + BS)]). In the multi-compound systems, while the calibrated toluene kinetics for the A-BA and A-BA-PAC microcosms were not statistically different, they were statistically different from and improved compared to the calibrated toluene kinetics for the BA microcosms ($\bar{\mu}_{max}$ = 0.401 /d and $\overline{K_S}$ = 69 mg/L [BA], $\bar{\mu}_{max}$ = 0.420 /d and $\overline{K_S}$ = 62 mg/L [A-BA], $\bar{\mu}_{max}$ = 0.419 /d and $\overline{K_S}$ = 62 mg/L [A-BA-PAC]). $\bar{\mu}_{max}$ and $\overline{K_S}$ for toluene in multi-compound systems lay between the calibrated $\bar{\mu}_{max}$ and $\overline{K_S}$ parameters for toluene in single compound A-BA and A-BA-PAC microcosms ($\bar{\mu}_{max}$: A-BA-Tol < BA-BTX < A-BA-PAC-BTX < A-BA-BTX < A-BA-PAC-Tol, K_S: A-BA-Tol > BA-BTX > A-BA-PAC-BTX = A-BA-BTX > A-BA-PAC-Tol). This suggests that in the presence of co-contaminants like *o*-xylene and benzene and competitive sorption (sorbed percentage of toluene in a multi-compound system: 0% [BA, no solids], 3% [A-BA, BS], and 35-72% [A-BA-PAC, PAC + BS]), the effect of improved calibrated toluene kinetics due to sorption onto PAC, which was observed in the single compound experiments, is diminished. This relationship was consistent for calibration efforts using one (μ_{max}) or two (μ_{max} and K_S) calibration parameters (Figure 4.21 and Figure 4.22).

In the multi-compound systems, calibrated *o*-xylene kinetics were all statistically different ($p < 0.05$). Kinetics in BA and A-BA microcosms were less than in the A-BA-PAC microcosms ($\bar{\mu}_{max}$: 0.304 < 0.325 < 0.414 /d [A-BA < BA < A-BA-PAC], $\overline{K_S}$: 133 > 123 > 35 [A-BA > BA > A-BA-PAC]). Improved kinetics corresponded to a significant increase in the amount of sorbed *o*-xylene due to sorption onto PAC (sorbed percentage of *o*-xylene in a multi-compound system: 0% [BA, no solids], 7% [A-BA, BS], and 68-94% [A-BA-PAC, PAC + BS]). This relationship was consistent for calibration efforts using one (μ_{max}) or two (μ_{max} and K_S) calibration parameters [Figure 4.21 and Figure 4.22].

Based on evidence that:

- Calibrated toluene kinetics are improved in the presence of PAC in single compound systems,
- Calibrated toluene kinetics for A-BA and A-BA-PAC multi-compound systems are not statistically different from each other, but are poorer than toluene kinetics in single compound A-BA-PAC microcosms, and
- Calibrated *o*-xylene kinetics are improved in the presence of PAC in multi-compound systems,

the simulation results suggest that while PAC seems to increase degradation kinetics of PHCs (i.e., toluene in single compound systems and *o*-xylene in multi-compound systems), this effect is inhibited to some degree in the presence of more competitive compounds (i.e., toluene kinetics were slower in a multi-compound PAC system than in a single compound PAC system). In the case of a single compound system, there are more opportunities for that compound (i.e., toluene) to sorb, and it is speculated that this creates a higher concentration of the PHC available for destruction by its associated degraders present on the surface of the PAC through an extension of the contact time between PHCs and biomass (Fan et al., 2017). Higher rates of PHC degradation and higher biomass concentrations can promote the formation of biofilm on the surface of PAC, which causes nutrient and genetic exchange between populations and resistance against predation (Kjellerup & Edwards, 2013). If a more competitive compound (e.g., *o*-xylene) is introduced in the system, the sorption affinity of the original compound decreases, and its degradation kinetics become slower. Likewise, the kinetics of the more competitive compound are improved.

4.2 One-Dimensional Model

The 1D model was used to investigate the behaviour of various scenarios representing a PAC treatment zone within an experimental column. Validation of the model's ability to represent advective-dispersive transport was completed using results from a conservative tracer study on a 12-cm long column with a central BS+PAC zone and comparison with an existing analytical solution. Using the transport parameters from the tracer study, simulations reflecting a single compound (toluene) adsorption-desorption experiment were completed to investigate the ability of the 1D model to accurately reflect effluent toluene concentrations. Building on the findings from the microcosm modelling effort and 1D simulation of the 12-cm column, a series of scenarios were completed reflecting hypothetical conditions of a longer 37-cm long column.

4.2.1 Tracer Study

Transport parameter (ϕ and α_L) estimation was completed using aqueous effluent concentration data from a tracer test in the 12-cm long column. The objective function was the RMSE between observed and simulated bromide effluent concentrations. A single DDS trial of 100 iterations was completed for the data set, and simulated values were validated using the Ogata-Banks solution (Figure 4.23).

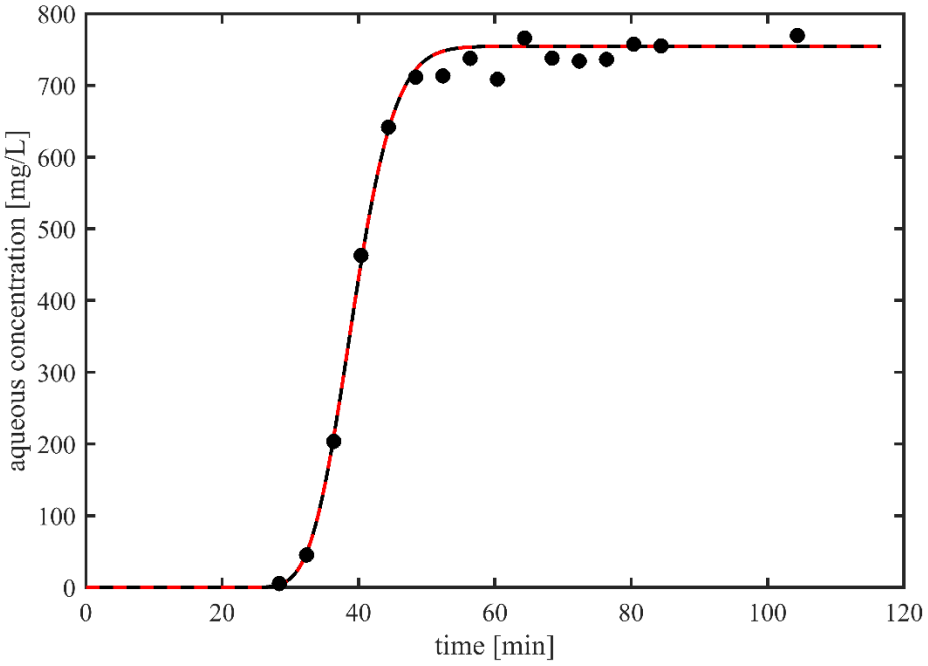

Figure 4.23 12 cm column effluent observed (●) and simulated aqueous bromide concentrations (ϕ = 0.348 and α_L = 9.30×10^{-4} m) using the 1D model (—) and the Ogata-Banks solution (– –). Each data point represents a single aqueous phase bromide measurement.

Calibrated ϕ and α_L were 0.348 [-] and 9.30×10^{-4} m respectively. The 1D model yields effluent concentrations essentially identical to the Ogata-Banks solution, validating the advective-dispersive transport component of the 1D model.

4.2.2 Adsorption/Desorption Experiment

Simulation of the single compound (toluene) adsorption/desorption experiment was completed to investigate the ability of the model to simulate PHC sorption on BS and PAC. Simulation results (1) without PAC, (2) with PAC and no hysteresis, and (3) with PAC and reversible hysteresis are displayed in Figure 4.24.

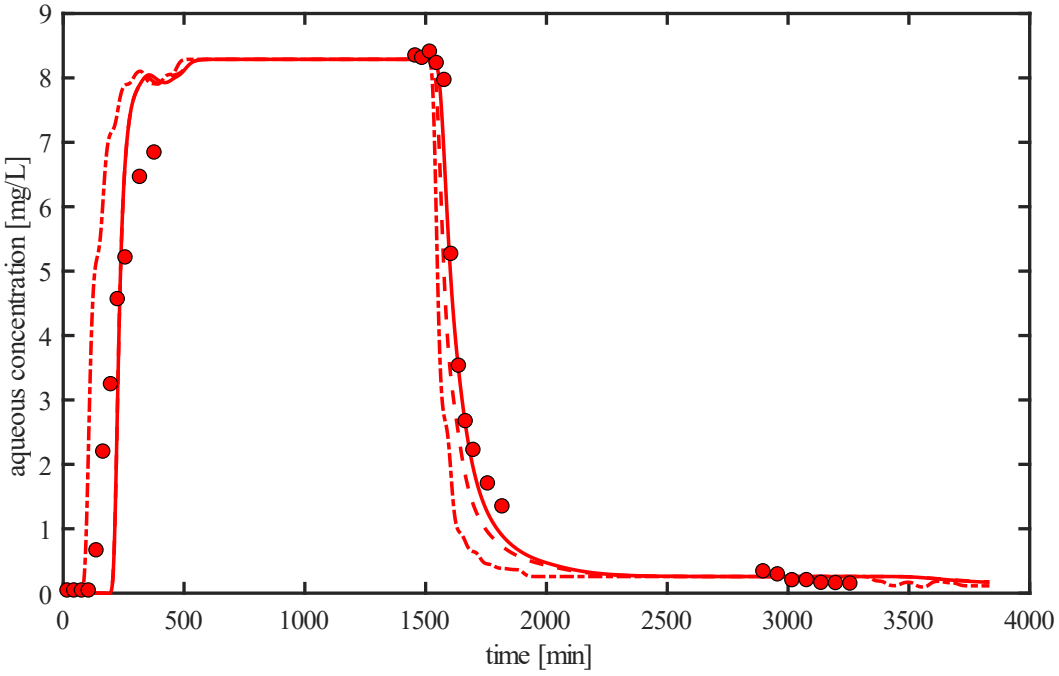

Figure 4.24 12 cm column effluent observed (●) and simulated aqueous toluene concentrations with no PAC (—·—), with PAC and no hysteresis (—), and with PAC and reversible hysteresis (—) (Equations (3.10) to (3.12), a = 0, b = 864, c = 1.11).

The oscillations near the peak of the rising limb of the effluent breakthrough curve (BTC) near 400 minutes is attributed to the rising and falling influent time series used to generate the influent signal (Figure 3.16). The RMSE for simulation (1), (2), and (3) were 11.48, 5.15, and 6.36 mg/L respectively. The simulation with no PAC had the largest overall RMSE and greatest mismatch of the rising and falling limbs of the toluene BTC, indicating, as expected, that PAC had an impact on toluene transport. While the simulations for PAC with hysteresis and no hysteresis coincide on the rising limb of the BTC because hysteresis is only relevant during desorption, the simulation with no hysteresis has a lower RMSE (1.39 mg/L) for the falling limb of the toluene BTC (1,456 minutes to

the end of the experiment) than the simulation with hysteresis (4.01 mg/L). The simulation with hysteresis has higher sorbed phase concentrations during desorption, leading to less toluene mass in the aqueous phase during desorption and a faster decrease in aqueous concentrations in the simulated column effluent. Based on evidence from comparing simulated BTCs to observed effluent toluene concentrations, the addition of hysteresis does not improve prediction and will be ignored in the investigative scenarios.

4.2.3 Investigative Scenarios

All scenarios simulated the transport of a multi-compound solution of PHCs (BTX, 20 mg/L for each compound) in a 37-cm long column with and without a central BS+PAC zone (6 cm, 0.02% f_{PAC}).

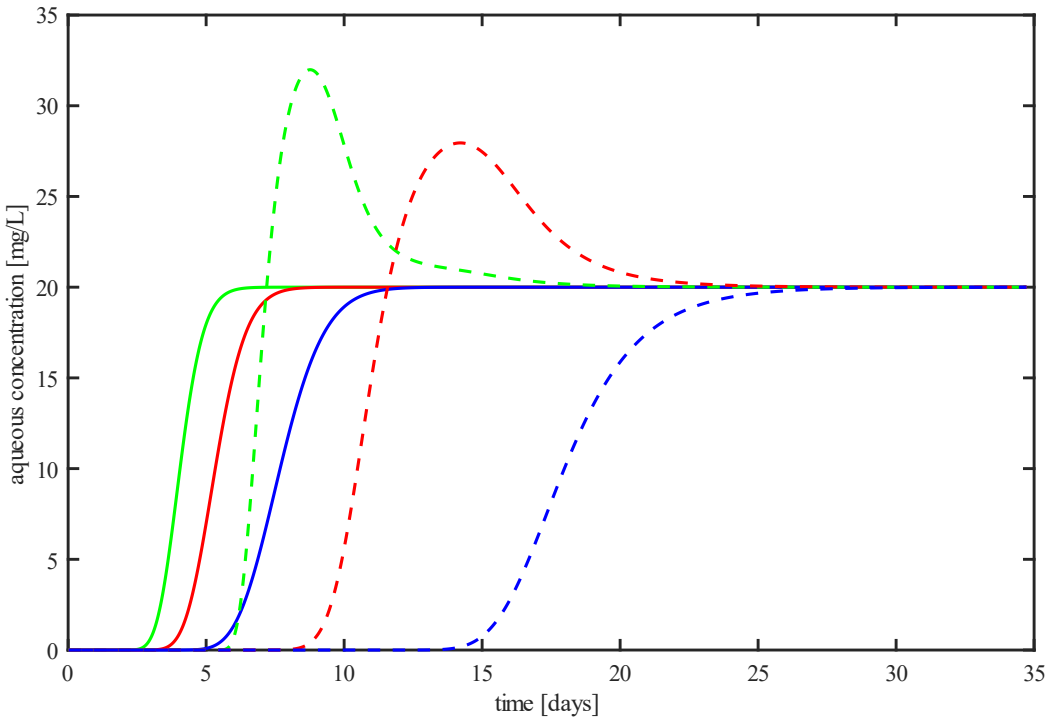

Figure 4.25 Scenario 1 simulated aqueous BTC concentrations with no PAC for benzene (—), toluene (—), and *o*-xylene (—), and with PAC for benzene (— —), toluene (— —), and *o*-xylene (— —).

The effluent BTC concentrations for Scenario 1 (no biodegradation) with and without a PAC zone is displayed in Figure 4.3. As expected, arrival of BTX occurs earlier with no PAC present due to lower sorbed PHC concentrations with breakthrough occurring in an order predicted by the linear partition coefficient (K_p) (B < T < X). When a PAC zone is present, breakthrough follows the order expected based on the Freundlich sorption parameters (K_f and n_f) and competition coefficients (a_i) for each PHC (B < T < X). Effluent concentrations higher than influent concentrations (20 mg/L for each

of B, T, and X) are observed for benzene and toluene, which is a result observed in multi-compound breakthrough experiments (Lillo-Ródenas et al., 2006) and manifests in the simulation because of competitive sorption and ISIAS theory.

Simulated aqueous effluent concentrations for Scenario 2 with biodegradation of benzene, toluene, and *o*-xylene using kinetic parameters from the batch reactor simulations (Section 4.1.2) are displayed in Figure 4.26. Yield coefficients (Y) and endogenous decay coefficients (K_d) for BTX in both BS and PAC zones were the same fixed values used in the batch reactor modelling (Y = 0.12 g/g and K_d = 0.01 /d). Calibrated maximum specific growth rates (μ_{max}) and half-velocity constants (K_S) for benzene from the SiREM culture vessel simulations were used for both BS and BS+PAC zones (μ_{max} = 0.165 /d and K_S = 147 mg/L). For toluene and *o*-xylene, separate calibrated maximum specific growth rates (μ_{max}) and half-velocity constants (K_S) were used for BS and BS+PAC zones based on the results from the A-BA (BS: μ_{max} = 0.420 /d, K_S = 62 mg/L for toluene and μ_{max} = 0.304 /d, K_S = 133 mg/L for *o*-xylene) and A-BA-PAC microcosm simulations (BS+PAC: μ_{max} = 0.419 /d, K_S = 62 mg/L for toluene and μ_{max} = 0.414 /d, K_S = 35 mg/L for *o*-xylene).

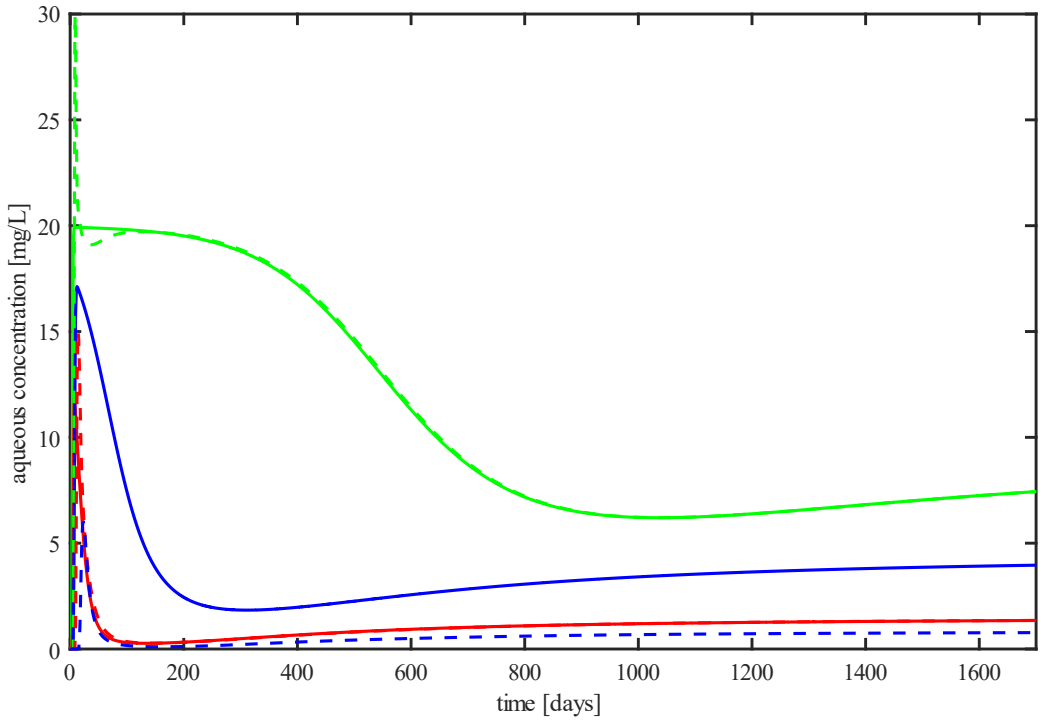

Figure 4.26 Scenario 2 simulated aqueous BTC concentrations in a bioaugmented column with no PAC for benzene (—), toluene (—), and *o*-xylene (—), and with PAC for benzene (— —), toluene (— —), and *o*-xylene (— —).

After initial breakthrough in the first ~20 days, simulated effluent toluene concentrations decrease the fastest, followed by *o*-xylene and eventually benzene. After breakthrough, the simulated effluent concentrations for benzene and toluene with and without PAC essentially overlap. Fixed benzene and toluene kinetic parameters are identical in the PAC and no-PAC systems except for the toluene maximum specific growth rate, which are only marginally different (μ_{max} = 0.420 /d for BS and 0.419 /d for BS+PAC). The simulated effluent aqueous concentrations at 1700 days for benzene, toluene, and *o*-xylene were 7.44, 1.35, and 3.96 mg/L respectively. Figure 4.27 displays various mass compartments in the 1D simulation, including cumulative influent, effluent, and biodegraded mass. Instantaneous compartment masses including aqueous, sorbed (sand and PAC) and biomass are also shown only for the central 6 cm zone in the column to facilitate comparison between scenarios. Initial decreases in aqueous BTX effluent concentrations are due to the growth of biomass in the central zone, which eventually reaches a peak at ~400 days for toluene and *o*-xylene, and ~1100 days for benzene. Biomass concentrations decrease after this point and appear to be approaching steady-state. The only significant difference in cumulative mass biodegraded is that the cumulative biodegraded mass of *o*-xylene in the column with PAC is higher.

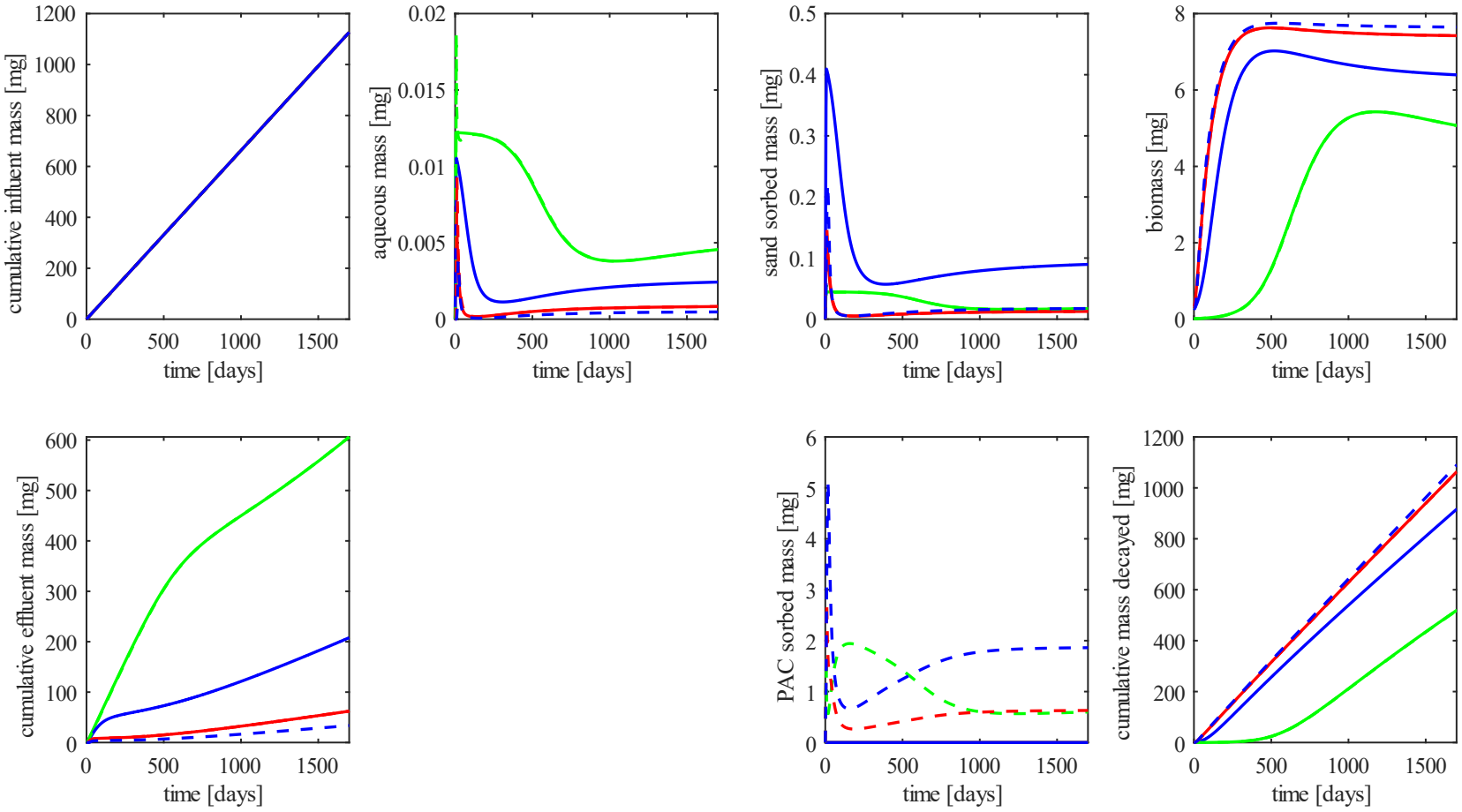

Figure 4.27 Scenario 2 simulated cumulative and compartment PHC masses in column with no PAC for benzene (—), toluene (—), and *o*-xylene (—), and with PAC for benzene (— —), toluene (— —), and *o*-xylene (— —). Aqueous mass, sorbed mass (sand and PAC), and biomass plots represent the central (BS+PAC) zone only.

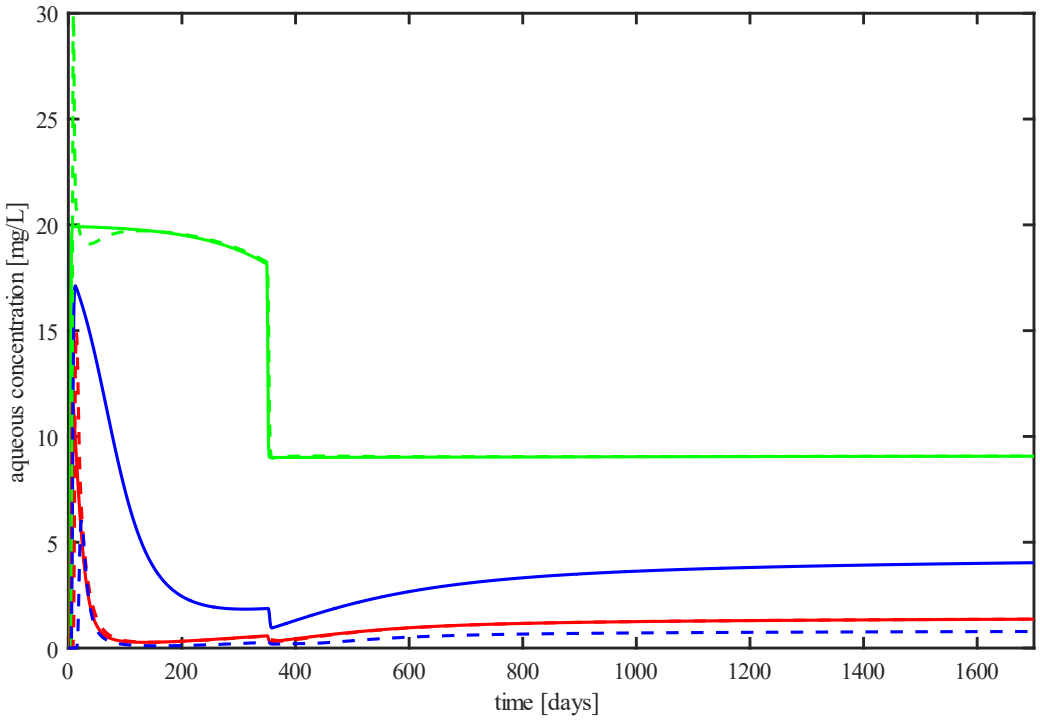

Figure 4.28 Scenario 3 simulated aqueous BTC concentrations in a bioaugmented column with no PAC for benzene (—), toluene (—), and *o*-xylene (—), and with PAC for benzene (– –), toluene (– –), and *o*-xylene (– –). A reduction in influent aqueous phase concentration from 20 mg/L to 10 mg/L for each of benzene, toluene, and *o*-xylene occurs on Day 347.

Figure 4.28 shows the results from Scenario 3 where a reduction in influent aqueous BTX concentrations from 20 mg/L to 10 mg/L at 347 days (20% of the total simulation time) was implemented. All kinetic parameters were the same as Scenario 2. As expected, the BTC results are the same as Scenario 2 for the first 347 days, followed by a drop in aqueous effluent concentrations. Benzene appears to reach a steady-state concentration, while toluene and *o*-xylene concentrations increase and approach what appears to be near steady-state concentrations. The simulated effluent aqueous concentrations at 1700 days for benzene, toluene, and *o*-xylene were 9.07, 1.37, and 4.03 mg/L respectively, which are comparable to Scenario 2 (7.44, 1.35, and 3.96 for benzene, toluene, and *o*-xylene respectively).

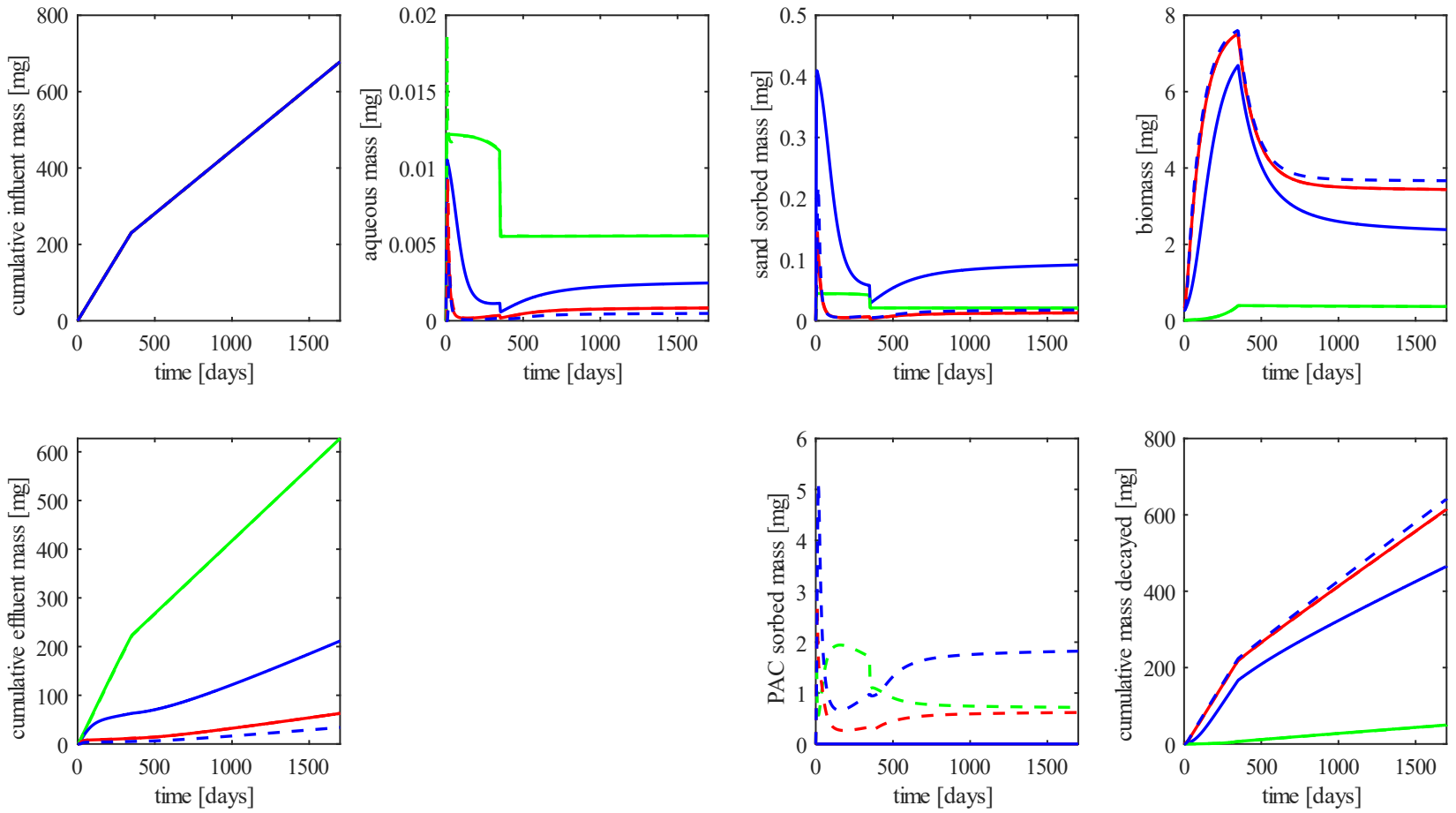

Figure 4.29 Scenario 3 simulated cumulative and compartment PHC masses in column with no PAC for benzene (—), toluene (—), and *o*-xylene (—), and with PAC for benzene (— —), toluene (— —), and *o*-xylene (— —). Aqueous mass, sorbed mass (sand and PAC), and biomass plots represent the central (BS+PAC) zone only. A reduction in influent aqueous phase concentration from 20 mg/L to 10 mg/L for each of benzene, toluene, and *o*-xylene occurs on Day 347.

When simulated aqueous influent concentrations decrease (Day 347) there is a corresponding drop in PHC aqueous mass. Since the aqueous mass of toluene and *o*-xylene are already low due to significant biodegradation when the influent concentration reduction occurs, there is little impact on the aqueous and sorbed masses of both these compounds. Conversely, benzene is not degraded significantly before the influent concentration reduction, so the drop in aqueous and sorbed masses for benzene is much more severe. Biomass for toluene and *o*-xylene experience significant decay after the influent concentration reduction, while benzene biomass remains constant. While the cumulative biodegraded mass for toluene and *o*-xylene is reduced compared to Scenario 2 (at Day 1700, reductions from 1,060 to 614 and 1,090 to 641 mg from Scenario 2 to Scenario 3 for toluene and *o*-xylene respectively), benzene displayed significantly reduced cumulative decayed mass (at Day 1700, reduction from 518 to 49 mg). This is due to lower biomass for benzene which plateaued at Day 347 in Scenario 3 but experienced significant growth after Day 347 in Scenario 2 without the reduction in influent aqueous concentrations.

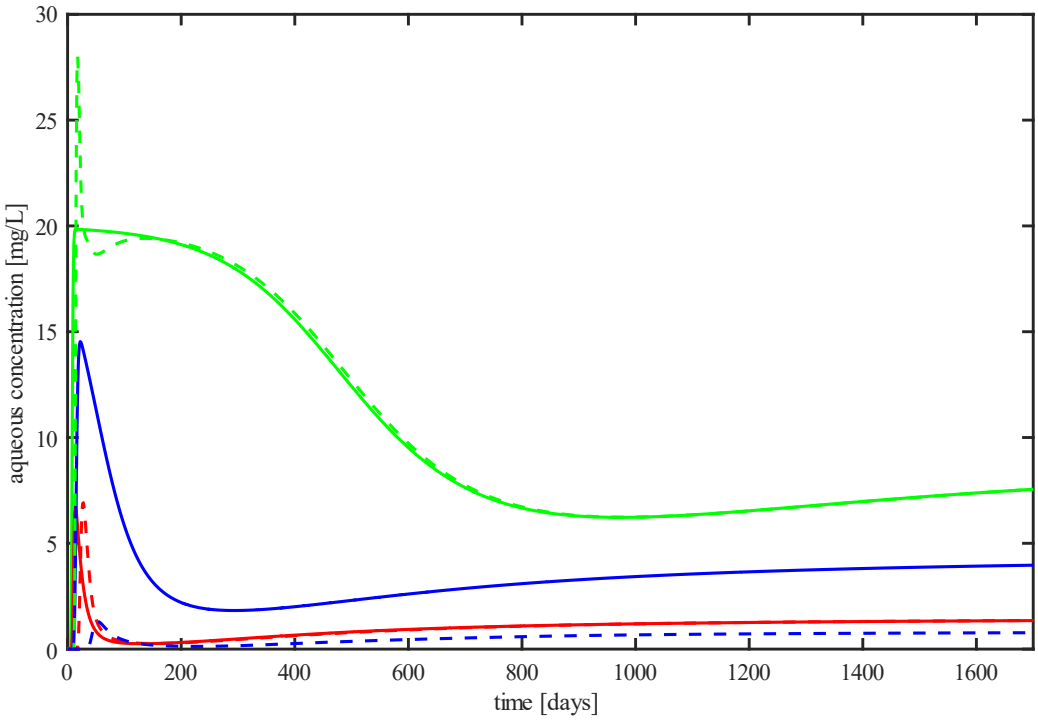

Figure 4.30 Scenario 4 simulated aqueous BTC concentrations in a bioaugmented column with no PAC for benzene (—), toluene (—), and *o*-xylene (—), and with PAC for benzene (— —), toluene (— —), and *o*-xylene (— —). This simulation had a 50% reduction in flowrate compared to Scenario 2.

The simulated BTCs for Scenario 4 with a reduced flowrate ($q = 1.74\times10^{-7}$ m/s, a 50% reduction from the Scenario 2 of 3.47×10^{-7} m/s) are shown in Figure 4.8. All kinetic parameters were the same as used in Scenario 2. The BTCs are like Scenario 2, with a slightly later breakthrough of BTX which

is pronounced for *o*-xylene when PAC is present. The simulated effluent aqueous concentrations at 1700 days for benzene, toluene, and *o*-xylene were 7.54, 1.35, and 3.97 mg/L respectively, which are comparable to Scenario 3 (7.44, 1.35, and 3.96 for benzene, toluene, and *o*-xylene respectively). The temporal variation of mass in each compartment is similar to Scenario 2, with the aqueous, sand, and PAC sorbed BTX masses showing the same trends and approach the same steady-state concentrations. The cumulative influent, effluent, and biodegraded mass for all compounds are 50% of those for Scenario 2, corresponding to the 50% reduction in BTX mass loading resulting from the lower flow rate. Biomass for each PHC was also halved and exhibited the same shape as the biomass profiles for Scenario 2.

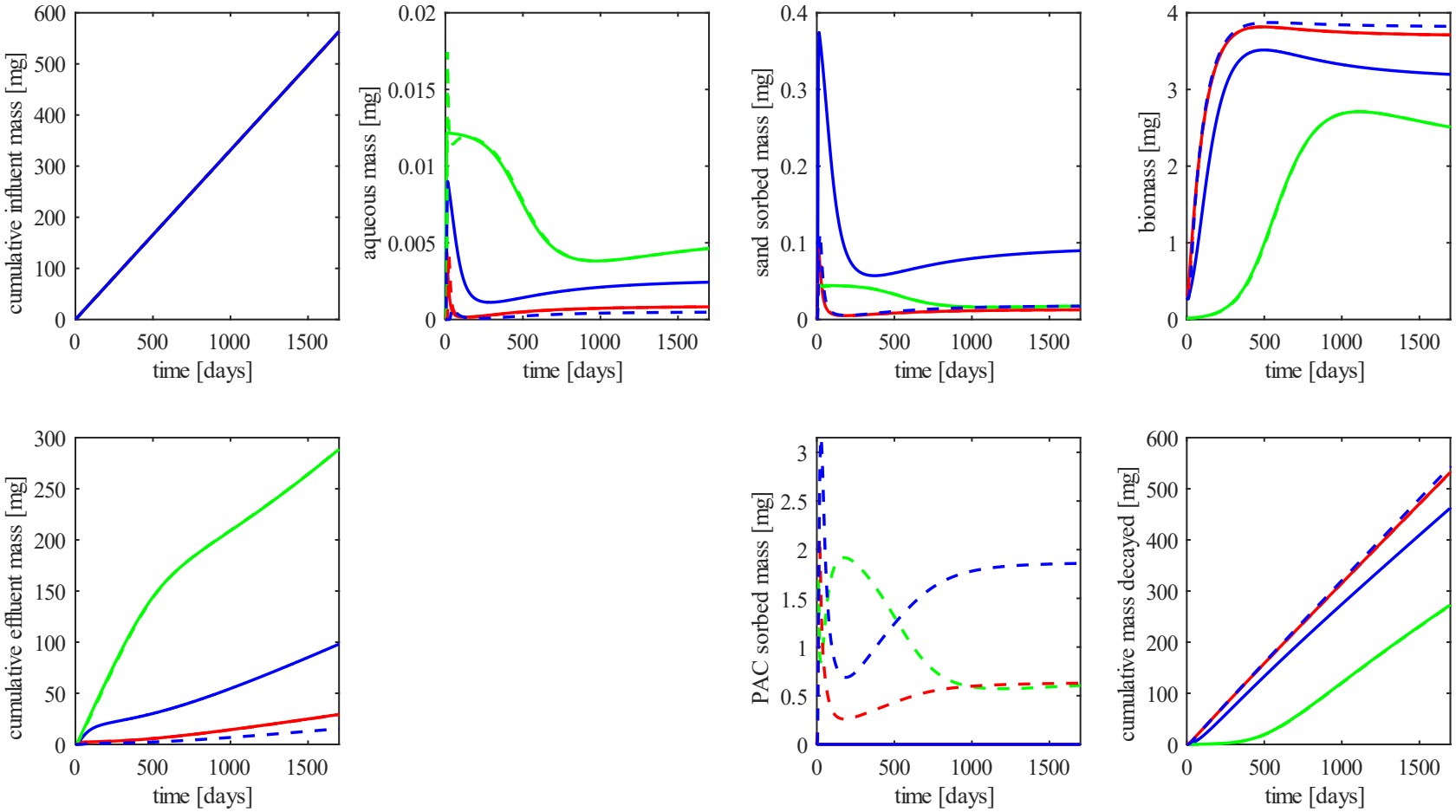

Figure 4.31 Scenario 4 simulated cumulative and compartment PHC masses in column with no PAC for benzene (—), toluene (—), and *o*-xylene (—), and with PAC for benzene (— —), toluene (— —), and *o*-xylene (— —). Aqueous mass, sorbed mass (sand and PAC), and biomass plots represent the central (BS+PAC) zone only. This simulation had a 50% reduction in flowrate compared to Scenario 2.

The results for Scenario 5 (where the biomass growth rate was assumed to be proportional to the biomass concentration) are shown in Figure 4.32, and with no PAC they are the same as Scenario 2 (μ_{max} is constant) as expected. When PAC is present, there is essentially no aqueous effluent concentration for toluene and *o*-xylene (completely biodegraded in the column). Benzene appears in the effluent but experiences a steep decline in concentration from Day 100 to Day 160, eventually reaching an aqueous concentration of essentially zero. The mass for toluene and *o*-xylene in all compartments overlap when PAC is present (Figure 4.11). Mass in the aqueous and sorbed compartments when PAC is present approach zero with benzene taking the longest time to decrease (Day 100 to Day 160). This is likely due to a delay in biomass growth for benzene, which has a smaller μ_{max} compared to toluene and *o*-xylene. The cumulative mass biodegraded for benzene, toluene, and *o*-xylene are all higher compared to Scenario 2 when PAC is present. The aqueous effluent benzene concentration is essentially zero after Day 160 while for toluene and *o*-xylene effluent concentrations are essentially zero after Day 20.

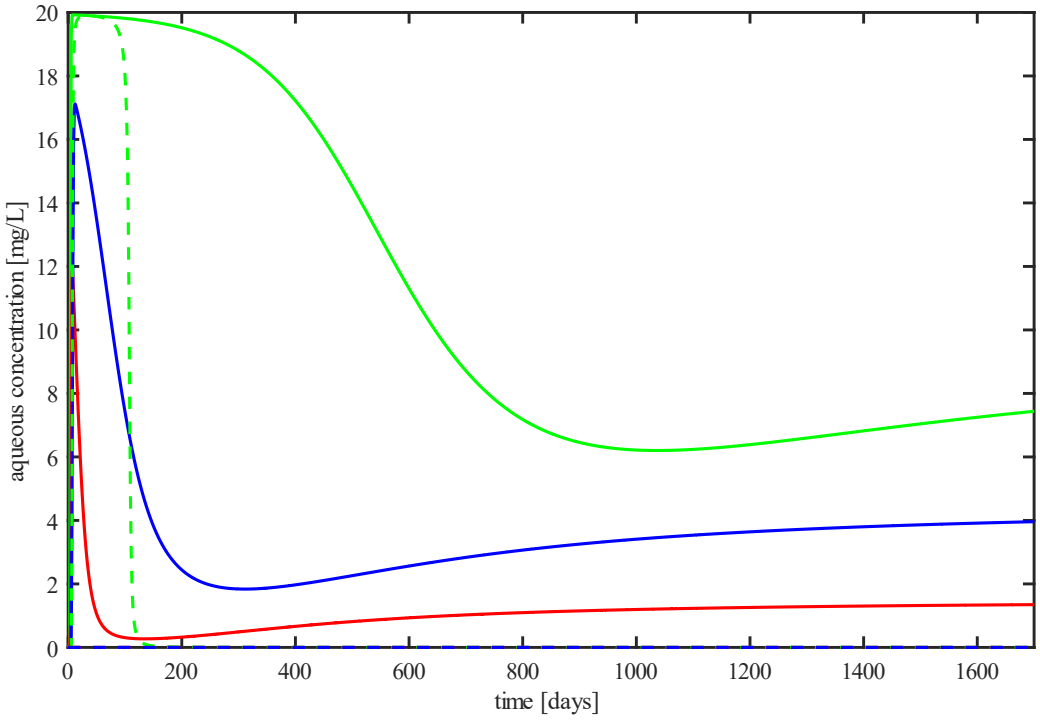

Figure 4.32 Scenario 5 simulated aqueous BTC concentrations in a bioaugmented column with no PAC for benzene (—), toluene (—), and *o*-xylene (—), and with PAC for benzene (— —), toluene (— —), and *o*-xylene (— —). This simulation is a hypothetical relationship where growth is proportional to biomass concentration.

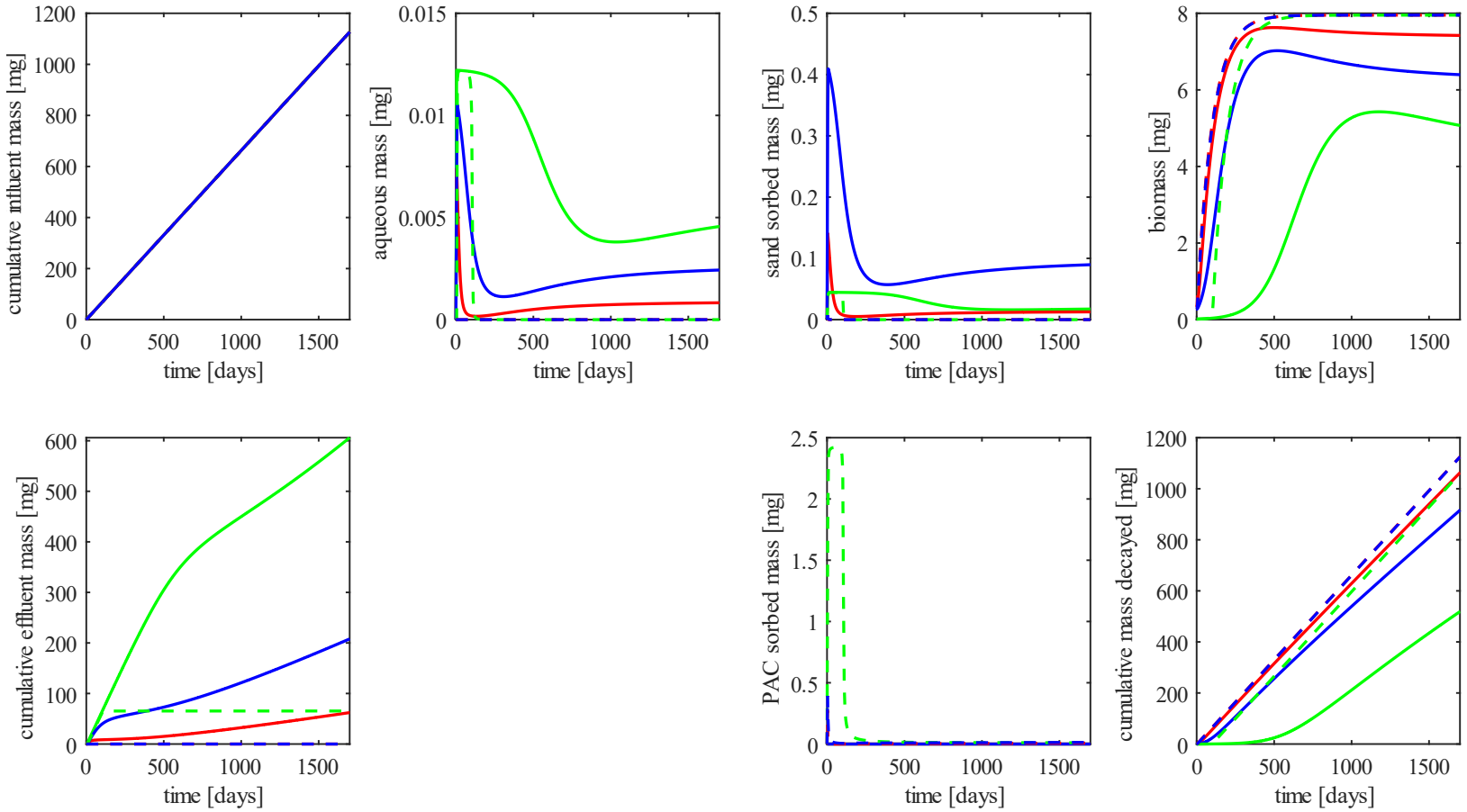

Figure 4.33 Scenario 5 simulated cumulative and compartment PHC masses in column with no PAC for benzene (—), toluene (—), and *o*-xylene (—), and with PAC for benzene (— —), toluene (— —), and *o*-xylene (— —). Aqueous mass, sorbed mass (sand and PAC), and biomass plots represent the central (BS+PAC) zone only. This simulation is a hypothetical relationship where growth is proportional to biomass concentration.

4.2.4 Summary

The results of the adsorption/desorption experiment indicated that the inclusion of hysteresis in the model did not improve the comparison between simulated and observed effluent toluene concentrations.

An increase in cumulative mass biodegraded for *o*-xylene with PAC present compared to simulations with no PAC was observed across all investigative scenarios and was due to a higher *o*-xylene maximum specific growth rate (μ_{max}) for the PAC zone. A reduction in PHC mass loading (Scenarios 3 and 4) had the expected impact with breakthrough occurring later; however, the steady-state concentrations for the PAC and no-PAC systems were similar. Scenario 5 with a maximum specific growth rate that increased with biomass concentration in the PAC zone displayed the lowest simulated effluent aqueous BTX concentration. Effluent toluene and *o*-xylene concentrations in this scenario were essentially zero for the duration of the simulation, and while benzene initially broke through, simulated effluent aqueous concentrations were reduced to essentially zero by Day 160 following an increase in biomass.

These results suggest that if the presence of PAC improves biodegradation kinetics (such as a higher maximum specific growth rate), effluent aqueous PHC concentrations will be significantly reduced. This was observed for *o*-xylene in all scenarios using kinetic parameters from the microcosm simulations, and for BTX in the Scenario 5 where the maximum specific growth rates were an assumed function of biomass concentrations (a scenario meant to represent conditions potentially resulting from biofilm formation on the PAC).

Chapter 5
Conclusions and Recommendations

5.1 Conclusions

A batch reactor model and a one-dimensional (1D) model were primarily developed to simulate sorption, desorption and biodegradation of multiple petroleum hydrocarbons (PHCs) in experimental laboratory systems (i.e., microcosms and columns) containing powdered activated carbon (PAC). The batch reactor model was used to simulate two large vessels of benzene-degrading bioaugmentation cultures as well as a series of single (toluene) and multi-compound (benzene, toluene, and *o*-xylene; BTX) sand/PAC microcosms with both indigenous and bioaugmentation cultures. The 1D model was used to investigate the impact of desorption hysteresis in a column packed with sand and PAC and subjected to a finite step injection of toluene, as well as a series of scenarios representing a PAC treatment zone in an experimental column subjected to benzene, toluene, and *o*-xylene.

Aqueous benzene concentration data from the large vessels of benzene-degrading culture were used to evaluate the biodegradation portion of the batch reactor model. Results indicated that when five calibration parameters (X_0, μ_{max}, Y, K_S, and K_d) were used a unique solution was difficult to obtain. Therefore, restricting the decision space to two calibration parameters (μ_{max} and K_S) permitted comparison of benzene degradation kinetics between culture vessels but required an analysis of parameter uncertainty. This strategy is only feasible when estimates of fixed kinetic parameters are readily available, whether from relevant literature (e.g., for Y and K_d) or from direct measurement (e.g., for X_0). While the maximum specific growth rates (μ_{max}) and half-velocity constants (K_S) for the two vessels were similar but statistically different, the older of the two vessels may have improved kinetics (higher μ_{max} and lower K_S) because the culture was more established. A sensitivity analysis identified that the calibrated value of μ_{max} was most sensitive to variations in the fixed parameter K_d.

Sorbed concentrations simulated using single compound isotherm parameters and multi-compound competition coefficients tended to overpredict observed sorbed concentrations in both the single and multi-compound microcosm systems. The observed experimental data indicated that when aqueous toluene was < MDL in the single compound microcosms, sorbed concentrations were also < MDL. In this case, reversible hysteresis would overpredict sorbed concentrations even more severely while irreversible hysteresis would predict non-zero sorbed concentrations at aqueous concentrations < MDL. A toluene adsorption/desorption experiment was conducted to investigate the impact of multiple desorption cycles on sorbed concentrations, and the data indicated that hysteresis was

insignificant. For these reasons, hysteresis was not included in the simulations involving PAC. The use of single compound isotherm parameters was sufficient to represent the equilibrium aqueous toluene concentrations in single compound microcosms with no biodegradation, and the addition of multi-compound competition coefficients permitted the prediction of equilibrium BTX concentrations in multi-compound systems with no biodegradation.

Observed microcosm data indicated that biodegradation by the indigenous microbial population was negligible and that aqueous benzene concentrations remained essentially constant in all microcosms. Therefore, indigenous biodegradation and biodegradation of benzene by bioaugmentation cultures was ignored in all microcosm simulations. Simulation results indicated that the calibrated kinetic parameters can generate the observed trends in aqueous PHC concentrations in both single and multi-compound bioaugmented microcosm systems, including systems with competitive PHC sorption onto PAC. Kinetics improved (i.e., higher μ_{max} and lower K_S) for the compound with the highest sorption affinity in the system, which was toluene in the single compound microcosms and *o*-xylene in the multi-compound systems. This finding was supported by simulations with two (μ_{max} and K_S) and one (μ_{max} alone) calibration parameter. The effect of PAC sorption on improved toluene kinetics for the single-compound system was significantly diminished in the multi-compound system. A sensitivity analysis was conducted on bioaugmented systems with PAC present and indicated that calibrated kinetic parameters (μ_{max} and K_S) were most sensitive to variations in initial biomass (X_0), and sorption parameters for PHCs present at high concentrations (benzene) and those with high sorption affinity (*o*-xylene).

Simulation results of an adsorption/desorption experiment involving a sand and PAC packed column demonstrated that the inclusion of desorption hysteresis in the 1D model does not improve the comparison to observed toluene breakthrough data. A series of investigative scenarios representing a PAC treatment zone in an experimental column showed that changes in multi-compound (BTX) PHC mass loading (lower flow rate or changes in influent concentration) had a minimal impact on the effluent PHC concentrations for both PAC and non-PAC systems. However, using kinetic parameters determined from the microcosm simulations with PAC present (i.e., a higher μ_{max} and lower K_S for *o*-xylene) resulted in increased cumulative mass biodegraded for *o*-xylene in all scenarios. In a hypothetical scenario where the maximum specific growth rate (μ_{max}) was assumed to be a function of biomass concentration, increased cumulative mass biodegraded and reduced steady-state aqueous effluent concentrations for all PHCs were observed. This suggests that kinetic improvements resulting from biofilm formation on PAC may lead to more effective long-term PHC treatment.

The following specifically addressed the two research questions presented in Section 1.2:

1. Can the complex dynamics involving AC particulate amendments be simulated at the bench-scale?

   Culture vessel and microcosm simulations demonstrated that the model was capable of simulating systems with biodegradation through the calibration of Monod kinetics parameters (μ_{max}, and K_S). Single compound sorption isotherms and competition coefficients were able to predict steady-state aqueous PHC concentrations in microcosm systems with PAC and no biodegradation. Evidence from simulated and sorbed concentration comparisons in microcosms with biodegradation suggest that hysteresis was minimal, and that sorption was primarily non-linear and competitive.

2. Does the presence of AC enhance the biodegradation of PHCs in bench-scale experiments?

   Single compound bioaugmented microcosm simulations displayed improved biodegradation kinetics (higher μ_{max}, lower K_S) in systems with PAC than those with no PAC. This effect was diminished in multi-compound systems with benzene, toluene, and *o*-xylene, with kinetic improvements instead seen in the compound with the highest sorption affinity (i.e., *o*-xylene). Using kinetic parameters obtained in the batch reactor modelling, 1D investigative scenarios of a hypothetical PAC treatment zone in an experimental column showed that while contaminant mass loading had minimal impact on treatment efficiency, improved kinetics in simulations with PAC displayed the most significant reduction in aqueous effluent PHC concentrations and increase in cumulative PHC mass biodegraded. A hypothetical scenario representing biofilm formation where the maximum specific growth rate (μ_{max}) was assumed a function of biomass concentration demonstrated that AC amendment performance can significantly degrade PHC mass and provide persistent and effective remediation in the long-term.

In summary, this research showed that sorption of PHCs onto PAC impacts biodegradation kinetics. The models developed provided insight into the synergy between sorption and biodegradation and provide a framework for comprehensive simulation of PAC treatment zones in the future.

5.2 Recommendations

Changes to experimental methods could be implemented to aid in model use and data interpretation. Batch reactor simulations assumed that the system was fully mixed, when it was only mixed briefly after re-spikes. Continuous shaking was not considered feasible so as not to interfere with the establishment of PHC degrading microorganisms; it is suspected that this lack of mixing resulted in non-equilibrium conditions between aqueous and sorbed PHC concentrations.

- Care should be taken in future work to ensure adequate mixing of batch reactors if sorption is assumed to occur instantaneously

Evidence from microcosm data with no biodegradation suggests that sampling losses accumulate over time if microcosms are repeatedly sampled.

- Efforts to minimize unknown sampling losses over time, such as the use of a greater number of bottles which are sacrificed after a sampling event, would provide greater certainty in concluding that mass loss is occurring due to mass removal rather than biodegradation

The uncertainty of mass re-spikes in both the culture vessels and microcosms necessitated the use of the initial aqueous phase PHC measurements (assumed to be in equilibrium with all phases) to determine the initial PHC system mass. All subsequent mass re-spikes had no immediate aqueous phase PHC measurement immediately following them, so they were assumed to be the actual spiked mass.

- Having aqueous phase PHC measurements after each subsequent mass re-spike would permit the use of these measurements to determine true initial PHC system mass after all mass additions

Estimates of some kinetic parameters (Y and K_d from literature and X_0 through measurement) were required to enable meaningful comparison between calibrated kinetic parameters across data sets. In future work, assuming calibration and optimization exercises utilize a similar strategy (minimizing RMSE between simulated and observed aqueous PHC concentrations), estimates of these parameters are required to restrict the decision space to a reasonable size.

- Measuring biomass over the experimental duration would permit the use of an additional calibration target (simulated and observed biomass concentrations) and thereby restrict the decision space

The modelling approach presented can simulate hysteresis for single compounds and competition for multiple compounds, but not both.

- Efforts to characterize simultaneously hysteretic and competitive sorption require a complete new set of multi-compound batch adsorption/desorption experiments; developing such an experiment and characterizing its results is likely a significant effort.

This research demonstrated the significant impact of competition on multi-compound sorption of PHCs on PAC but did not consider the impact of other sorbing compounds. In natural groundwater environments, NOM is ubiquitous to the aqueous phase and would interfere significantly with the adsorption capacity of AC. While concentrations in groundwater are highly variable, NOM is suspected to compete for sorption sites and may significantly reduce the treatment efficiency of an AC particulate amendment.

- Using more complex groundwater matrices (i.e., NOM, other PHCs) in isotherm development would permit the simulation of environmental conditions more representative of an *in situ* AC PRB

The developed models were used to simulate BTX. Model application can be extended to other contaminants with equally or less complex physical and chemical characteristics.

- Through the collection of relevant physical and chemical properties and sorption isotherms, numerous other contaminants (e.g., NOM, PFAS, pesticides, PAHs) can be modelled using both the batch reactor and 1D models

The models were also limited in numerous ways, providing opportunities for their extension. Both the batch reactor and 1D models assumed sorption was instantaneous.

- Accounting for sorption kinetics would permit the simulation of kinetically controlled sorption, as in a stagnant batch reactor or a flow through column experiment

More formal biofilm models have been developed for BAC systems, as discussed in Section 2.2.3. A simplistic approach was adopted for the models developed in this work, where biomass degrades

aqueous PHC mass according to a single set of Monod kinetics parameters that remain constant over the simulation duration.

- More complex models of biofilm development and PHC degradation may better represent the relationship between sorption and biodegradation in a PAC amendment system

The 1D model assumes saturated, steady-state, and isotropic groundwater flow, which is not representative of field-scale AC particulate amendments used to treat contamination in the vadose zone or in highly heterogeneous aquifers.

- The inclusion of unsaturated, variable, and anisotropic groundwater flow would extend the applicability of the model to three dimensions

The investigative scenarios presented in this research were limited in scope. Contaminant loading was varied by reductions in flow rate and influent concentrations of BTX, and biodegradation kinetics were altered using an assumed function relating the maximum specific growth rate to biomass concentrations.

- Various contaminant loading scenarios (e.g., different combinations of step loadings representing variation in contaminant source, or variations in groundwater flow rate due to precipitation events) would provide further insight into the effect of mass loading on treatment performance
- Further experimentation to relate biodegradation rates and biofilm growth are required to represent the dynamic behaviour of a biofilm

References

Abtahi, M., Fakhri, Y., Conti, G. O., Ferrante, M., Taghavi, M., Tavakoli, J., Heshmati, A., Keramati, H., Moradi, B., Amanidaz, N., & Khaneghah, A. M. (2018). The concentration of BTEX in the air of Tehran: A systematic review-meta analysis and risk assessment. *International Journal of Environmental Research and Public Health; Int J Environ Res Public Health*, *15*(9), 1837. https://doi.org/10.3390/ijerph15091837

Ahmad, A., Idris, A., & Hameed, B. (2013). Organic dye adsorption on activated carbon derived from solid waste. *Desalination and Water Treatment*, *51*(13–15), 2554–2563. https://doi.org/10.1080/19443994.2012.749019

Aktas, O., & Cecen, F. (2007). Competitive adsorption and desorption of a bi-solute mixture: effect of activated carbon type. *Adsorption : Journal of the International Adsorption Society*, *13*(2), 159–169. https://doi.org/10.1007/s10450-007-9017-5

Aktaş, Ö., & Çeçen, F. (2007). Adsorption, desorption and bioregeneration in the treatment of 2-chlorophenol with activated carbon. *Journal of Hazardous Materials*, *141*(3), 769–777. https://doi.org/10.1016/J.JHAZMAT.2006.07.050

Al-Hashimi, O., Hashim, K., Loffill, E., Marolt Čebašek, T., Nakouti, I., Faisal, A. A. H., & Al-Ansari, N. (2021). A Comprehensive Review for Groundwater Contamination and Remediation: Occurrence, Migration and Adsorption Modelling. *Molecules 2021, Vol. 26, Page 5913*, *26*(19), 5913. https://doi.org/10.3390/MOLECULES26195913

ASTM International. (2017). *ASTM D2862-16: Standard Test Method for Particle Size Distribution of Granular Activated Carbon*. https://www.astm.org/d2862-16.html

ASTM International. (2019). *ASTM D5158-98(2019): Standard Test Method for Determination of Particle Size of Powdered Activated Carbon by Air-Jet Sieving*. https://www.astm.org/d5158-98r19.html

Barker, J. P., Patrick, G. C., & Major, D. (1987). Natural Attenuation of Aromatic Hydrocarbons in a Shallow Sand Aquifer. *Ground Water Monitoring & Remediation*, *7*(1), 64–71. https://doi.org/10.1111/j.1745-6592.1987.tb01063.x

Bartlett, C. K., Slawson, R., & Thomson, N. R. (2019). Response of sulfate-reducing bacteria and supporting microbial community to persulfate exposure in a continuous flow system. *Journal of Environmental Monitoring; Environ.Sci.: Processes Impacts*, *21*(7), 1193–1203. https://doi.org/10.1039/c9em00094a

Bender, K. S., M., S. O., Coates, J. D., Lack, J. G., Chakraborty, R., Achenbach, L. A., & Cole, K. A. (2001). Anaerobic benzene oxidation coupled to nitrate reduction in pure culture by two strains

of Dechloromonas. *Nature (London); Nature*, *411*(6841), 1039–1043. https://doi.org/10.1038/35082545

Black & Veatch. (2008). *Evaluation & Assessment of Removal Technology for Specific Organic Contaminants in NJ Drinking Water*. https://www.nj.gov/dep/watersupply/pdf/treatment_b&v_final08_rpt.pdf

Bolden, A. L., Kwiatkowski, C. F., & Colborn, T. (2015). New Look at BTEX: Are Ambient Levels a Problem? *Environmental Science & Technology; Environ.Sci.Technol*, *49*(9), 5261–5276. https://doi.org/10.1021/es505316f

Bonaglia, S., Broman, E., Brindefalk, B., Hedlund, E., Hjorth, T., Rolff, C., Nascimento, F. J. A., Udekwu, K., & Gunnarsson, J. S. (2020). Activated carbon stimulates microbial diversity and PAH biodegradation under anaerobic conditions in oil-polluted sediments. *Chemosphere*, *248*, 126023. https://doi.org/10.1016/J.CHEMOSPHERE.2020.126023

Braida, W., Pignatello, J., Lu, Y., & Ravikovitch, P. (2003). Sorption hysteresis of benzene in charcoal particles. *Environmental Science & Technology*, *37*(2), 409–417. https://doi.org/10.1021/es020660z

Brosselin, P., Rudant, J., Orsi, L., Leverger, G., Baruchel, A., Bertrand, Y., Nelken, B., Robert, A., Michel, G., Margueritte, G., Perel, Y., Mechinaud, F., Bordigoni, P., Hémon, D., & Clavel, J. (2009). Acute childhood leukaemia and residence next to petrol stations and automotive repair garages: the ESCALE study (SFCE). *Occupational and Environmental Medicine (London, England); Occup Environ Med*, *66*(9), 598–606. https://doi.org/10.1136/oem.2008.042432

Carey, G. R., Mcgregor, R., Pham, A. L., Sleep, B., & Hakimabadi, S. G. (2019). Evaluating the longevity of a PFAS in situ colloidal activated carbon remedy. *Remediation Journal*, *29*(2), 17–31. https://doi.org/10.1002/rem.21593

Çeçen, F., & Aktaş, Ö. (2011). *Activated carbon for water and wastewater treatment; integration of adsorption and biological treatment* (Vol. 26, Issue 6). Ringgold, Inc.

Chan, P. Y., Lim, P. E., Ng, S. L., & Seng, C. E. (2018). Bioregeneration of granular activated carbon loaded with phenolic compounds: effects of biological and physico-chemical factors. *International Journal of Environmental Science and Technology*, *15*(8), 1699–1712. https://doi.org/10.1007/S13762-017-1527-4/FIGURES/6

Chatzopoulos, D., Varma, A., & Irvine, R. L. (1993). Activated carbon adsorption and desorption of toluene in the aqueous phase. *AIChE Journal*, *39*(12), 2027–2041. https://doi.org/10.1002/aic.690391213

Chen, W., & Wagenet, R. J. (1995). Solute Transport in Porous Media with Sorption-Site Heterogeneity. *Environmental Science & Technology; Environ.Sci.Technol*, *29*(11), 2725–2734. https://doi.org/10.1021/es00011a005

Considine, R., Denoyel, R., Pendleton, P., Schumann, R., & Wong, S.-H. (2001). The influence of surface chemistry on activated carbon adsorption of 2-methylisoborneol from aqueous solution. *Colloids and Surfaces A: Physicochemical and Engineering Aspects*, *179*, 271–280. www.elsevier.nl/locate/colsurfa

Crank, J., & Nicolson, P. (1947). A practical method for numerical evaluation of solutions of partial differential equations of the heat-conduction type. *Mathematical Proceedings of the Cambridge Philosophical Society*, *43*(1), 50–67. https://doi.org/10.1017/S0305004100023197

Cunningham, J. A., Rahme, H., Hopkins, G. D., Lebron, C., & Reinhard, M. (2001). Enhanced In Situ Bioremediation of BTEX-Contaminated Groundwater by Combined Injection of Nitrate and Sulfate. *Environmental Science & Technology; Environ.Sci.Technol*, *35*(8), 1663–1670. https://doi.org/10.1021/es001722t

de Jonge, J. R., Breure, A. M., & van Andel G., J. (1996). Reversibility of adsorption of aromatic compounds onto powdered activated carbon (PAC). *Water Research (Oxford)*, *30*(4), 883–892. https://doi.org/10.1016/0043-1354(95)00248-0

de León, G. R. R. D. (2021). *Impact of Anaerobic Biofilm Formation on Sorption Characteristics of Powdered Activated Carbon*. University of Waterloo.

DiGiano, F., Baldauf, G., Frick, B., & Sontheimer, H. (1980). *Simplifying the description of competitive adsorption for practical application in water treatment* (I. Suffett & M. McGuire, Eds.; pp. 213–228). Ann Arbor Science Publishers.

Doucette, W. J. (2003). Quantitative structure-activity relationships for predicting soil-sediment sorption coefficients for organic chemicals. *Environmental Toxicology and Chemistry; Environmental Toxicology and Chemistry*, *22*(8), 1771–1788. https://doi.org/10.1897/01-362

Edwards, E., & Grbić-Galić, D. (1992). Complete mineralization of benzene by aquifer microorganisms under strictly anaerobic conditions. *Applied and Environmental Microbiology; Appl Environ Microbiol*, *58*(8), 2663–2666. https://doi.org/10.1128/AEM.58.8.2663-2666.1992

Edwards, E., & Grbić-Galić, D. (1994). Anaerobic degradation of toluene and (omicron)-xylene by a methanogenic consortium. *Applied and Environmental Microbiology*, *60*(1), 313. https://doi.org/10.1128/AEM.60.1.313-322.1994

Edwards, S. J., & Kjellerup, B. v. (2013). Applications of biofilms in bioremediation and biotransformation of persistent organic pollutants, pharmaceuticals/personal care products, and

heavy metals. *Applied Microbiology and Biotechnology*, *97*(23), 9909–9921. https://doi.org/10.1007/S00253-013-5216-Z/FIGURES/2

Ehrlich, R., White, N., Tewaternaude, J., Walt, A. van der, Ravenscroft, G., & Roberts, W. (2009). Meteorologically estimated exposure but not distance predicts asthma symptoms in schoolchildren in the environs of a petrochemical refinery: A cross-sectional study. *Environmental Health; Environ Health*, *8*(1), 45. https://doi.org/10.1186/1476-069X-8-45

el Gamal, M., Mousa, H. A., El-Naas, M. H., Zacharia, R., & Judd, S. (2018). Bio-regeneration of activated carbon: A comprehensive review. *Separation and Purification Technology*, *197*, 345–359. https://doi.org/10.1016/J.SEPPUR.2018.01.015

Faisal, A. A. H., Sulaymon, A. H., & Khaliefa, Q. M. (2017). A review of permeable reactive barrier as passive sustainable technology for groundwater remediation. *International Journal of Environmental Science and Technology*, *15*. https://doi.org/10.1007/s13762-017-1466-0

Fan, D., Gilbert, E. J., & Fox, T. (2017). Current state of in situ subsurface remediation by activated carbon-based amendments. *Journal of Environmental Management*, *204*, 793–803. https://doi.org/10.1016/j.jenvman.2017.02.014

Farhadian, M., Vachelard, C., Duchez, D., & Larroche, C. (2008). In situ bioremediation of monoaromatic pollutants in groundwater: A review. *Bioresource Technology; Bioresour Technol*, *99*(13), 5296–5308. https://doi.org/10.1016/j.biortech.2007.10.025

Farhat, S. K., Newell, C. J., Seyedabbasi, M. A., McDade, J. M., Mahler, N. T., Sale, T. C., Dandy, D. S., & Wahlberg, J. J. (2012). *Matrix Diffusion Toolkit. User's Manual. Version 1.0*. https://apps.dtic.mil/sti/citations/ADA610154

Ficker, M., Krastel, K., Orlicky, S., & Edwards, E. (1999). Molecular Characterization of a Toluene-Degrading Methanogenic Consortium. *Applied and Environmental Microbiology*, *65*(12), 5576. https://doi.org/10.1128/AEM.65.12.5576-5585.1999

Figueiredo, J. L., Pereira, M. F. R., Freitas, M. M. A., & Órfão, J. J. M. (1999). Modification of the surface chemistry of activated carbons. *Carbon (New York)*, *37*(9), 1379–1389. https://doi.org/10.1016/S0008-6223(98)00333-9

Freidman, B. L., Gras, S. L., Snape, I., Stevens, G. W., & Mumford, K. A. (2017). A bio-reactive barrier sequence for petroleum hydrocarbon capture and degradation in low nutrient environments. *International Biodeterioration & Biodegradation*, *116*, 26–37. https://doi.org/10.1016/J.IBIOD.2016.09.025

Georgi, A., Schierz, A., Mackenzie, K., & Kopinke, F.-D. (2015). Colloidal activated carbon for in-situ groundwater remediation — Transport characteristics and adsorption of organic compounds

in water-saturated sediment columns. *Journal of Contaminant Hydrology; J Contam Hydrol*, *179*, 76–88. https://doi.org/10.1016/j.jconhyd.2015.05.002

Gödeke, S., Gödeke, S., Vogt, C., Vogt, C., Schirmer, M., & Schirmer, M. (2008). Estimation of kinetic Monod parameters for anaerobic degradation of benzene in groundwater. *Environmental Geology (Berlin)*, *55*(2), 423–431. https://doi.org/10.1007/s00254-007-0988-z

Gupta, H., & Gupta, B. (2016). Adsorption of polycyclic aromatic hydrocarbons on banana peel activated carbon. *Desalination and Water Treatment*, *57*(20), 9498–9509. https://doi.org/10.1080/19443994.2015.1029007

Gupta, V. K. (2001). Kinetics of mercury adsorption from wastewater using activated carbon derived from fertilizer waste . *Colloids and Surfaces*, 169–181. https://www.academia.edu/27270292

Hackbarth, F., Vilar, V., Souza, G., Souza, S., & Souza, A. (2014). Benzene, toluene and o -xylene (BTX) removal from aqueous solutions through adsorptive processes. *Adsorption; Journal of the International Adsorption Society*, *20*(4), 577–590. https://doi.org/10.1007/s10450-014-9602-3

Harris, P. J. F., Liu, Z., & Suenaga, K. (2008). Imaging the atomic structure of activated carbon. *Journal of Physics.Condensed Matter*, *20*(36), 362201. https://doi.org/10.1088/0953-8984/20/36/362201

Health Canada. (2020). *Guidelines for Canadian Drinking Water Quality* (Vol. 2021, Issue June). https://www.canada.ca/en/health-canada/services/environmental-workplace-health/reports-publications/water-quality/guidelines-canadian-drinking-water-quality-summary-table.html

Heath, J. S., Koblis, K., & Sager, S. L. (1993). Review of chemical, physical, and toxicologic properties of components of total petroleum hydrocarbons. *Journal of Soil Contamination*, *2*(1), 1–25. https://doi.org/10.1080/15320389309383426

Heidarinejad, Z., Dehghani, M. H., Heidari, M., Gholamali Javedan, ·, Ali, I., & Sillanpää, M. (2020). *Methods for preparation and activation of activated carbon: a review*. *18*, 393–415. https://doi.org/10.1007/s10311-019-00955-0

Ho, Y. S. (1995). *Adsorption of heavy metals from waste streams by peat*. University of Birmingham.

Ho, Y.-S. (2004). Citation review of Lagergren kinetic rate equation on adsorption reactions. *Budapest Scientometrics*, *59*(1), 171–177.

Hoang, T. T. L., Vigneswaran, S., Ngo, H. H., Kandasamy, J., Shim, W. G., Chaudhary, D. S., Gotety, P., & Peiris, P. (2008). Performance evaluation and mathematical modelling of granular activated carbon biofiltration in wastewater treatment. *Korean Journal of Chemical Engineering*, *25*(2), 259–267. https://doi.org/10.1007/s11814-008-0046-x

Julien, F., Baudu, M., & Mazet, M. (1998). Relationship between chemical and physical surface properties of activated carbon. *Water Research (Oxford)*, *32*(11), 3414–3424. https://doi.org/10.1016/S0043-1354(98)00109-2

Kan, A. T., Fu, G., Hunter, M., Chen, W., Ward, C. H., & Tomson, M. B. (1998). Irreversible sorption of neutral hydrocarbons to sediments: Experimental observations and model predictions. *Environmental Science and Technology*, *32*(7), 892–902. https://doi.org/10.1021/ES9705809/ASSET/IMAGES/MEDIUM/ES9705809E00010.GIF

Kan, A. T., Fu, G., & Tomson, M. B. (1994). Adsorption/Desorption hysteresis in organic pollutant and soil/sediment interaction. *Environmental Science & Technology*, *28*(5), 859. https://doi.org/10.1021/es00054a017

Karickhoff, S. W., Brown, D. S., & Scott, T. A. (1979). Sorption of hydrophobic pollutants on natural sediments. *Water Research (Oxford)*, *13*(3), 241–248.

Khan, F. I., Husain, T., & Hejazi, R. (2004). An overview and analysis of site remediation technologies. *Journal of Environmental Management*, *71*(2), 95–122. https://doi.org/10.1016/j.jenvman.2004.02.003

Kilduff, J. E., & Wigton, A. (1999). Sorption of TCE by Humic-Preloaded Activated Carbon: Incorporating Size-Exclusion and Pore Blockage Phenomena in a Competitive Adsorption Model. *Environmental Science & Technology; Environ.Sci.Technol*, *33*(2), 250–256. https://doi.org/10.1021/es980321z

Kjellerup, B., & Edwards, S. (2013). *FINAL REPORT-PHASE I Application of Biofilm Covered Activated Carbon Particles as a Microbial Inoculum Delivery System for Enhanced Bioaugmentation of PCBs in Contaminated Sediment*.

Knettig, E., Thomson, B. M., & Hrudey, S. E. (1986). Competitive activated carbon adsorption of phenolic compounds. *Environmental Pollution.Series B.Chemical and Physical*, *12*(4), 281–299. https://doi.org/10.1016/0143-148X(86)90016-9

Lagergren, S. (1898). About the theory of so-called adsorption of soluble substances. *Kungliga Svenska Vetenskapsakademiens*, *24*(4), 1–39.

Lamichhane, S., Bal Krishna, K. C., & Sarukkalige, R. (2016). Polycyclic aromatic hydrocarbons (PAHs) removal by sorption: A review. *Chemosphere*, *148*, 336–353. https://doi.org/10.1016/J.CHEMOSPHERE.2016.01.036

Leahy, J. G., & Colwell, R. R. (1990). Microbial degradation of hydrocarbons in the environment. *Microbiological Reviews; Microbiol Rev*, *54*(3), 305–315. https://doi.org/10.1128/mmbr.54.3.305-315.1990

Leglize, P., Alain, S., Jacques, B., & Corinne, L. (2008). Adsorption of phenanthrene on activated carbon increases mineralization rate by specific bacteria. *Journal of Hazardous Materials*, *151*(2–3), 339–347. https://doi.org/10.1016/J.JHAZMAT.2007.05.089

Li, L., Quinlivan, P. A., & Knappe, D. R. U. (2002). E ffects of activated carbon surface chemistry and pore structure on the adsorption of organic contaminants from aqueous solution. *Carbon*, *40*, 2085–2100.

Lillo-Ródenas, M. A., Fletcher, A. J., Thomas, K. M., Cazorla-Amorós, D., & Linares-Solano, A. (2006). Competitive adsorption of a benzene–toluene mixture on activated carbons at low concentration. *Carbon*, *44*(8), 1455–1463. https://doi.org/10.1016/j.carbon.2005.12.001

Lin, Y.-H. (2016). Adsorption and biodegradation of 2-chlorophenol by mixed culture using activated carbon as a supporting medium-reactor performance and model verification. *Applied Water Science*, *7*(7), 3741–3757. https://doi.org/10.1007/s13201-016-0522-0

Lindelöf, E. (1894). Sur l'application de la méthode des approximations successives aux équations différentielles ordinaires du premier ordre. *Comptes Rendus Hebdomadaires Des Séances de l'Académie Des Sciences*, *118*, 454–457. https://gallica.bnf.fr/ark:/12148/bpt6k3074r/f454.table

López, E., Schuhmacher, M., & Domingo, J. L. (2008). Human health risks of petroleum-contaminated groundwater. *Environmental Science and Pollution Research International; Environ Sci Pollut Res Int*, *15*(3), 278–288. https://doi.org/10.1065/espr2007.02.390

Lueders, T. (2017). The ecology of anaerobic degraders of BTEX hydrocarbons in aquifers. *FEMS Microbiology Ecology; FEMS Microbiol Ecol*, *93*(1), fiw220. https://doi.org/10.1093/femsec/fiw220

Luo, F., Devine, C. E., & Edwards, E. A. (2016). Cultivating microbial dark matter in benzene-degrading methanogenic consortia. *Environmental Microbiology*, *18*(9), 2923–2936. https://doi.org/10.1111/1462-2920.13121

Luo, F., Gitiafroz, R., Devine, C. E., Gong, Y., Hug, L. A., Raskin, L., & Edwards, E. A. (2014). Metatranscriptome of an anaerobic benzene-degrading, nitrate-reducing enrichment culture reveals involvement of carboxylation in benzene ring activation. *Applied and Environmental Microbiology*, *80*(14), 4095–4107. https://doi.org/10.1128/AEM.00717-14/SUPPL_FILE/ZAM999105467SO1.PDF

Luz, A., & Luz, C. da. (2013). Multicomponent Adsorption and Desorption of BTX Compounds Using Coconut Shell Activated Carbon: Experiments, Mathematical Modeling, and Numerical Simulation. *Industrial & Engineering Chemistry Research*, *52*(23), 7896–7911. https://doi.org/10.1021/ie302849j

Ma, C., Li, J., Xia, W., Ding, Y., Zhang, L., & Xu, Y. (2021). Effect of additives on the remediation of arsenic and chromium co-contaminated soil by an electrokinetic-permeable reactive barrier. *Environmental Science and Pollution Research*, 11966–11975. https://doi.org/10.1007/s11356-021-16357-1/Published

Magne, P., & Walker, P. L. (1986). Phenol adsorption on activated carbons: Application to the regeneration of activated carbons polluted with phenol. *Carbon*, *24*(2), 101–107. https://doi.org/10.1016/0008-6223(86)90102-8

Marais, G. v R., & Ekama, G. (1976). The activated sludge process Part 1 - Steady state behaviour. *Water SA*, *2*(4), 165–199. https://www.researchgate.net/publication/284774604

Marchal, G., Smith, K. E. C., Rein, A., Winding, A., Trapp, S., & Karlson, U. G. (2013). Comparing the desorption and biodegradation of low concentrations of phenanthrene sorbed to activated carbon, biochar and compost. *Chemosphere*, *90*(6), 1767–1778. https://doi.org/10.1016/J.CHEMOSPHERE.2012.07.048

Marrocco, A. L. (2022). *In progress - Activated Carbon-Based Amendments for the Treatment of Petroleum Hydrocarbons in Anaerobic Groundwater Systems*. University of Waterloo.

Matott, L. S. (2017). *OSTRICH: an Optimization Software Tool, Documentation and User's Guide, Version 17.12.19*. .

Mcdougall, G. (1991). The Physical Nature and Manufacture of Activated Carbon. *Journal of The South African Institute of Mining and Metallurgy*, *91*(4), 109–120.

McKenzie, L. M., Witter, R. Z., Newman, L. S., & Adgate, J. L. (2012). Human health risk assessment of air emissions from development of unconventional natural gas resources. *The Science of the Total Environment; Sci Total Environ*, *424*, 79–87. https://doi.org/10.1016/j.scitotenv.2012.02.018

Middeldorp, P. J. M., van Aalst, M. A., Rijnaarts, H. H. M., Stams, F. J. M., de Kreuk, H. F., Schraa, G., & Bosma, T. N. P. (1998). Stimulation of reductive dechlorination for in situ bioremediation of a soil contaminated with chlorinated ethenes. *Water Science and Technology*, *37*(8), 105–110. https://doi.org/10.2166/WST.1998.0314

Miller, L., Xu, X., Grgicak-Mannion, A., Brook, J., & Wheeler, A. (2012). Multi-season, multi-year concentrations and correlations amongst the BTEX group of VOCs in an urbanized industrial city. *Atmospheric Environment (1994)*, *61*, 305–315. https://doi.org/10.1016/j.atmosenv.2012.07.041

Millington, R. J. (1959). Gas Diffusion in Porous Media. *Science*, *130*(3367), 100–102.

Mohamed, E. F., Andriantsiferana, C., Wilhelm, A. M., & Delmas, H. (2011). Competitive adsorption of phenolic compounds from aqueous solution using sludge-based activated carbon.

Environmental Technology; Environ Technol, *32*(12), 1325–1336. https://doi.org/10.1080/09593330.2010.536783

Monod, J. (1949). The Growth of Bacterial Cultures. *Annual Reviews in Microbiology*, *3*(1), 371–394.

Myers, A. L., & Prausnitz, J. M. (1965). Thermodynamics of mixed-gas adsorption. *AIChE Journal; AIChE J*, *11*(1), 121–127. https://doi.org/10.1002/aic.690110125

Naeimi, M., Shavandi, M., & Alaie, E. (2020). *Determining the impact of biofilm in the bioaugmentation process of benzene-contaminated resources*. https://doi.org/10.1016/j.jece.2020.104976

Obiri-Nyarko, F., Grajales-Mesa, S., & Malina, G. (2014). An overview of permeable reactive barriers for in situ sustainable groundwater remediation. *Chemosphere*, *111*, 243–259. https://doi.org/10.1016/j.chemosphere.2014.03.112

Odermatt, J. R. (1994). Natural chromatographic separation of benzene, toluene, ethylbenzene and xylenes (BTEX compounds) in a gasoline contaminated ground water aquifer. *Organic Geochemistry*, *21*(10), 1141–1150. https://doi.org/10.1016/0146-6380(94)90076-0

Ogata, A., & Banks, R. B. (1961). A Solution of the Differential Equation of Longitudinal Dispersion in Porous Media. In *Fluid Movement in Earth Materials*.

Ontario Ministry of Environment. (2011). *Soil, ground water and sediment standards for use under Part XV.1 of the Environmental Protection Act | Ontario.ca*. https://www.ontario.ca/page/soil-ground-water-and-sediment-standards-use-under-part-xv1-environmental-protection-act

Ossai, I. C., Ahmed, A., Hassan, A., & Hamid, F. S. (2020). Remediation of soil and water contaminated with petroleum hydrocarbon: A review. *Environmental Technology & Innovation*, *17*, 100526. https://doi.org/10.1016/j.eti.2019.100526

Ozis, F., Bina, A., & Devinny, J. S. (2007). Biofilm Growth-Percolation Models and Channeling in Biofilter Clogging. *Journal of the Air & Waste Management Association; J Air Waste Manag Assoc*, *57*(8), 882–892. https://doi.org/10.3155/1047-3289.57.8.882

Pagnozzi, G., Carroll, S., Reible, D. D., & Millerick, K. (2021). Powdered activated carbon (PAC) amendment enhances naphthalene biodegradation under strictly sulfate-reducing conditions. *Environmental Pollution*, *268*, 115641. https://doi.org/10.1016/J.ENVPOL.2020.115641

Piai, L., Blokland, M., van der Wal, A., & Langenhoff, A. (2020). Biodegradation and adsorption of micropollutants by biological activated carbon from a drinking water production plant. *Journal of Hazardous Materials*, *388*, 122028. https://doi.org/10.1016/J.JHAZMAT.2020.122028

Piai, L., Langenhoff, A., Jia, M., de Wilde, V., & van der Wal, A. (2022). Prolonged lifetime of biological activated carbon filters through enhanced biodegradation of melamine. *Journal of Hazardous Materials*, *422*, 126840. https://doi.org/10.1016/J.JHAZMAT.2021.126840

Picard, E. (1890). Mémoire sur la théorie des équations aux dérivées partielles et la méthode des approximations successives. *Journal de Mathématiques Pures et Appliquées*, *6*, 145–210. https://eudml.org/doc/235808

Pikaar, I., Koelmans, A. A., & van Noort, P. (2006). Sorption of organic compounds to activated carbons. Evaluation of isotherm models. *Chemosphere (Oxford); Chemosphere*, *65*(11), 2343–2351. https://doi.org/10.1016/j.chemosphere.2006.05.005

Piwoni, M. D., & Keeley, J. W. (1990). *Basic concepts of contaminant sorption at hazardous waste sites (ground-water issue)*. https://www.osti.gov/biblio/5606332

Pui, W. K., Yusoff, R., & Aroua, M. K. (2019). A review on activated carbon adsorption for volatile organic compounds (VOCs). *Reviews in Chemical Engineering*, *35*(5), 649–668. https://doi.org/10.1515/revce-2017-0057

Qiu, T., Zeng, Y., Ye, C., & Tian, H. (2012). Adsorption Thermodynamics and Kinetics of p -Xylene on Activated Carbon. *Journal of Chemical & Engineering Data*, *57*(5), 1551–1556. https://doi.org/10.1021/je300138a

Qu, W., Yuan, T., Yin, G., Xu, S., Zhang, Q., & Su, H. (2019). *Effect of properties of activated carbon on malachite green adsorption*. https://doi.org/10.1016/j.fuel.2019.03.058

Rabus, R., & Widdel, F. (1995). Anaerobic degradation of ethylbenzene and other aromatic hydrocarbons by new denitrifying bacteria. *Archives of Microbiology; Arch Microbiol*, *163*(2), 96–103. https://doi.org/10.1007/BF00381782

Radke, C. J., & Prausnitz, J. M. (1972). Thermodynamics of multi-solute adsorption from dilute liquid solutions. *AIChE Journal*, *18*(4), 761–768. https://doi.org/10.1002/aic.690180417

Razzaque, M. M., & Grathwohl, P. (2008). Predicting organic carbon–water partitioning of hydrophobic organic chemicals in soils and sediments based on water solubility. *Water Research (Oxford); Water Res*, *42*(14), 3775–3780. https://doi.org/10.1016/j.watres.2008.07.003

Regenesis. (2022). *PlumeStop® Liquid Activated Carbon™*. https://regenesis.com/eur/remediation-products/plumestop-liquid-activated-carbon/

Rittmann, B. E., & McCarty, P. L. (2018). *Environmental Biotechnology*. McGraw-Hill Education. https://www.accessengineeringlibrary.com/content/book/9781260440591

Rittmann, B. E., Stilwell, D., & Ohashi, A. (2002). The transient-state, multiple-species biofilm model for biofiltration processes. *Water Research (Oxford); Water Res*, *36*(9), 2342–2356. https://doi.org/10.1016/s0043-1354(01)00441-9

Samaddar, P., Kim, K.-H., Yip, A. C. K., Zhang, M., Szulejko, J. E., & Khan, A. (2019). The unique features of non-competitive vs. competitive sorption: Tests against single volatile aromatic hydrocarbons and their quaternary mixtures. *Environmental Research; Environ Res*, *173*, 508–516. https://doi.org/10.1016/j.envres.2019.03.046

Schaffer, M., & Licha, T. (2015). A framework for assessing the retardation of organic molecules in groundwater: Implications of the species distribution for the sorption-influenced transport. *The Science of the Total Environment; Sci Total Environ*, *524–525*, 187–194. https://doi.org/10.1016/j.scitotenv.2015.04.006

Schirmer, M., Frind, E. O., Barker, J. F., Molson, J. W., & Butler, B. J. (1998). Identifying scale relationships between the laboratory and field scale using numerical modelling to demonstrate intrinsic bioremediation. *IAHS-AISH Publication*, *250*(250), 229–236.

Schirmer, M., Molson, J. W., Frind, E. O., & Barker, J. F. (2000). Biodegradation modelling of a dissolved gasoline plume applying independent laboratory and field parameters. *Journal of Contaminant Hydrology*, *46*(3–4), 339–374. https://doi.org/nfo:doi/

Schneider, A. E. (2022). *In progress - Bioaugmentation to Increase the Effectiveness of Activated Carbon Amendments to Treat PHCs*. University of Waterloo.

Scott, D. I., Ashmore, M. H., & Nathanail, C. P. (2005). Operating windows to assess whether monitored natural attenuation is a technically feasible remediation option for BTEX-contaminated groundwater. *Remediation (New York, N.Y.); Remediation*, *15*(3), 65–82. https://doi.org/10.1002/rem.20050

Shim, W., Chaudhary, D. S., Vigneswaran, S., Ngo, H.-H., Lee, J., & Moon, H. (2004). Mathematical modeling of granular activated carbon (GAC) biofiltration system. *Korean Journal of Chemical Engineering*, *21*(1), 212–220. https://doi.org/10.1007/BF02705401

Simon, J. A. (2015). Editor's Perspective-An In Situ Revelation: First Retard Migration, Then Treat. *Remediation (New York, N.Y.); Remediation*, *25*(2), 1–7. https://doi.org/10.1002/rem.21420

Simpson, D. R. (2008). Biofilm processes in biologically active carbon water purification. *Water Research*, *42*(12), 2839–2848. https://doi.org/10.1016/J.WATRES.2008.02.025

Smolin, S., Kozyatnyk, I., & Klymenko, N. (2020). New approach for the assessment of the contribution of adsorption, biodegradation and self-bioregeneration in the dynamic process of biologically active carbon functioning. *Chemosphere*, *248*, 126022. https://doi.org/10.1016/J.CHEMOSPHERE.2020.126022

Sochard, S., Fernandes, N., & Reneaume, J.-M. (2010). Modeling of adsorption isotherm of a binary mixture with real adsorbed solution theory and nonrandom two-liquid model. *AIChE Journal; AIChE J*, *56*(12), 3109–3119. https://doi.org/10.1002/aic.12220

Swanson, R., & Dutt, G. (1973). Chemical and Physical Processes that Affect Atrazine and Distribution in Soil Systems. *Soil Science Society of America Journal*, *37*, 872–876.

Teng, H., Ho, J. A., & Hsu, Y. F. (1997). Preparation of activated carbons from bituminous coals with CO2 activation—Influence of coal oxidation. *Carbon*, *35*(2), 275–283. https://doi.org/10.1016/S0008-6223(96)00137-6

Teramoto, E. H., & Chang, H. K. (2019). Geochemical conceptual model of BTEX biodegradation in an iron-rich aquifer. *Applied Geochemistry*, *100*, 293–304. https://doi.org/10.1016/j.apgeochem.2018.11.019

Tessmer, C., Vidic, R., Uranowski, L., & Vidic, R. (1997). Impact of oxygen-containing surface functional groups on activated carbon adsorption of phenols. *Environmental Science & Technology*, *31*(7), 1872–1878. https://doi.org/10.1021/es960474r

Tolson, B. A., & Shoemaker, C. A. (2007). Dynamically dimensioned search algorithm for computationally efficient watershed model calibration. *Water Resources Research; Water Resour.Res*, *43*(1), W01413-n/a. https://doi.org/10.1029/2005WR004723

Tolson, B. A., & Shoemaker, C. A. (2008). Efficient prediction uncertainty approximation in the calibration of environmental simulation models. *Water Resources Research; Water Resour.Res*, *44*(4), W04411-n/a. https://doi.org/10.1029/2007WR005869

Toth, C. R. A., Luo, F., Bawa, N., Webb, J., Guo, S., Dworatzek, S., & Edwards, E. A. (2021). Anaerobic Benzene Biodegradation Linked to the Growth of Highly Specific Bacterial Clades. *Environmental Science & Technology; Environ.Sci.Technol*, *55*(12), 7970–7980. https://doi.org/10.1021/acs.est.1c00508

Treasury Board of Canada Secretariat. (2022). *Federal Contaminated Sites Inventory*. https://www.tbs-sct.gc.ca/fcsi-rscf/cm-eng.aspx

Tsuno, H., Kawamura, M., & Oya, T. (2006). Application of biological activated carbon anaerobic reactor for treatment of hazardous chemicals. *Water Science and Technology; Water Sci Technol*, *53*(11), 251–260. https://doi.org/10.2166/wst.2006.360

Ulrich, A. C., & Edwards, E. A. (2003). Physiological and molecular characterization of anaerobic benzene-degrading mixed cultures. *Environmental Microbiology; Environ Microbiol*, *5*(2), 92–102. https://doi.org/10.1046/j.1462-2920.2003.00390.x

USEPA. (1996). *Superfund Soil Screening Guidance*. https://www.epa.gov/superfund/superfund-soil-screening-guidance

USEPA. (2020a). *Superfund Remedy Report, 16th Edition*. https://www.epa.gov/sites/production/files/2020-07/documents/100002509.pdf

USEPA. (2020b). *US EPA Semiannual Report of UST Performance Measures*.

USEPA. (2021). *Superfund Chemical Data Matrix* (Vol. 2021, Issue June). https://www.epa.gov/superfund/superfund-chemical-data-matrix-scdm-query

Vaccari, D. A., & Kaouris, M. (1988). A model for irreversible adsorption hysteresis. *Journal of Environmental Science and Health .Part A: Environmental Science and Engineering*, *23*(8), 797–822. https://doi.org/10.1080/10934528809375453

van Genuchten, M. T., Davidson, J. M., & Wierenga, P. J. (1974). An Evaluation of Kinetic and Equilibrium Equations for the Prediction of Pesticide Movement Through Porous Media. *Soil Science Society of America Journal*, *38*(1), 29. http://soil.scijournals.org/cgi/content/abstract/38/1/29

Warner, S. D. (2015). Permeable Reactive Barrier. *Radwaste Solutions*, *18*(4), 333. https://doi.org/10.1201/9781351228886

Weber, W. J., Huang, W., & Yu, H. (1998). Hysteresis in the sorption and desorption of hydrophobic organic contaminants by soils and sediments: 2. Effects of soil organic matter heterogeneity. *Journal of Contaminant Hydrology*, *31*(1), 149–165. https://doi.org/10.1016/S0169-7722(97)00059-4

Weelink, S. A. B., van Eekert M.H.A., & Stams, A. J. M. (2010). Degradation of BTEX by anaerobic bacteria: physiology and application. *Reviews in Environmental Science and Biotechnology*, *9*(4), 359–385. https://doi.org/10.1007/s11157-010-9219-2

Wei, Y., Thomson, N. R., Aravena, R., Marchesi, M., Barker, J. F., Madsen, E. L., Kolhatkar, R., Buscheck, T., Hunkeler, D., & Derito, C. M. (2018). Infiltration of Sulfate to Enhance Sulfate-Reducing Biodegradation of Petroleum Hydrocarbons. *Groundwater Monitoring & Remediation*, *38*(4), 73–87. https://doi.org/10.1111/gwmr.12298

Widdel, F., Knittel, K., & Galushko, A. (2010). *Anaerobic Hydrocarbon-Degrading Microorganisms: An Overview* (pp. 1997–2021). https://doi.org/10.1007/978-3-540-77587-4_146

Xia, Y., Cheng, Y., Li, L., Chen, Y., & Jiang, Y. (2020). A microcosm study on persulfate oxidation combined with enhanced bioremediation to remove dissolved BTEX in gasoline-contaminated groundwater. *Biodegradation (Dordrecht); Biodegradation*, *31*(3), 213–222. https://doi.org/10.1007/s10532-020-09904-z

Xu, X., & Thomson, N. (2008). Estimation of the Maximum Consumption of Permanganate by Aquifer Solids Using a Modified Chemical Oxygen Demand Test. *Journal of Environmental Engineering*, *134*(5), 353–361. https://doi.org/10.1061/(ASCE)0733-9372(2008)134:5(353)

Yakout, S., & Daifullah, A. (2014). Adsorption/desorption of BTEX on activated carbon prepared from rice husk. *Desalination and Water Treatment*, *52*(22–24), 4485–4491. https://doi.org/10.1080/19443994.2013.821629

Yang, K., & Xing, B. (2007). Desorption of polycyclic aromatic hydrocarbons from carbon nanomaterials in water. *Environmental Pollution*, *145*(2), 529.

Yonge, D. R., & Keinath, T. M. (1986). The Effects of Non-Ideal Competition on Multi-Component Adsorption Equilibria. *Journal (Water Pollution Control Federation)*, *58*(1), 77–81.

Yonge, D. R., Keinath, T. M., Poznanska, K., & Jiang, Z. P. (1985). Single-solute irreversible adsorption on granular activated carbon. *Environmental Science & Technology*, *19*(8), 690. https://doi.org/10.1021/es00138a006

Zhang, J. X., & Ou, L. L. (2013). Kinetic, isotherm and thermodynamic studies of the adsorption of crystal violet by activated carbon from peanut shells. *Water Science and Technology : A Journal of the International Association on Water Pollution Research*, *67*(4), 737. https://doi.org/10.2166/wst.2012.605

Zhang, S., & Huck, P. M. (1996). Parameter estimation for biofilm processes in biological water treatment. *Water Research*, *30*(2), 456–464. https://doi.org/10.1016/0043-1354(95)00162-X

Appendix A

Supplementary Materials

Batch Adsorption/Desorption Experimental Method and Results

In this section, the experimental protocol and results from the modified adsorption/desorption experiment are detailed, including recipes for the solutions used in the experimental work.

Artificial Groundwater Recipe

Recipe for 1 L of artificial groundwater (AGW) salt solution in Milli-Q® water (adapted from de León (2021) which was modified from (Middeldorp et al., 1998)).

- 0.05 g/L NH_4Cl (53.49 g/mol, 0.93 mM)
- 0.01 g/L $MgCl_2$ (203.31 g/mol, 0.05 mM)
- 0.0019 g/L $MnCl_2$ $4H_2O$ (197.91 g/mol, 0.0096 mM)
- 0.007 g/L NaCl (58.44 g/mol, 0.12 mM)
- 0.15 g/L $CaCl_2$ (147.02 g/mol, 1 mM)
- 0.0620 g/L $Na_2HPO_4 \cdot 2H_2O$ (141.96 g/mol, 0.43 mM)
- 0.0204 g/L KH_2PO_4 (136.09 g/mol, 0.14 mM)
- 0.009 g/L Na_2SO_4 (142.0 g/mol, 0.06 mM)
- 0.86 g/L $NaHCO_3$ (86.01 g/mol, 1 M)

Measure pH, should be around 7.

Toluene Stock Solution

Recipe for 4.5 L of toluene amended – AGW salt solution

1. Place 4.5 L of AGW salt solution in a dispensing bottle with a Teflon coated magnetic stirrer.
2. Place the bottle on top of the stirrer at speed 8.
3. Add 250 µL of neat toluene and cap immediately, securing the cap with tape, this volume gives a final concentration of ~ 30 mg/L.
4. Leave for at least 12 h to allow toluene to dissolve completely.

Batch Adsorption/Desorption Experiment Protocol (adapted from de Léon (2021))

1. Fill three 160 mL serum bottles containing 10 mg PAC and three 160 mL serum bottles without PAC (controls) per initial concentration (10, 15, 20, 25, and 30 mg/L toluene) without headspace and crimp with aluminum seal + Teflon silicon septa.
2. Transfer to a platform shaker and agitate at 100 rpm for 24 h.
3. Stop agitation.
4. Leave undisturbed for 24 h to allow PAC to sediment from the aqueous phase.
5. Perform aqueous phase extraction for each sample.
6. Remove 130 mL from the sorption assay bottles leaving the PAC inside.
7. Replenish with fresh AGW solution (toluene free) and seal tightly.
8. Repeat Steps 2-7 for a total of seven desorption cycles.
9. After final desorption cycle (Step 6), remove all aqueous phase from sorption assay bottles leaving the PAC inside.
10. Perform PAC sorbent extraction for each sorption assay bottle
11. Transfer dichloromethane phase to 2 mL autosampler vials
12. Analyze extracted samples in a GC-FID.

The results of the first 48h adsorption cycle are displayed in Figure A1.

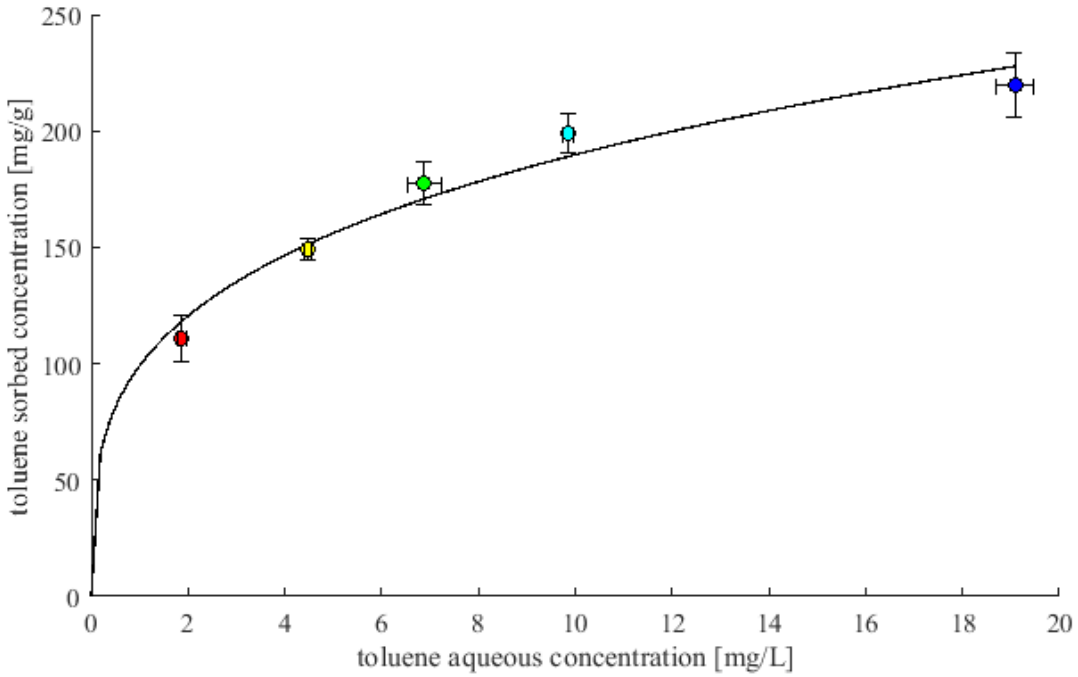

Figure A1 Adsorption data for toluene at initial aqueous concentrations of 10 (red), 15 (yellow), 20 (green), 25 (light blue), and 30 (dark blue) mg/L sorbed to ~10 mg of PAC. Calculated K_f and n_f adsorption parameters were 99.09 ± 24.98 and 0.282 ± 0.110 (± 95% CI) respectively. Error bars represent ± one standard deviation.

After equilibrium was reached, desorption cycles were completed by decanting ~81% of the aqueous phase (130 mL out of 160 mL total), measuring the toluene concentration in the decanted phase, and replacing the decanted aqueous phase with toluene-free AGW. This represents a modification of the method used in the previous desorption experiments; previously, a majority of the aqueous phase was decanted. PAC was potentially removed from the system during this process, leading to a lower amount of mass available to desorb to the aqueous phase. This lost mass would then be included in the mass balance calculation used to determine sorbed concentrations under an erroneous assumption that the same amount of PAC remained in the reactor. Half of the aqueous phase was decanted in the new experiments to avoid this. The desorption process was repeated seven times, and sorbed concentrations were calculated using a mass balance calculation. The results of the desorption exercise are superimposed on the adsorption results in Figure A2.

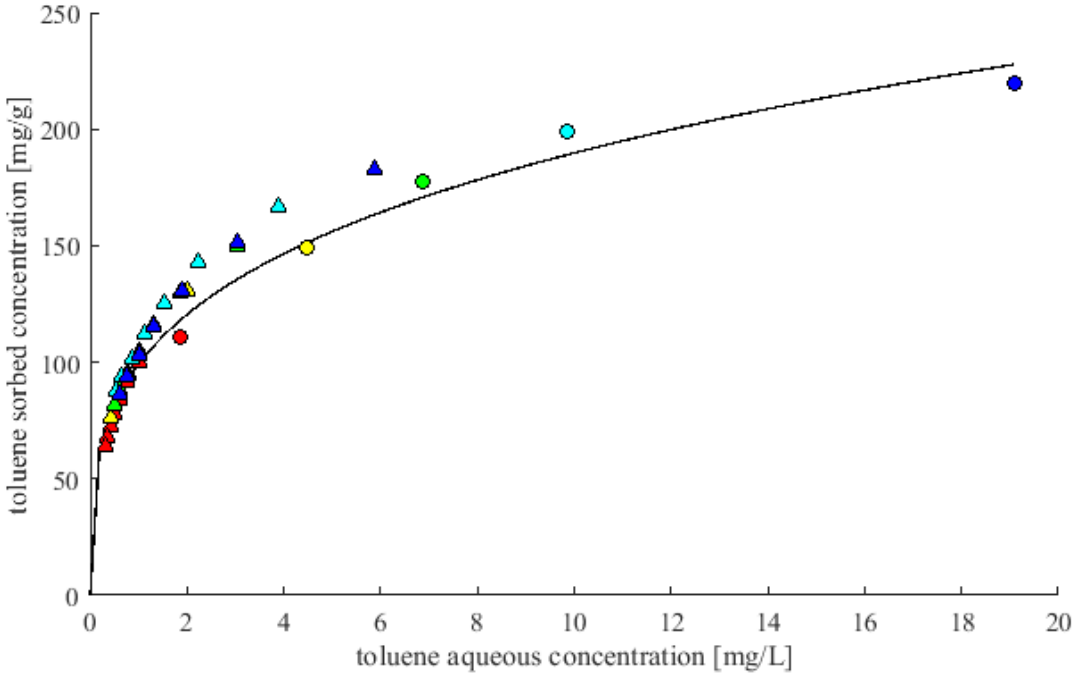

Figure A2 Adsorption (circles) and desorption (triangles) data for toluene at initial aqueous concentrations of 10 (red), 15 (yellow), 20 (green), 25 (light blue), and 30 (dark blue) mg/L sorbed to ~10 mg of PAC. The solid line represents the adsorption isotherm described in Figure 3.11(b).

Solid phase extractions conducted at the end of each experiment were not significantly different than those predicted by the mass balance calculations ($p > 0.05$) and all lay on or below the adsorption isotherm, suggesting there is no irreversible hysteresis of toluene in the system [A3].

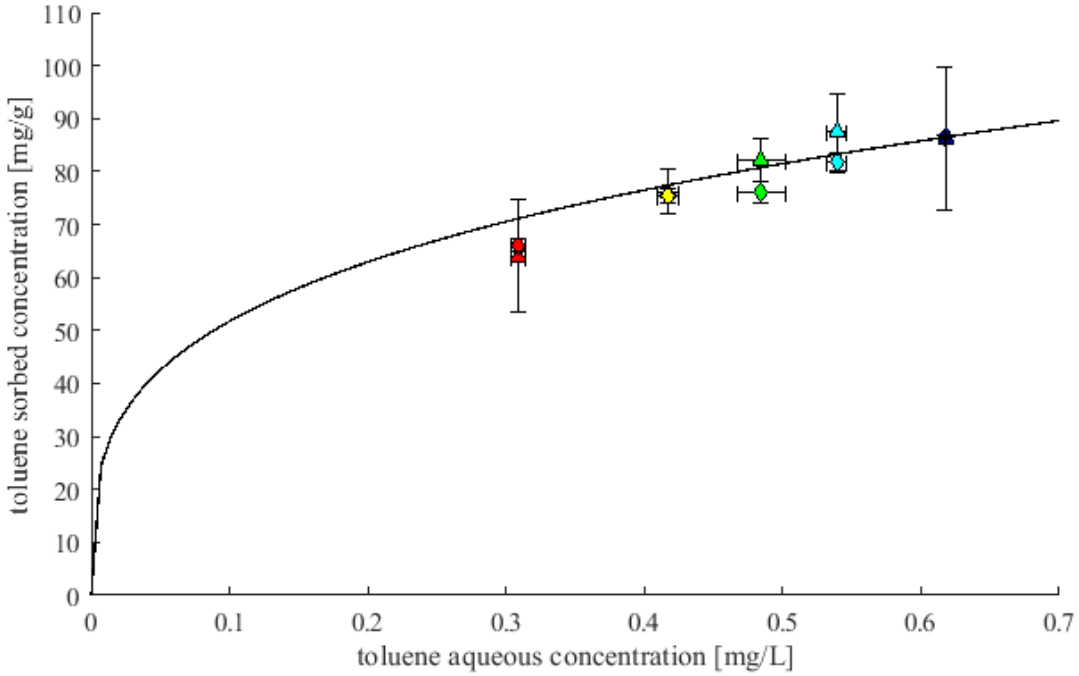

Figure A3 Isotherm data points for toluene at initial aqueous concentrations of 10 (red), 15 (yellow), 20 (green), 25 (light blue), and 30 (dark blue) mg/L sorbed to ~10 mg of PAC. Sorbed concentrations were calculated based on a mass balance (triangles) and measured through solid phase extraction (diamonds). Calculated and measured sorbed concentrations were not significantly different ($p > 0.05$). The solid line represents the adsorption isotherm described in Figure A1. Error bars represent ± one standard deviation.

The fitting of reversible hysteresis parameters conducted in the previous sorption experiments was inconclusive for the new data (i.e., reversible hysteresis cannot be modelled using this data set). The results of both (A) the original sorption experiment detailed in Section 3.1.4.4, and (B) the seven-cycle desorption experiment are plotted on Figure A4 to facilitate comparison.

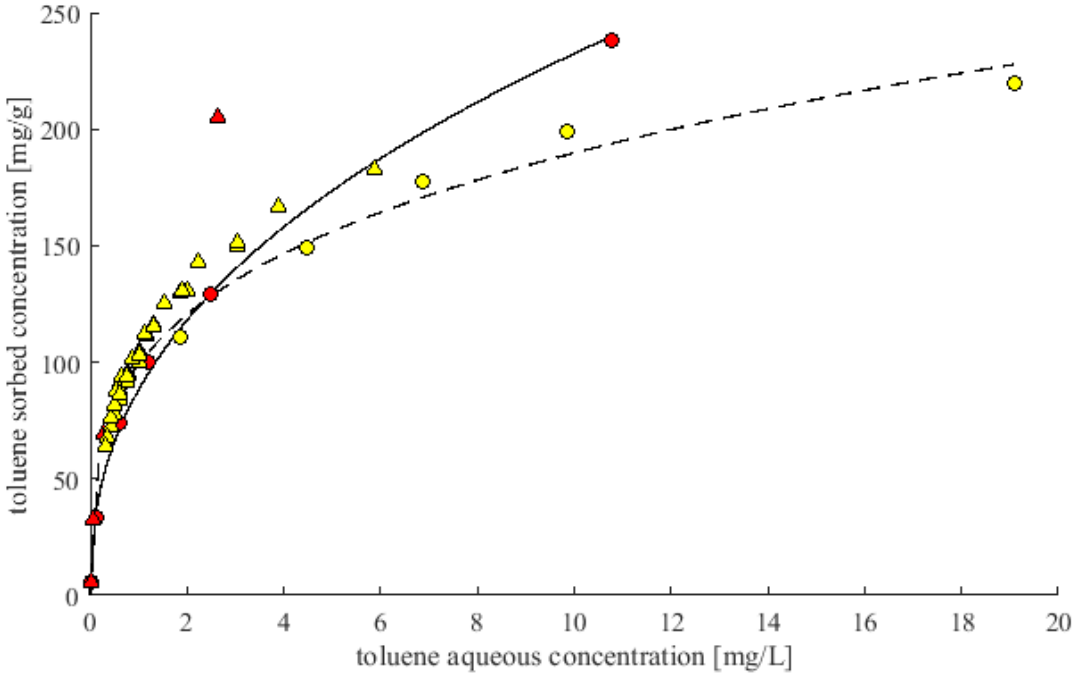

Figure A4 Adsorption (circles) and desorption (triangles) isotherm data for (A) a single desorption cycle (red) and (B) multiple desorption cycles (yellow).

The most significant deviation between experiments (A) and (B) arises in the highest concentration adsorption/desorption pair in experiment (A). Ignoring this cycle, all data is tightly clustered around the sorption isotherms for (B). These results would seemingly indicate that there is no irreversible hysteresis and potentially a slight degree of reversible hysteresis.

Table A1 Hysteretic sorption parameters for BTX on Calgon WPC® powdered activated carbon.

Compound	Reversible			Reversible + Irreversible			
	a	**b**	**c**	$\mathbf{K_f^r}$ ($mg^{1-nf}\ L^{nf}\ g^{-1}$)	$\mathbf{n_f^r}$ **[-]**	$\mathbf{K_f^{irr}}$ ($mg^{1-nf}\ L^{nf}\ g^{-1}$)	$\mathbf{n_f^{irr}}$ **[-]**
Benzene	1.46	517	2.02	26.40	0.543	15.34	0.110
Toluene	0	813	1.10	39.29	0.457	55.12	0.380
o-Xylene	0	577,000	2.14	89.86	0.353	56.89	0.286

Statistical Comparison of Calibrated Monod Kinetic Parameters

The following tables display the full results for all pairwise statistical tests performed on calibrated Monod kinetics parameters (μ_{max} and K_S for multi-parameter calibration exercises and μ_{max} alone for single parameter calibration exercises).

Table A2 Statistical comparisons for optimized maximum specific growth rates of toluene. Statistical measure used was the Wilcoxon rank sum test (comparison of medians) at 95% confidence levels. Displayed are p-values: <0.05 is a significant difference.

	BA-Tol	**A-BA-Tol**	**A-BA-PAC-Tol**	**BA-BTX**	**A-BA-BTX**	**A-BA-PAC-BTX**
BA-Tol	1	1.00E-13	4.19E-36	8.84E-22	3.56E-34	7.40E-32
A-BA-Tol		1	2.93E-05	4.64E-02	4.23E-05	3.13E-05
A-BA-PAC-Tol			1	2.51E-02	0.983	0.882
BA-BTX				1	2.80E-02	2.70E-02
A-BA-BTX					1	0.867
A-BA-PAC-BTX						1

Table A3 Statistical comparisons for optimized half-velocity constants of toluene. Statistical measure used was the Wilcoxon rank sum test (comparison of medians) at 95% confidence levels. Displayed are the p-values: <0.05 is a significant difference.

	BA-Tol	**A-BA-Tol**	**A-BA-PAC-Tol**	**BA-BTX**	**A-BA-BTX**	**A-BA-PAC-BTX**
BA-Tol	1	1.43E-50	1.85E-144	2.42E-90	1.25E-105	8.49E-106
A-BA-Tol		1	2.19E-09	1.31E-18	7.48E-34	8.39E-34
A-BA-PAC-Tol			1	3.05E-72	1.75E-65	3.05E-67
BA-BTX				1	9.27E-07	1.15E-06
A-BA-BTX					1	0.973
A-BA-PAC-BTX						1

Table A4 Statistical comparisons for optimized maximum specific growth rates of *o*-xylene. Statistical measure used was the Wilcoxon rank sum test (comparison of medians) at 95% confidence levels. Displayed are the p-values: <0.05 is a significant difference.

	BA-BTX	**A-BA-BTX**	**A-BA-PAC-BTX**
BA-BTX	1	1.22E-03	1.39E-26
A-BA-BTX		1	5.24E-40
A-BA-PAC-BTX			1

Table A5 Statistical comparisons for optimized half-velocity constants of *o*-xylene. Statistical measure used was the Wilcoxon rank sum test (comparison of medians) at 95% confidence levels. Displayed are the p-values: <0.05 is a significant difference.

	BA-BTX	**A-BA-BTX**	**A-BA-PAC-BTX**
BA-BTX	1	1.37E-03	1.41E-130
A-BA-BTX		1	5.32E-142
A-BA-PAC-BTX			1

Table A6 Statistical comparisons for optimized growth rates of toluene in response to a fixed half-velocity constant. Statistical measure used was the Welch t-test (comparison of means, unequal variance) or Student t-test (comparison of means, equal variance) at 95% confidence levels. Displayed are the p-values: < 0.05 is a significant difference. Values of zero represent values lower than the numerical precision of the software.

	BA-Tol	**A-BA-Tol**	**A-BA-PAC-Tol**	**BA-BTX**	**A-BA-BTX**	**A-BA-PAC-BTX**
BA-Tol	1	0	0	0	0	0
A-BA-Tol		1	0	0	0	0
A-BA-PAC-Tol			1	0	0	0
BA-BTX				1	1.07E-313[S]	3.00E-91[S]
A-BA-BTX					1	4.05E-248[S]
A-BA-PAC-BTX						1

[S]Paired comparisons using the Student's t-test.

Table A7 Statistical comparisons for optimized growth rates of *o*-xylene in response to a fixed half-velocity constant. Statistical measure used was the Welch t-test (comparison of means, unequal variance) or Student t-test (comparison of means, equal variance) at 95% confidence levels. Displayed are the p-values: < 0.05 is a significant difference. Values of zero represent values lower than the numerical precision of the software.

	BA-BTX	**A-BA-BTX**	**A-BA-PAC-BTX**
BA-BTX	1	6.90E-67[S]	0
A-BA-BTX		1	0
A-BA-PAC-BTX			1

[S]Paired comparisons using the Student's t-test.

Flow Through Column Adsorption/Desorption Experimental Method

Column Packing Method

Glass columns used have a core length of 12.0 cm and an inner diameter of 1.5 cm. The 2.5 cm long tip has an inner diameter of 0.4 cm. All syringes used are reusable glass syringes with stainless-steel needles. Note column length.

1. Pack the narrow tip with Pyrex fiberglass wool and fill with glass beads until the internal core diameter is reached. Cover with a piece of stainless-steel wire mesh. Record masses of each piece, as well as full setup weight after combination.
2. Pack the column with the desired sand (PAC mixture notes are in the next step). Add gradual amounts, packing after every addition with a glass rod. Record total setup weight over the course of packing, as well as the length of the first sand zone.
3. Pack the column with the desired sand-PAC mixture. Add gradual amounts, packing after every addition with a glass rod. Record the total setup weight over the course of packing, as well as the length of the sand-PAC zone. This volumetric measurement of mass will be compared with the measured mass for QA/QC. **The mixture added should be of known composition** (mass PAC + mass sand (and thus, ratio) known).
4. Repeat step 2 to fill the column.
5. Cover the soil with a fine mesh piece, followed by a courser mesh piece.
6. Screw the 316 Swagelok fittings onto the ends of the column. **Make sure the tubing used is compatible with BTEX (no sorption in tubing).** The required size of O-rings for the influent are 1/4 and 1/8 inch, while the effluent are 3/4 and 1/4 inch.
7. Attach 3-way ball-valves to the influent and effluent ends with Viton tubing. One of the three attachments contains a septum, into which a 18G needle and syringe (10 and 5 mL for effluent and influent ends respectively). Connect the other influent valve to the Cole-Parmer pump.

Tracer Test Method

Materials:

- Small plastic centrifuge tubes
- Centrifuge tube tray (dark blue)
- Plastic IC sample vials and stoppers
- IC tube tray
- IC stopper insertion tool
- Stopwatch
- Influent flask (200 mL) with **~150 mL of 1000 mg/L NaBr solution** prepared in DI water
- Stopper with hole for influent tubing
- Effluent flask (200 mL)
- 2x pneumatic micropipettes (1 mL and 10 mL) with one tip for each
- 200 mL beaker with DI (for pipette rinsing)
- 200 mL beaker (for DI waste during pipette rinsing)
- 2x column clamps

Column Tracer Flowthrough Protocol:

1. Record test and column information. This includes the date of the test, the column name, length, and diameter, injection concentration, and pump flow rate.
2. Measure two tubing lengths: 1) the influent tubing for the column and 2) the effluent tubing for the column. Record these lengths (cm) at the bottom of the data sheet beside "Tubing length notes".
3. Label record mass of x small plastic centrifuge tubes.
   Note: always weigh the centrifuge tubes using the analytical balance. The influent and effluent flasks can be weighed using the larger balance.
4. Record mass of empty effluent flask (200 mL).
5. Record mass of influent flask with NaBr solution (200 mL).
6. Take 3x 1 mL samples of the NaBr solution using a 1 mL pipette and store in centrifuge tubes labelled "Init 1", "Init 2", and "Init 3". Rinse the mechanical pipette 3x with the 200 mL beaker of DI water, wasting into the empty 200 mL beaker.
7. Clamp the effluent end of the column tubing and disconnect and clamp the influent end of the influent end of the column tubing from the pump effluent tubing. Position the uptake tubing in the NaBr solution.
8. Start pump at elevated flow rate and wait until the NaBr solution is exiting the effluent end of the pump. Once this happens, stop pump, connect the effluent end of the pump tubing to the influent of the column tubing (unclamping the influent), and reset flow rate to the lower one specified on the data sheet. Unclamp the column effluent tubing, positioning it in the effluent flask.
9. Start injection of NaBr solution at specified flow rate. Start the stopwatch when the first drop of water falls into the effluent flask. Record the time of day.
10. Switch the effluent tubing to either: 1) the appropriate vial in the series, or 2) the effluent flask. Timings are unique to each tracer test and should be pre-determined based on effective porosity estimates. Weigh the vial/effluent flask the effluent tubing was just removed from and record its mass.
    Note: periodically mix the influent flask by swirling (~4-5 times over the course of the experiment).
11. Repeat step 10 for all samples.
12. Once last sample is collected, stop stopwatch. Record the time of day.
13. Record the mass of the influent flask.
14. Prepare all IC samples using "Ion Chromatography Sample Preparation" below.
    Note: each IC sample can be prepared during downtime in step 10. This way the samples can be taken straight to the IC at the end of the experiment. Just make sure to **weigh the centrifuge tube before sampling for IC**.

Ion Chromatography Sample Preparation:

1. Using a pneumatic micropipette, add 0.5 mL effluent sample from each glass vial to a corresponding, clearly labelled, plastic Ion Chromatography (IC) vial. Do this for the "Init 1/2/3" samples as well. Rinse the mechanical pipette 3x with the 200 mL beaker of DI water after each sample, wasting into the empty 200 mL beaker. DI beaker may require refilling.
2. Using a 5 mL pneumatic pipette, add 4.5 mL Millipore DI water to each plastic IC vial.
3. Install the filter cap on each IC vial and invert gently 3-5 times to ensure mixing.

4. Leave the labelled samples in the lab beside the IC machine. E-mail the appropriate lab technician after leaving the samples, mentioning the total number of samples **and that they are all diluted 10x**.

Adsorption/Desorption Test Method

Materials:

- 2 mL glass autosampler vials
- Dichloromethane for aqueous phase extraction
- Stopwatch
- Tedlar bag (1 L) with 600 mL of anaerobic 8 mg/L toluene solution prepared in AGW
- Effluent flask (1 L)
- 2x pneumatic micropipettes (1 mL and 10 mL) with one tip for each
- 200 mL beaker with DI (for pipette rinsing)
- 200 mL beaker (for DI waste during pipette rinsing)
- 2x column clamps

Adsorption/Desorption Flowthrough Protocol:

1. Replace all lines with stainless steel lines to prevent toluene adsorption during experiment. Calculate volume of voids in lines.
2. Record test and column information. This includes the date of the test, the column name, length, and diameter, injection concentration, and pump flow rate.
3. Weigh and record influent tedlar bag mass.
4. Record mass of empty effluent flask (200 mL).
5. Take 3x 1 mL samples of the toluene AGW solution using a glass syringe and store in 2 mL autosampler vials.
6. Position the uptake tubing in the toluene AGW solution.
7. Start injection of toluene AGW solution at specified flow rate. Start the stopwatch when the first drop of water falls into the effluent flask. Record the time of day.
8. Take influent and effluent samples using a glass syringe at specified time intervals and store in 2 mL autosampler vials.
9. Repeat step 8 until injection has reached 24 hours. Switch the influent from the toluene AGW solution to toluene-free AGW.
10. Repeat step 8 until toluene-free AGW has been injected for 32 hours (total experimental duration of 56 hours).
11. Once last sample is collected, stop stopwatch. Record the time of day.
12. Record the mass of the tedlar bag and effluent flask.
13. Complete aqueous extraction on all collected samples.
14. Transfer dichloromethane phase to 2 mL autosampler vials
15. Analyze extracted samples in a GC-FID.
16. Upon disassembly of column, complete methylene chloride solid phase extraction on the influent and effluent sand zones and the central sand+PAC zone.